CHARLES UNIVERSITY PRAGUE

faculty of mathematics and physics

Optical Properties of Semiconductor Double Quantum Wells in Magnetic Fields

A thesis submitted to the Charles University
for the degree of Doctor of Philosophy

Milan Orlita

This thesis was submitted by:

Milan Orlita

Enrolled in PhD study program: Physics, Branch of Quantum optics and optoelectronics (F-6) since 2002

Address:

Charles University in Prague
Faculty of Mathematics and Physics
Institute of Physics
Department of semiconductors and semiconductor optoelectronics
Ke Karlovu 5
CZ-121 16 Prague 2
Czech Republic

Email address:

orlita@karlov.mff.cuni.cz

This thesis was supervised by:

Assoc. Prof. Milan Zvára, PhD

Address:

Charles University in Prague
Faculty of Mathematics and Physics
Institute of Physics
Department of semiconductors and semiconductor optoelectronics
Ke Karlovu 5
CZ-121 16 Prague 2
Czech Republic

Email address:

mzvara@karlov.mff.cuni.cz

Acknowledgement

I hope it is obvious to all readers that the thesis could not have been finished without significant help of many people. First I would like to emphasise the help and guidance of my supervisor Assoc. Prof. Milan Zvára and advisor Assoc. Prof. Roman Grill. Precious advice was often given by Assoc. Prof. Pavel Hlídek. Many thanks should be expressed to Dr. Stefan Malzer and Prof. Gottfied H. Döhler, who helped me in several not only working problems during my stay at Institute of Technical Physics I at University Erlangen-Nuremberg. Thanks should go to Isabel Gäßner, who introduced me into the optical lithography and processed several samples for us. Priceless was also the help from Dr. Marcin Byszewski, our local contact person in Grenoble High Magnetic Field Laboratory, CNRS, where the main results summarised in this thesis were attained. In this respect, I am also very grateful to Dr. Ludvík Smrčka, who devoted to me a great deal of time for valuable discussions and persuaded me to perform the experiment in Grenoble's laboratory.

I acknowledge the support received from several institutions:

German Academic Exchange Office (DAAD), which provided me with the scholarship for young researchers and doctoral students and enabled thus my stay at Institute of Technical Physics I, University Erlangen-Nuremberg (October 2003-July 2004).

Grenoble High Magnetic Field Laboratory, CNRS, which accepted several proposals of our group and enabled thus the use of their facilities for our experiments. In addition, they offered a financial support through the program *Transnational Access to Infrastructures – Specific Support Action*, contract No. RITA-CT-2003-505474 of the European Commission.

Grant Agency of Charles University for the support of my doctoral project *Optical properties of coupled double quantum wells in magnetic fields*, contract No. 281/2004.

FRVS fund for the support of the research project: *Optical properties of semiconductor quantum structures in magnetic fields*, contract No. 1841/2004.

Fraternity *Corps-Onoldia* in Erlangen that kindly supported me during the stay at Institute of Technical Physics I, University Erlangen-Nuremberg (March 2003-September 2003).

The whole thesis was finished as a part of the research plan MSM0021620834 that is financed by the Ministry of Education of the Czech Republic.

Used abbreviations

0D, 1D, 2D, 3D	Zero-, one- , two- and three-dimensional (system)
2DEG	Two-dimensional electron gas
2DHG	Two-dimensional hole gas
A	Antibonding (subband)
B	Bonding (subband)
BEC	Bose-Einstein condensation
BO	Bloch oscillation
BX	Biexciton
DOS	Density of states
DQW	Double quantum well
DX	Spatially direct exciton
EX	Exciton
FWHM	Full width at half maximum
HL	D. Huang and S. K. Lyo
IX	Spatially indirect exciton
LL	Landau level
MBE	Molecular beam epitaxy
ML	Atomic monolayer
MT	Mott transition
PL	Photoluminescence
QW	Quantum well
SL	Superlattice
TB	Tight-binding (model)

Important symbols

$B_{\parallel}$	magnetic field in in-plane direction
$B_{\perp}$	magnetic field in perpendicular orientation
Δ	distance between layers or wells
e	electron charge ($e = -1.602 \times 10^{-19}$ C)
E	subband or miniband energy
E_0	miniband width
F_x, F_z	components of electric-field vector
$\hbar$	reduced Planck constant ($\hbar = 1.054 \times 10^{-34}$ J.s)
H	Hamiltonian
k_x, k_y, k_z	components of particle wave vector (momentum)
k_B	Boltzmann constant ($k_B = 1.381 \times 10^{-23}$ J.K^{-1})
m	conduction electron or valence hole mass
m_0	bare electron mass ($m_0 = 9.109 \times 10^{-31}$ kg)
M	exciton mass
$n^{(2)}$	2D electron density
ω_{BO}	frequency of Bloch oscillations
$\omega_{B_{\parallel}}$	frequency of $B_{\parallel}$-controlled oscillations
P_x, P_y	momentum components of exciton
τ_r, τ_n	radiative and non-radiative exciton lifetimes
t	tunnelling coeffiecient
T	temperature
U_{pp}, U_{pn}	bias applied between p-p or p-n contacts
$V(z)$	potential energy, i.e. band profile of 2D structure
v_x	component of velocity in x-direction
x, y, z	spatial coordinates
x_0	amplitude of $B_{\parallel}$-controlled oscillations

Contents

Preface

A great deal of attention has been paid to physics of low-dimensional semiconductors within recent thirty years, resulting in crucial impacts on both current applications and the physics itself. Nevertheless, even though many problems have been solved, there is, in our opinion, a considerable number of questions to be answered. One such region, which certainly deserves our attention, are the optical properties of bilayer systems subject to the in-plane magnetic field. Many papers have dealt with the phenomena induced by the in-plane magnetic field both experimentally and theoretically, but mostly electron transport properties have been investigated. Hence, many measurements and calculations of the in-plane resistance, effective mass or thermopower can be found, but surprisingly few works addressed the optical properties. We try to fill partly this gap in this thesis.

The thesis can be basically considered as experimental but it is completed by some simple theoretical calculations useful for interpretation of achieved experimental results. All experiments were carried out on double quantum well structures under various experimental conditions involving the particle density, applied electric field, temperature etc. It is the application of the in-plane magnetic field, which is the connecting point in all cases. An exception is made in the last part of the thesis, which is purely theoretical and is concerned by properties of superlattices subject to the in-plane magnetic field. This part is based on our previous work on double quantum wells.

I have taken advantage of the possibility given by the university authorities to prepare the thesis as a commented set of already published or accepted papers. The reason I have chosen this way is my feeling that scientific articles contain all relevant results in a comprehensive and well-organised form. Hopefully, readers will appreciate this still not so widely spread way of presenting PhD thesis. Hence, the work is divided into two separate parts. The first one is generally devoted to physics of semiconductor double quantum wells and summarises the most important achievements in the physics of bilayer systems. The main emphasis was put on the optical properties in the external electric and magnetic fields. This overview was written with respect to the results presented in our papers, which form the second part of the thesis as Appendices A-E.

Chapter 1

Double quantum wells in semiconductor physics

The double quantum well (DQW) represents a typical example of a bilayer system. These structures are characterised by a 2D translation symmetry amended by an additional binary degree of freedom due to the possible tunnelling between layers. Therefore, the bilayer structures are sometimes referred to as the simplest 3D systems. The presence of a quantised motion in the growth direction of these structures has a huge impact on their physical properties, which strongly differ from properties of narrow single quantum wells (QWs) representing a physical realisation of an ideal 2D system. The distinctive behaviour of DQWs becomes apparent especially when the in-plane magnetic or perpendicular electric fields are applied as will be discussed in the following chapters.

The quantum well structures are usually realised as sandwich-like semiconductor devices, where the width of individual wells is controlled with the precision of single atomic layers. Among materials used for their preparation appear usually III-V or II-VI semiconductors. The most frequent method of growth is without any doubt the molecular beam epitaxy (MBE). Other methods such as the metal organic chemical vapour deposition or the liquid phase epitaxy are nowadays very rarely used for the preparation of high quality samples and are especially important in the industrial use. In this thesis, we discuss results achieved on DQW structures grown by MBE using the GaAs/$Ga_{1-x}Al_xAs$ (binary/ternary) system, which is in the field of low-dimensional semiconductors the most common combination of technology and materials at all. Its material parameters such as electron and hole effective masses or band offsets are relatively well known. For the sake of completeness, other materials often used for preparation of semiconductor quantum structures are e.g. GaAs/$Ga_{1-x}In_xAs$, CdTe/$Cd_{1-x}Zn_xTe$ or CdTe/$Cd_{1-x}Mn_xTe$.

The topic of DQWs have appeared in the literature since the middle of 1980s when the first experimental results have been published, see e.g. Kawai *et al.* [1, 2]. Gradually, DQWs and bilayer structures in general were recognised as very promising systems for the fundamental physical research. The reasons for this are apparent, not more than the simple quantum mechanics is necessary for their sufficiently accurate description, see Yariv *et al.* [3] or Austin and Jaros [4], their parameters are easy to be controlled using standard tools of the band gap engineering, and additionally, DQWs are a nice example of a realisation of a two-level system, so widely treated in various theoretical models.

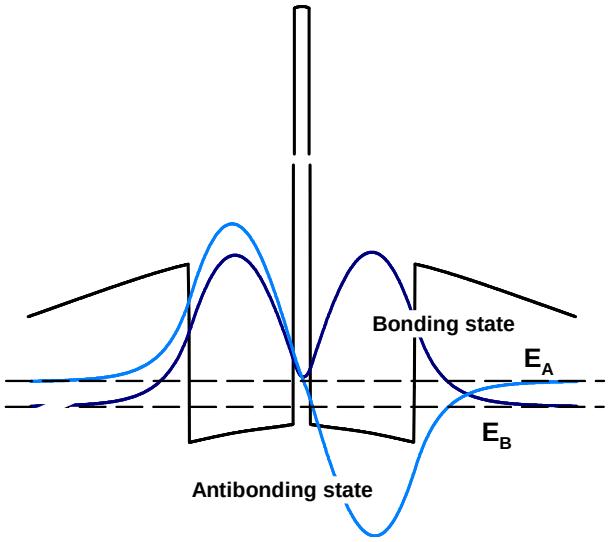

Figure 1.1: An illustrative picture of an n-doped double quantum well. Wave functions of two lowest lying bonding and antibonding subbands are shown.

Many theoretical and experimental papers concerned with DQWs have appeared up to nowadays. We summarise at least some of them in this chapter. We intentionally skip a large number of articles dealing with the DQW properties in normal electric and in-plane magnetic fields, as these are closely related to results achieved by our group and are therefore extensively discussed in the following chapters.

We start with the topic of phase transitions in quantum well systems, which is certainly an up-to-date problem in the contemporary semiconductor physics. A great deal of attention has been paid to the character of the Mott transition (MT), which in the context of the optical properties of 2D semiconductor structures denotes the transition between the gas of interband excitons (EXs) and electron-hole plasma, i.e between insulating and conducting phases. This transition is mentioned although it is not a special feature of DQWs, but due to its importance for the further discussion. The recent experimental results suggest that MT is probably smooth without any abrupt changes in the physical parameters of the system, see Kappei *et al.* [5].

The differences between QWs and DQWs emerge when these systems are studied at temperatures below the critical temperature of MT. In single QWs, excitons are supposed to bind themselves into pair states – so-called biexcitons (BXs). More interesting effects are anticipated in DQWs, as the transition into the BX gas is prevented owing to the strong repulsive exciton-exciton interaction emerging when the electron and hole layers are spatially separated. Namely, the appearance of a spontaneously spin-polarised phase and at lower temperatures even a transition into a superfluid phase – so-called Kosterlitz-Thouless transition – are expected in coupled well systems. For further reading see e.g. [6] and other references therein.

Another phase transition anticipated in DQW systems is the Bose-Einstein condensation (BEC) predicted for a dilute exciton gas. Even though BEC is theoretically forbidden in ideal 2D systems at finite temperatures, it becomes allowed in real DQWs due to po-

tential fluctuations and inhomogeneities giving rise to some discrete levels under the 2D continuum of states. The properties of interband excitons in DQWs, i.e. of EXs in the standard "optical" meaning and their possible BEC is discussed in the next chapter.

Different way how the excitonic BEC could be proven in semiconductor DQWs has been investigated very recently. Nevertheless, in this case, the excitons are no longer formed by an electron in the conduction band bound to a hole in the valence band. The basic idea is to prepare an n-doped symmetric DQW with the same electron density in both QWs and apply the perpendicular magnetic field strong enough to achieve the filling factor $\nu = 1/2$ in each well. Under such conditions, a special type of excitons is supposed to appear consisting from an electron in one layer that is bound to an empty state[1] in the second layer, see e.g. [7]. The main advantage of such "conduction-band" excitons to standard interband ones is their infinite lifetime, as they exist also in thermodynamical equilibrium. Hence, no thermal heating of the system standardly caused by the optical generation is present. This concept has been proven experimentally in transport experiments and brought impressive results [8, 9]. Note that design of samples prepared for this investigation of BEC allowed a proper study of Coulomb drag effects, see e.g. [10].

The discussed collective behaviour of excitons represents a typical example of many-particle effects studied in DQWs. However, numerous other examples can be given. We mention e.g the phenomena of charged exciton states, sometimes referred to as trions. Whilst the binding energy of such complexes in bulk materials is probably too small to find them experimentally, they have been many times observed in systems with a significant quantum confinement such as quantum wells and quantum dots, see e.g. Kheng *et al.* [11] and Warburton *et al.* [12], respectively. As shown e.g. by Shields *et al.* [13] or Timofeev *et al.* [14], the additional degree of freedom in the growth direction of DQW systems has a significant impact on properties of these charged exciton states. Our group touched this problem in Zvára *et al.* [15].

The DQWs are no longer only promising systems for fundamental research, but are definitely important for the future industrial applications. On the basis of DQW systems, several nanoelectronic devices have been suggested and already realised. DQWs based on various semiconductor materials appear frequently in lasers emitting light in a wide range of wave lengths including the region 1.3-1.5 μm that is of great importance in optical communications. DQWs are also considered as effective THz detectors, see [16]. Naturally, also other applications of DQWs can be found.

[1] This empty state can be understood as an effective hole in the conduction band.

Chapter 2

Double quantum wells in electric fields

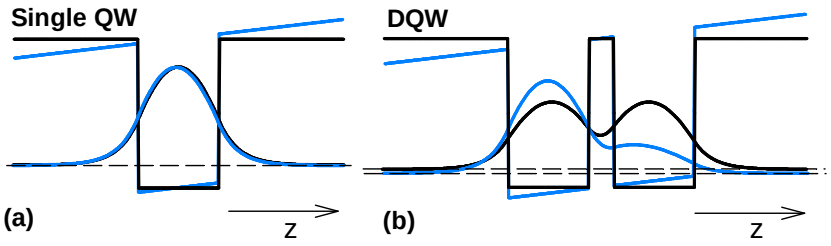

Figure 2.1: A comparison of electron states in (a) QW and (b) symmetric DQW at zero (black curve) and at a finite (blue curve) electric field applied along the growth direction, $\mathbf{F} = (0, 0, F_z)$. The same electric field is applied in both cases.

Quantum states in bilayer systems are rather sensitive to the electric field F_z applied along the growth direction of the structure. We demonstrate this effect in Fig. 2.1, where the ground-state wave functions are calculated for (a) a single QW and (b) a symmetric DQW at zero and at a finite F_z. The DQW considered in Fig. 2.1b was simply created by a coupling of two identical QWs from Fig. 2.1a. The same electric field F_z was considered in both cases.[1] Whereas the wave function in a single QW changes weakly with F_z, the influence on the symmetric DQW is considerably enhanced. This can be understood, when we realise that the energy spectrum of a symmetric DQW originates in energy levels of two independent QWs which are resonantly coupled. Each energy level from a single QW is then split in the symmetric DQW. When the coupling is weak, we practically obtain twofold degeneracy of each level. The additionally applied electric field then lifts this degeneracy and brings the wells out of resonance, i.e. effectively decouples the wells. This explains a rather steep change in the shape of the wave function. When the wells are coupled non-resonantly only, the whole energy spectrum consists of levels related to the particle localised predominantly in the left or in the right QW. The change in the electric field then mutually shifts energy levels in such two wells by $\delta E \approx e\Delta\delta F_z$. Δ denotes the characteristic distance of layers in DQW. Note that the non-resonant coupling is a common case of asymmetric DQWs, but obviously, an appropriate F_z can bring any two

[1] As the results in Figs. 2.1a,b serve as an illustration only, we do not explicitly discuss parameters of wells chosen realistically for the GaAs/GaAlAs system.

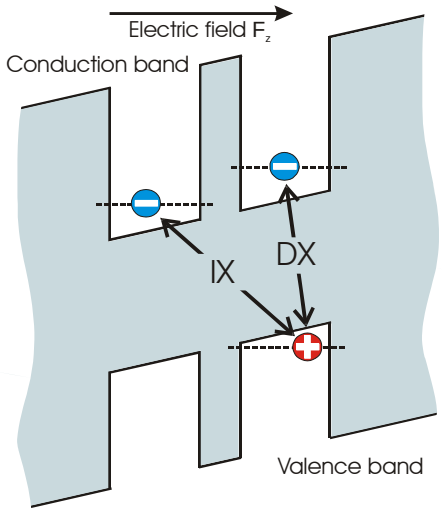

Figure 2.2: Spatially direct and indirect excitons in a tilted DQW.

levels in opposite wells into resonance. Finally, we can conclude that the Stark effect is strongly enhanced in both symmetric and asymmetric DQWs in comparison with single QWs.

The presented electric-field-induced effects are currently observed in experiments. The strong Stark shift in bilayer systems is especially apparent in optical measurements and was identified in photoluminescence (PL), photoluminescence excitation or photoconductivity spectra, see e.g. Chen *et al.* [17] or Little and Leavitt [18]. All these experiments allow a study of intersubband transitions. Such transitions can be divided into spatially direct and indirect ones, depending if they occur between electron and hole states localised in the same or in the opposite well, respectively. The transition energy of the latter ones varies with the applied electric field as $\delta E \approx e\Delta\delta F_z$.

The samples used in experiments are usually undoped to prevent the screening of the external electric field by 2D electron or hole gases (2DEG or 2DHG). However, the optical spectra obtained from undoped DQWs are significantly influenced by the mutual Coulomb interaction between recombining electrons and holes. Similar to bulk crystals, the excitonic interaction leads to the formation of bound states – excitons whose binding energy is due to the 2D spatial confinement considerably enhanced in comparison with EXs in the bulk. A proper calculation of EX binding energies is thus necessary to get a quantitatively applicable description of undoped DQWs in optical experiments, see e.g. Westgaard *et al.* [19] or Soubusta *et al.* [20]. Since the excitonic interaction leads to a formation of stable excitons in undoped DQWs, we usually speak about the recombination of the spatially direct (DX) and indirect (IX) excitons instead of the optical transitions, see Fig. 2.2. An example of such excitons in PL spectra of a biased DQW can be found in Fig. 2.3, where the redshift of the IX line with the increasing electric field on DQW is apparent. The DX energy is influenced only weakly by this electric field, as well as the energy of peaks A and B which were identified as charged excitons. The electric field on DQW is supplied by the external bias voltage. For a deeper discussion of these spectra see Zvára *et al.* [15].

The applied electric field enables not only the changing of the IX recombination energy,

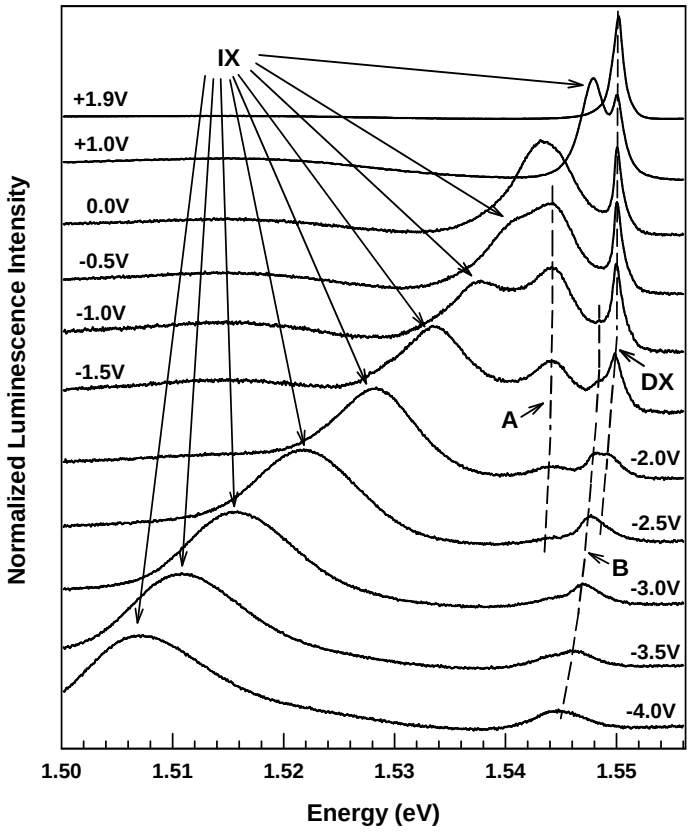

Figure 2.3: IXs in PL spectra of 35-ML DQW in the sample TP313. For sample description see Chapter 7. Data are taken from a previous work of our group [15].

but brings also a possibility to control the IX radiative lifetime in DQWs as well. This is simply caused by the spatial separation of electrons and holes in the tilted DQW, since the mutual overlap of electron and hole wave functions strongly decreases with the electric field F_z. The IX radiative lifetime can thus be increased up to μs region, see [21, 22, 23], i.e. almost three orders of magnitude longer than for intrawell excitons. Note that the probability of the radiative recombination can be further reduced when the in-plane magnetic field is applied. The Chapter 5 will be concerned with this problem.

Observation of long exciton lifetimes in DQW structures once more attracted attention to the problem of the Bose-Einstein condensation (BEC) in semiconductors, which was widely studied in 1980s. Even though the excitonic BEC is not studied in this thesis it is worth to devote some space to its description. Excitons having an integer spin and a relatively low mass seemed to be ideal particles for study of BEC at rather easily achievable experimental conditions. For such excitonic systems, the critical temperature of the transition into the Bose-Einstein condensate was predicted to be close to the liquid helium temperature. This topic was extensively investigated both theoretically and experimentally, promising appeared for instance the material Cu_2O, where the exciton recombination is forbidden within the electric-dipole approximation, see e.g. Snoke *et al.* [24]. Nevertheless, all attempts to find conclusive evidence for BEC in bulk semiconductors failed. The

problem encountered lay in the optical generation of relatively short-living excitons, which either did not provide a sufficient density of the cold exciton gas or created a dense exciton gas at temperatures too high to allow the condensation. However, when the advantage of long lifetimes of IXs in DQWs is taken, we can achieve the needed exciton density at a significantly reduced excitation intensity. Hence, IXs brought about a renaissance of BEC in excitonic systems.

Since 1990s, several groups have been concerned by the possibility of BEC in the dilute IX gas and interesting results mainly from PL experiments have been published. The collective behaviour of IXs was reported e.g. Larionov *et al.* [25], Butov *et al.* [26] and Krivolapchuk *et al.* [27]. The seminal papers presenting the spatially resolved PL experiment were simultaneously published by groups of Butov and Snoke, see [23, 28], where a clear evidence for the collective properties in the IX gas was found. However, no direct evidence for the excitonic BEC has been given. Additionally, the interpretation of these fascinating experiments is not definite up to now, see e.g. [29, 30]. In this respect, a good deal of effort is now devoted to the investigation of transport properties of IXs, see e.g. Gärtner *et al.* [31] or Vörös *et al.* [32], which are likely essential for understanding of the experimental data. A thorough study of IX PL was published by Lai *et al.* [33]. The interpretation of their spatially resolved PL experiment suggests a presence of statistically degenerate lakes of IXs localised in potential traps. Recall that just the potential traps are necessary for a possible appearance of BEC in 2D systems.

However, one fundamental question concerning BEC in the dilute IX gas is still to be answered. It is not definitely clarified if the cold gas of IXs is really a good way how to physically realise the system of non-interacting bosons for which the BEC was originally proposed. The main problem lies in a rather strong repulsive dipole-dipole interaction between IXs, which, in our opinion, could exclude the formation of a dense IX gas, where IXs could be treated as mutually non-interacting. In our experiment, this repulsive interaction was likely responsible for the narrowing of IX PL line with the increasing excitation density, see Orlita *et al.* [34] in Appendix D. The rather broad PL emission of localised IXs was at a higher excitation power replaced by a narrowed PL line from weakly bound IXs, since the additionally created IXs could not relax to the already occupied states in deeper potential traps. Other experimental results indicating the strong dipole-dipole repulsion among IXs can be found e.g in Negoita *et al.* [35]. Very roughly, the dipole-dipole interaction acts as an effective Pauli principle in the bosonic (!) system in these cases. Evidently, the system of interacting IXs can also give rise to many interesting collective effects, but such a system is not so unique, since the collective behaviour of (relatively strongly) interacting bosons at the liquid helium temperature was widely studied in many types of materials (superfluidity, superconductivity etc.).

Very similar situation is encountered in case of "conduction-band" EXs investigated by groups of Eisenstein and von Klitzing [8, 9]. However, the dipole-dipole interaction among these EXs can be both attractive and repulsive, as EXs are not oriented by the external electric field as in case of the spatially indirect interband excitons. In addition, we should also emphasise the general feature of excitons. These boson-like particles consist of rather loosely bound fermions in a very dense environment of solid state materials, which can significantly modify the possible BEC.

Chapter 3

Quantum wells in magnetic fields - general remarks

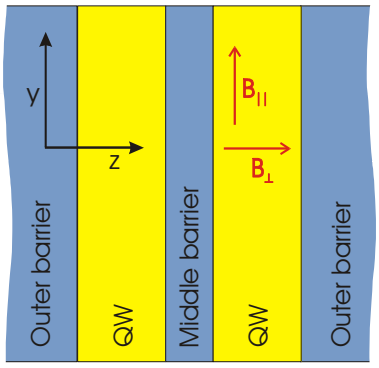

Figure 3.1: A schematic picture of a DQW structure, where both in-plane ($B_{\|}$) and perpendicular ($B_{\perp}$) orientations of the magnetic field considered in this thesis are shown.

The 2D translation symmetry of quantum wells defines two principal directions in which the magnetic field can be applied: along ($B_{\perp}$) or perpendicular ($B_{\|}$) to the growth axis of the system, see Fig. 3.1. Whilst the former is usually denoted as the Faraday configuration or the perpendicular direction of the field, the latter is often referred to as the Voigt configuration or simply as the "in-plane" orientation of the field. In this chapter, we discuss some important features of quasi-2D systems under influence of the magnetic field applied in both principal directions. Let us emphasise that one fixed orientation of the in-plane field $B_{\|}$ along the y-axis is consistently considered in the whole thesis, for simplicity. Obviously, all other directions of the in-plane field lying in the x-y plane would be physically equivalent. Note that we completely omit the very interesting and in recent years frequent tilted orientation of the field.

3.1 Perpendicular magnetic field

The perpendicular magnetic field strongly modifies the in-plane motion of an electron[1] in QW structures and we can combine both quasi-classical and quantum-mechanical considerations in its description. The simple (quasi) classical theory predicts a standard circular trajectory and the electron in QW is thus effectively confined in all three spatial directions. Therefore, the quantum well at finite $B_\perp$ resembles 0D instead of 2D systems. The proper quantum-mechanical treatment allows us to deepen these quasi-classical considerations, to calculate corresponding wave functions and to obtain the corresponding energy spectrum. This spectrum, so-called Landau levels (LLs), $E_n = \hbar\omega_c(n + 1/2)$, where $\omega_c = |e|B_\perp/m$ and $n = 0, 1, 2\ldots$, is discrete in energy and again resembles 0D features of QW systems at finite $B_\perp$. In this respect, the LL degeneracy $\zeta = |e|B_\perp/\pi\hbar$ can be understood as the spatial density of 0D systems in the QW plane. The spin state of electrons is involved in these considerations simply as a twofold degeneracy. Apparently, the Zeeman splitting might be experimentally important at higher magnetic fields.

The presented conclusions can be easily utilised in experiments. For instance, we could have estimated the electron density and confirmed the expected structure of the electron subbands in the sample TP811, see Orlita *et al.* [36, 37] in Appendices A and B. Let us note that there are no principal differences between the application of the field $B_\perp$ to a pure 2D and to a bilayer system. This is no longer valid in the case of the in-plane magnetic field $B_\parallel$ as will be clarified in the next section.

3.2 In-plane magnetic field

Apparently, also the magnetic field in the in-plane orientation affects the energy spectrum of quantum well systems but in a way completely different from $B_\perp$. If quantum well structures at finite $B_\perp$ are in some features close to 0D systems the in-plane magnetic field, as will be shown, brings about the confinement leading to the DOS that has similarities to 1D systems. Let us now consider the magnetic field $\mathbf{B} = (0, B_\parallel, 0)$ with the vector potential gauge $\mathbf{A} = (B_\parallel z, 0, 0)$ applied to a 2D system defined by the band profile $V(z)$. The Hamiltonian of such a system reads:

$$H = \frac{\hbar^2}{2m}\left(k_x - \frac{eB_\parallel z}{\hbar}\right)^2 + \frac{\hbar^2 k_y^2}{2m} - \frac{\hbar^2}{2m}\frac{d^2}{dz^2} + V(z). \tag{3.1}$$

We implicitly suppose the wave function in a form of a plane wave in both in-plane directions and the components of the particle in-plane momentum are labelled by k_x and k_y. Actually, these components are wave vectors and not momenta, but we keep the terminology standardly used in the literature. Other symbols in (3.1) have their usual meaning. The Hamiltonian (3.1) evidently leads to the coupling of the electron motion in the x- and z-direction and the electron energy takes a general form of $E(k_x, k_y) = E(k_x) + \hbar^2 k_y^2/2m$, where the dispersion $E(k_x)$ strongly differs from a parabolic shape common at $B_\parallel = 0$. Now, we look at this dispersion closer.

We start with a simple example of a single n-doped QW. Using the self-consistent model developed in [36], we calculated the dispersion curve $E(k_x)$ and the related DOS for an

[1] We speak about electrons, for simplicity, but all conclusions in this chapter are valid also for holes.

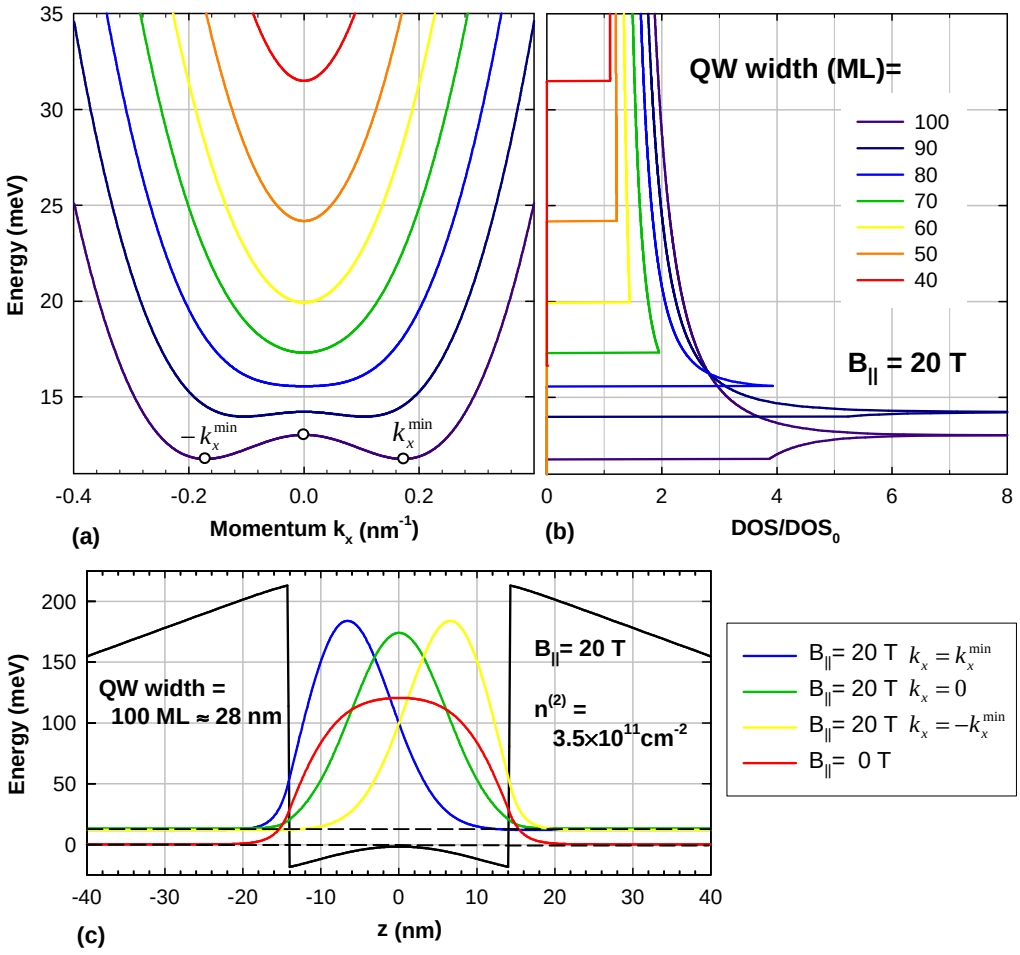

Figure 3.2: (a) The electron dispersion curve $E(k_x)$ and (b) the related DOS for a single GaAs/$Ga_{0.7}Al_{0.3}$As QW at $B_{\|} = 20$ T for various well thicknesses. The DOS is normalised to $DOS_0 = m/\pi\hbar^2$, i.e. to the DOS of a pure 2D system. Part (c) shows the wave functions for selected electron momenta k_x in 100-ML QW again at $B_{\|} = 20$ T. Zero energy corresponds to the ground state of 100-ML QW at $B_{\|} = 0$ in all three parts of this figure.

electron in GaAs/$Ga_{0.7}Al_{0.3}$As QW at $B_{\|} = 20$ T and plotted the results into figures 3.2a and 3.2b, respectively. The QW thickness given in units of monoatomic layers (ML) serves as a parameter.[2] The 2D electron density, which is an input to our calculations, was chosen as $n^{(2)} = 3.5 \times 10^{11}$ cm^{-2}. We can clearly observe a gradual flattening of $E(k_x)$ with the increasing well width which finally results in the creation of two independent minima. This significantly non-parabolic shape of $E(k_x)$ leads to DOS that strongly differs from an almost constant function found for very thin QWs. In a wide QW, even a singularity in DOS appears as a result of the saddle point developed in $E(k_x, k_y)$. This singularity can resemble DOS of a 1D system.

We see that the influence of $B_{\|}$ is enhanced in wider QWs, which illustrates the essential feature of all $B_{\|}$-induced effects – they are based on the quasi-two-dimensionality of the

[2] 1 ML $\doteq$ 0.283 nm in GaAs [38]

real 2D systems. Or reversely, the influence of $B_\parallel$ can measure how ideal is the 2D confinement in the studied system. For the sake of completeness, we should add that the two minima in $E(k_x)$ would not appear in the same but undoped QW, since these minima correspond to two potential minima of this doped QW, see the QW potential profile in Fig. 3.2c. However, the flattening of $E(k_x)$ appears in empty wells as well. For further reading about electron dispersions in single QWs at finite $B_\parallel$ see [39].

Up to now, we have just described calculations in Figs. 3.2a and 3.2b, but also their physical interpretation should be given. We can do it on the basis of Fig. 3.2c, where the wave functions corresponding to the dispersion $E(k_x)$ of 100-ML QW at $B_\parallel = 20$ T are plotted for three different k_x. Because the wave function at zero $B_\parallel$ is shown as well, for comparison, we can see that all wave functions are significantly narrowed at finite $B_\parallel$ due to the additional magneto-confinement. In addition, contrary to the case of $B_\parallel = 0$, the wave functions are strongly k_x-dependent owing to the above discussed coupling between electron motion in the x- and z-directions. Depending on the momentum k_x, electrons become localised at finite $B_\parallel$ closer to one barrier than to the other. This result can closely resemble quasi-classical expectations, i.e. the influence of the Lorentzian force, pushing electrons either towards the right or the left barrier depending on the sign of their velocity. However, these quasi-classical considerations must be done very carefully. As the electron velocity is given by the well-known relation $v_x = \hbar^{-1} dE(k_x)/dk_x$, we apparently get $v_x(k_x^{\min}) = v_x(-k_x^{\min}) = 0$, see Fig. 3.2c. Hence, also the wave functions of standing electrons are effected by $B_\parallel$. In addition, the fact that electrons with positive momentum k_x are localised close to the left barrier and vice versa would not be true if we choose another gauge, e.g. $\mathbf{A} = (eB_\parallel(z - z_0), 0, 0)$. We would then simply obtain the dispersion identical in shape but shifted in the reciprocal space by the amount of $eB_\parallel z_0/\hbar$. Nevertheless, the picture of the acting Lorentzian force can be useful at least for basic understanding of the physics of bilayer systems at finite $B_\parallel$.

The influence of $B_\parallel$ can be enhanced when the single QW is replaced by a DQW system whose bilayer character is clearly induced by its band profile. This fact is illustrated in Figs. 3.3a and 3.3b, where the dispersion curves for two lowest lying subbands of a DQW system together with the corresponding DOSs are plotted as a function of the molar fraction in the central barrier x_{Barrier}. This 4 ML (≈ 1 nm) wide barrier separates two identical 26-ML (≈ 7 nm) GaAs QWs. Hence, we have a 56-ML (≈ 16 nm) GaAs QW for $x_{\text{Barrier}} = 0$ and a well defined DQW with the barrier from pure AlAs at $x_{\text{Barrier}} = 1$. The outer barriers are assumed to be made from $Ga_{0.7}Al_{0.3}As$, the magnetic field is fixed at $B_\parallel = 16$ T and the same electron density $n^{(2)}$ is chosen as in previous calculations for single QWs. The increase in the strength of the central barrier has several impacts. We can omit the change of the subband energies[3] with x_{Barrier} since it appears at zero $B_\parallel$ as well, and focus our attention to the two minima developed in the dispersion of the lower subband. They correspond to electrons localised in the right or in the left well, see Fig. 3.3c, as can be expected when we recall calculations in Fig. 3.2c. Hence, standing or slowly running electrons can be localised in the right, in the left or in both wells, electrons with high velocities v_x just in one of them. In quasi-classical considerations, we could again carefully speak about the Lorentzian force pushing electrons through the central barrier.

[3]The subtle change in the energy of the first excited subband is caused by the shape of the wave function having a node in the central barrier.

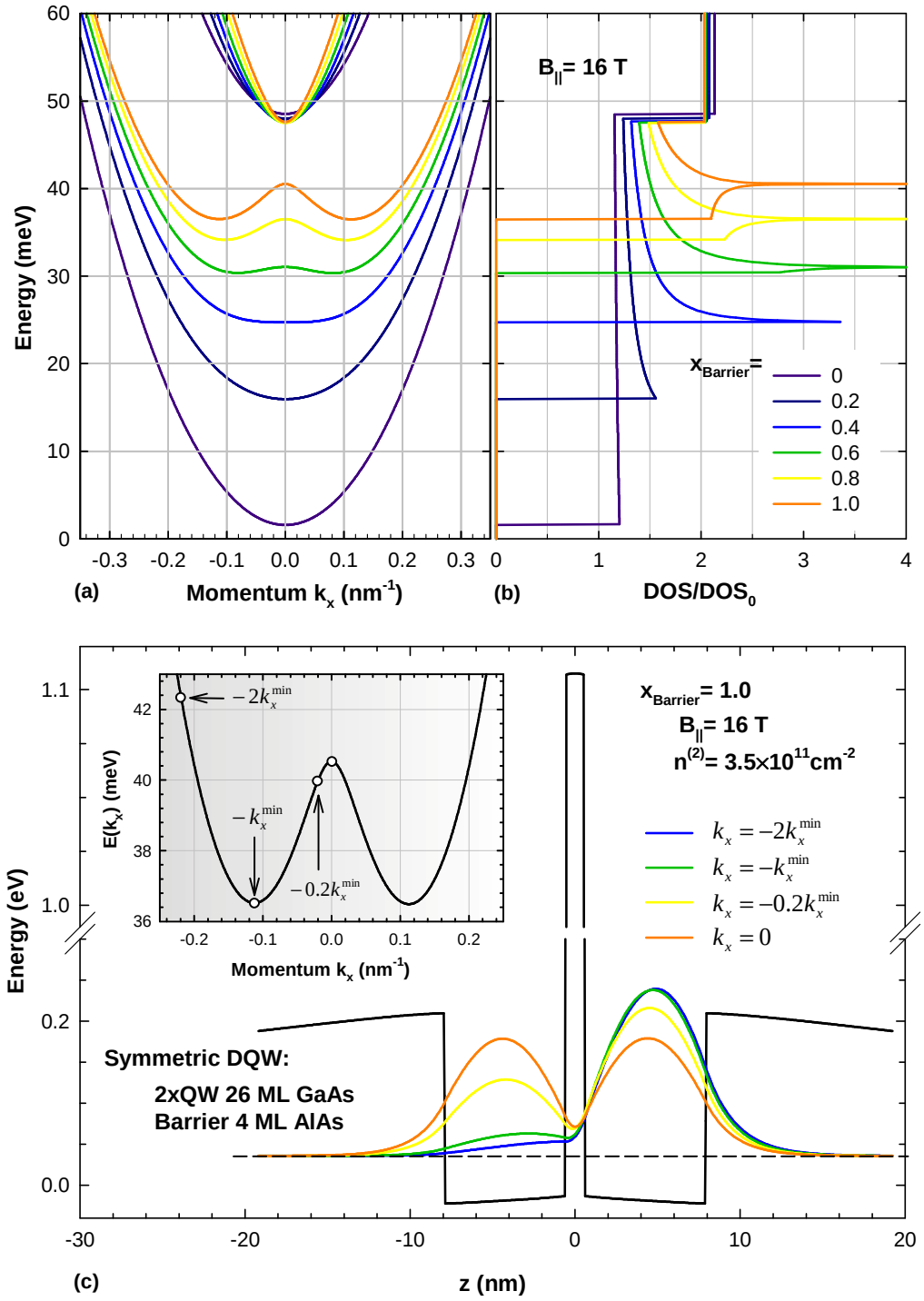

Figure 3.3: (a) Electron dispersion curves $E(k_x)$ and (b) corresponding DOSs in a symmetric DQW consisting of two 26-ML GaAs QWs separated by a 4-ML barrier at $B_{\parallel} = 16$ T and electron density $n^{(2)} = 3.5 \times 10^{11}$ cm^{-2}. The aluminum content in the central barrier x_{Barrier} serves as a parameter. (c) Electron wave functions for selected k_x at $B_{\parallel} = 16$ T for $x_{\mathrm{Barrier}} = 1$. The inset shows the enlarged dispersion $E(k_x)$ from part (a), where the chosen values of momentum k_x are depicted. The zero energy corresponds to the ground state of a single 56-ML QW at $B_{\parallel} = 0$ in all three parts.

A careful reader may be surprised that the potential profile inside the wells in Fig. 3.3c is convex instead of the concave shape which might be expected at the finite electron density. This is a consequence of the exchange-correlation potential involved in our self-consistent model [36], because the contribution of this term is at the given density roughly comparable to the Hartree contribution. This result is in agreement with calculations performed by Huang and Lyo [40].

In summary, we illustrated that effects induced by the in-plane magnetic field are essentially connected with the degree of the quantum confinement in the growth direction of the considered quasi-2D system. We discussed examples of a single QW of different widths and a symmetric DQW. In a wide single QW, the sufficiently high magnetic field $B_{\parallel}$ causes a transition from a single-layer system to a bilayer one. Similar behaviour but even at lower magnetic fields was demonstrated in DQWs, which thus represent a natural system, where the influence of $B_{\parallel}$ can be studied. In addition, contrary to the case of single QWs, where rather complicated calculations are necessary, the DQWs allow a simple and also intuitive way how to describe $B_{\parallel}$-induced effects when a tight-binding (TB) model is used. We will sketch it in the remaining part of this chapter.

The TB model, working with a superposition of electron states in isolated QWs, can be usefully extended for calculations at a finite $B_{\parallel}$, see [41, 42, 43]. The Hamiltonian (3.1) then takes a simple matrix form:

$$H_{i,j} = E_i\delta_{i,j} + \frac{\hbar^2}{2m}(k_x - K_0 i)^2\delta_{i,j} + t\delta_{i,j\pm1}, \tag{3.2}$$

where $i, j = 1, 2$, $K_0 = eB_{\parallel}\Delta/\hbar$ and the coefficient t ($t < 0$) characterises the tunnelling rate between wells. Parameter Δ denotes the centre-to-centre distance of QWs. The electron motion in the y-direction is not included, since it is not affected by $B_{\parallel}$. Solving the eigenvalue problem defined by the matrix (3.2), we obtain two electron subbands – a lower lying bonding (B) and an upper lying antibonding (A). Both subbands are parabolic in k_x only at $B_{\parallel} = 0$ or in a limit of fully separated QWs $t = 0$. At finite $B_{\parallel}$ we obtain general dispersions $E_{A,B}(k_x)$ that are formed by two "anti-crossed" parabolas which correspond to dispersions of isolated QWs mutually shifted in the reciprocal space by the amount of K_0.

The simplicity of this model can be used for effective calculations of both transport and optical properties of DQWs. Soubusta in his doctoral thesis [44] calculated joint density of states for symmetric DQWs and our group performed a similar calculation for DQWs with an electric-field-induced asymmetry [45]. In this thesis, the model was straightforwardly extended to a superlattice structure, see Chapter 6 and [46]. We just assumed that $i, j \in \mathcal{Z}$ and took $E_i = 0$. The same considerations can be found also in [47].

Chapter 4

Two-dimensional electron gas subject to in-plane magnetic fields – experimental aspects

The two-dimensional electron gas (2DEG) in bilayer systems in in-plane magnetic fields became the subject of interest in late 1980s when first theoretical works appeared, see e.g. Oliveira *et al.* [48]. This interest was intensified in early 1990s, when several experimental works concerning this topic have been published. In these experiments, the bilayer systems were represented by modulation-doped wide QWs or DQWs and transport properties were mainly investigated, whilst optical measurements appeared rather rarely. To get some insight, we review several relevant papers.

Boebinger *et al.* [49] investigated the Shubnikov-de Haas oscillations in DQWs as a function of the in-plane component of the magnetic field $B_{\|}$. The observed beating in these oscillations was explained as a result of the $B_{\|}$-induced mixing of the bonding (B) and antiboding (A) state in DQW. This interpretation was confirmed by a proper theoretical model developed by Hu and MacDonald [41]. Further results on DQW systems were achieved by the group of Eisenstein [50] who reported a strong decline of the tunnelling efficiency between wells with increasing $B_{\|}$. Their interpretation expected the mutual shift of the parabolic dispersions corresponding to electrons in opposite wells by the amount of $\delta k \approx eB_{\|}\Delta/\hbar$. As soon as the Fermi level dropped down under the crossing point of these parabolas, the tunnelling rate decreased significantly due to the momentum conservation of the tunnelling electrons. Zheng and MacDonald [51] supported this explanation by a theoretical model later on.

Another type of transport experiments –an in-plane conductance– was performed on an n-doped DQW by Simmons *et al.* [52]. The modulation of this conductance by the in-plane magnetic field revealed a strong variation of the electron DOS on the Fermi level, which was explained by a partial gap in the electron subband structure induced by $B_{\|}$. The interpretation was based on a simple theoretical model [42] published in advance by Lyo, one of the co-authors of [52]. A large number of papers dealing with similar problems followed this finding. Among others: Smrčka *et al.* [53] studied the cyclotron effective mass in a single heterojuction as a function of $B_{\|}$, Jungwirth *et al.* [54] investigated the in-plane magnetoresistance in a wide single QW, Blount *et al.* [55] in strongly coupled

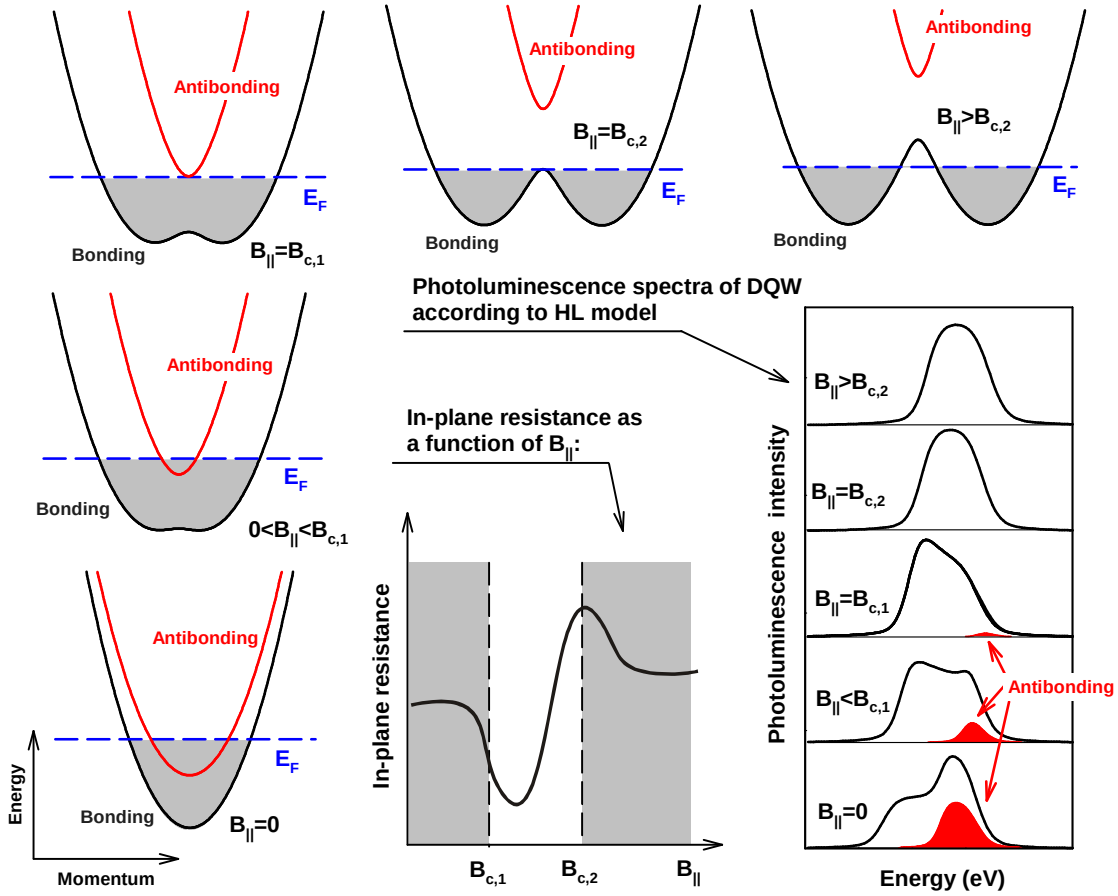

Figure 4.1: A symmetric double quantum well in the in-plane magnetic field. A schematic comparison of a typical result of the in-plane magnetoresistance with predictions done by HL for a PL experiment. The red area in spectra denotes the contribution of the subband A to the whole PL. Corresponding dispersion curves are plotted for both bonding and antibonding subbands.

DQWs and Makarovskii *et al.* [56] in asymmetric DQWs.

However, let us turn our attention to the optical properties. To the best of our knowledge, the first "optical" paper concerning a bilayer system with 2DEG at $B_{\|}$ was published by Whittaker *et al.* [57]. They studied PL from a wide QW where the asymmetric doping ensured a large spatial separation of electron and hole layers. The PL spectra revealed a formation of an indirect-band-gap structure at the finite in-plane magnetic field. Further papers that appeared were mostly theoretical. Soubusta calculated in [44] a joint density of states of a symmetric DQW in the framework of the TB model. Huang and Lyo (HL) suggested a far infrared detector based on DQWs tunable by $B_{\|}$ in [58] and the same authors calculated PL from both symmetric and asymmetric n-doped DQWs as a function of $B_{\|}$ in [40]. They predicted a so-called $\mathcal{N}$-type kink in PL spectra of sufficiently doped symmetric DQWs, i.e. the redshift of PL maximum appearing when the in-plane magnetic field is high enough to depopulate the antibonding subband. This effect proposed for the PL experiment represents an "optical" counterpart of the above discussed $B_{\|}$-induced

conductance (or resistance) modulation [52].

Since the HL prediction is essential for the discussion of our results, we explain it with the help of an illustrative diagram in Fig. 4.1, where dispersion curves and position of the Fermi level of a hypothetical symmetric DQW are depicted. We show there the evolution of the electron subbband structure with $B_{\|}$ and discuss the response of this system in both PL and in-plane magneto-resistance experiments. We start with the DQW system at $B_{\|} = 0$, when the electron dispersion corresponding to the bonding as well as antibonding subband is apparently of a common parabolic shape. The chosen position of the Fermi level E_F suggests that electrons occupy both of the considered subbands. This results in a "step-like" shape of the PL spectrum reflecting recombination of electrons from both subbands cut at the Fermi level. With increasing $B_{\|}$, the dispersion of the subband B becomes modulated, the total number of states close to the subband bottom increases and simultaneously the splitting of the subbands rises. As a result, the electron density in the subband A decreases and its contribution to the whole PL spectrum weakens. As soon as $B_{\|} = B_{c,1}$,[1] the Fermi level sweeps across the bottom of the subband A which does not practically contribute to the PL signal. The depopulation of the subband A has a significant impact on the resistivity which is roughly proportional to the DOS at the Fermi level.[2] Therefore, the resistivity rather abruptly decreases. At $B_{\|} > B_{c,1}$, the PL spectra are modified rather weakly, but the resistivity rises again, reflecting the increasing DOS at the Fermi level. The resistivity achieves its maximum when E_F reaches the saddle point in the electron subband structure, which leads to the logarithmic singularity in DOS. We define that this situation occurs at the critical field $B_{c,2}$, see Fig. 4.1.

In summary, the evolution of the DQW subband structure is observed in both experiments. The PL experiment allows a direct observation of the gradual depopulation of the subband A that is not seen in the magneto-resistance. On the other hand, the field induced logarithmic singularity in the DOS can be studied by transport measurements, but not in the PL experiment.

We should recall that we compared a typical result of the in-plane magneto-resistance measurement with a theoretical model of the PL experiment on an n-doped symmetric DQW published by HL. As their model is rather simple, we can ask how realistic these predictions are. In order to allow the experimental verification of their model, HL kept $B_{c,1}$ as low as possible. This can be achieved in common DQWs only when a relatively low electron density is assumed, but with the decreasing electron density the influence of the excitonic interaction on PL spectra significantly rises. Nevertheless, the HL model does not take the excitonic interaction into account. The density of 2.4×10^{11} cm^{-2} chosen by HL does not allow a simple decision whether or not the excitonic interaction is sufficiently screened in 2DEG. In addition, HL supposed that optically generated holes in DQW built up a low density Boltzmann distributed hole gas. Neither this assumption is obvious in n-doped systems, where the localisation of holes is often reported, allowing thus the observation of the Fermi edge singularity, see e.g. Kissel *et al.* [59].

As far as we know, there are only two published experiments relevant to the model of HL. The first experiment was performed by Kim *et al.* [60] and the second one by our group [36]. Kim and coworkers studied PL from three symmetric n-doped DQWs and

[1] The notation of the critical fields $B_{c,1}$ and $B_{c,2}$ are taken after [56].

[2] In the simplest consideration, the resistance is proportional to the total number of states on the Fermi level, i.e. to the number of states into which electrons can be elastically scattered, see [42, 52].

one of them qualitatively exhibited the expected behaviour. No theoretical calculation to support the interpretation was appended. The sample, where the $\mathcal{N}$-type kink was observed, showed the lowest mobility of the studied set and the hole localisation was expected.

Our experiment was carried out on a symmetric p-i-δn-DQW-δn-i-p structure, whose selective electrical contacts enabled to tune the electron density in DQW up to 3.5×10^{11} cm^{-2}, see the sample description in Chapter 7 or directly [36] in Appendix A. The PL spectra attained experimentally are in a very good agreement with those calculated using a simple self-consistent model based on the HL theory. $\mathcal{N}$-type kink was clearly observed. The main deviation from the original HL theoretical model was an assumption of localised holes, based on the experimental findings. The comparison of theory and experiment has proven that the excitonic interaction does not dominantly affect the PL spectra and thus the one-particle model of the band-to-band recombination is adequate at these electron densities.

The electron subband structure and the electron density were crosschecked by measurements at a finite $B_\perp$ that revealed the quantisation of 2DEG into LLs, see [36, 37]. We could clearly distinguish zero LLs corresponding to the subband A as well as B. The latter one was gradually depopulated by increasing $B_\perp$. Excited LLs occupied at lower magnetic fields $B_\perp$ were not clearly resolved in spectra due to the inhomogeneous broadening of the observed transitions.

HL in [40] have also done several predictions for asymmetric DQWs, depending on the electron density and the DQW asymmetry, which should be induced by the external electric field. In our sample, we could have created this field applying an appropriate bias U_{pp} to the top and bottom p-contacts, see Chapter 7. The performed experiment did not provide such easily interpretable results as in the case of $U_{pp} = 0$. The problem we encountered was the decline of the electron density with the increasing U_{pp}. This decrease could be partially compensated for by the forward bias U_{pn}, but the whole structure then became much more complicated and no simple conclusions were possible, see Orlita *et al.* [37]. We suppose that the symmetric DQWs with an asymmetric doping or directly asymmetric DQWs would be much better for this purpose than our symmetric DQW with the electric-field-induced asymmetry.

In summary, our experiment [36] (see Appendix A) confirmed the theoretical predictions for the PL measurement on a symmetric n-doped DQW published by Huang and Lyo [40]. To the best of our knowledge, the validity of their model was quantitatively confirmed for the first time. Unfortunately, our experimental approach did not allow the same in case of asymmetric DQWs, see [37] in Appendix B. Additionally, the PL spectra of a symmetric DQW were studied in a wide range of electron densities in [36], showing a gradual evolution of spectra from the excitonic- to free-electron-like. In our opinion, this result is important in the context of the Mott transition because it amends and supports recent findings published by Kappei *et al.* [5], where MT in the balanced electron-hole plasma was reported as smooth without any abrupt changes in PL spectra.

Apart from papers discussed in this chapter, other important PL measurements on DQWs at $B_\parallel$ have been published. Nevertheless, no 2DEG was present in DQWs in those cases, instead the excitonic properties were addressed. This topic is discussed in the next chapter.

Chapter 5

In-plane magnetic field and indirect excitons

In the previous chapter, we discussed the optical response of DQW systems at particle densities which allow a neglect of the excitonic interaction. Consequently, the simple band-to-band recombination model has been successfully utilised. However, also undoped DQWs, where the Coulomb interaction between recombining holes and electrons has a huge impact on the optical properties, exhibit a noticeable behaviour in the in-plane magnetic field. We will now discuss this topic.

The excitonic PL in DQW structures was theoretically investigated by Gorbatsevich and Tokatly [61] and later on also by Chang and Peeters [62]. The main attention was naturally paid to the properties of indirect excitons (IXs), as the possibility of their formation is the main advantage of DQW structures to uncoupled QWs. Their findings can be summarised as follows. The finite in-plane magnetic field $B_{\parallel}$ shifts the bottom of the IX dispersion from the zero point of the reciprocal space. The IXs dispersion at a finite $B_{\parallel}$ then takes the approximative form of:

$$E_{IX}(P_x, P_y) = E_{\text{rest}} + \frac{P_y^2}{2M} + \frac{(P_x - eB_{\parallel}\Delta)^2}{2M}, \tag{5.1}$$

where P_x and P_y are the in-plane components of the IX momentum, E_{rest} denotes the energy of IX at rest and M is the IX mass. The orientation of the in-plane magnetic field along the y-axis as well as its gauge are again taken in accordance with Chapter 3. We see that the displacement of the dispersion parabola (5.1) is linear in the magnetic field $B_{\parallel}$ and also in the parameter Δ which represents the mean distance between an electron and a hole from which IX consists. A good estimation for Δ at a higher tilting of DQW is simply the centre-to-centre distance of the wells.

The described displacement of the IX dispersion can be interpreted as the $B_{\parallel}$-induced transition from a direct-band-gap semiconductor to an indirect-band-gap one. The optical response of this system is in some features similar to that of the well-known semiconductors with an indirect band gap such as silicon, germanium or diamond. The optically excited excitons relax to the states close to the dispersion minimum at the finite momentum $\mathbf{P} = (eB_{\parallel}\Delta, 0, 0)$, i.e. to states that are optically inactive, since only excitons with nearly zero momentum $\mathbf{P} \approx \mathbf{0}$ can undergo a direct optical recombination. The slight relaxation of the momentum conservation appears due to the finite photon momentum and thus the recombination of excitons is allowed within the photon cone, as schematically depicted in

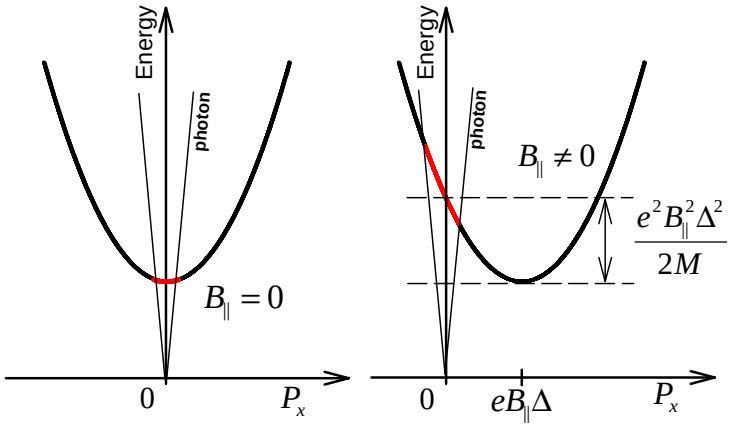

Figure 5.1: A schematically depicted shift of the IX dispersion parabola with the in-plane magnetic field $B_\parallel$. Owing to the momentum conservation, the optical recombination of IXs is allowed within the small red-coloured interval of momenta, see the text.

Fig. 5.1.[1] The main advantage to the standard materials with an indirect band gap is the smooth transition between the direct and indirect band gap controlled by $B_\parallel$. In this respect, Chang and Peeters [62] used the term "dispersion engineering" and referred to the IX states at finite $B_\parallel$ as "dark excitons". To avoid confusion, this term is also used for exciton states with spin $J_z = \pm 2$. However, the recombination of these excitons is not allowed due to the conservation of their angular momenta, i.e. for different reasons than for IXs at $B_\parallel$.

The possibility of the "dispersion engineering" mentioned above gave rise to the idea of a phonon laser, i.e. to the idea of a coherent source of phonons. This concept of the so-called "saser" was introduced and further investigated by Lozovik *et al.* [64, 65]. They suggested making use of the $B_\parallel$-induced displacement of the IX dispersion to prepare the phonon laser at a chosen energy of (acoustic) phonons. The stimulated emission of phonons is assumed to occur when the IX and DX energies differ just by the energy of a given acoustic phonon. The energy of sasers would be controlled by $B_\parallel$.

Now we describe a simple model of IX PL in the in-plane magnetic field $B_\parallel$ suggested by Parlangeli *et al.* [66]. They considered the IX dispersion in the simple parabolic form of (5.1) and supposed the Boltzmann statistics of the IX gas. Taking both assumptions into account, the occupation probability of the optically active states and thus also the corresponding PL intensity decreases as a gaussian function of $B_\parallel$:

$$I = I_0 \exp\left(-\frac{e^2\Delta^2 B_\parallel^2}{2Mk_BT}\right), \tag{5.2}$$

where all the symbols have their usual meaning. Simultaneously, the energy of PL line should increase quadratically with $B_\parallel$ by amount of $e^2\Delta^2 B_\parallel^2/2M$, cf. Fig. 5.1.

To find a simple interpretation of the proposed damping, we can take a simple picture of very weakly bound IX states. The electron and hole forming the IX state can then be

[1] For extended discussion about the exciton linewidth in 2D quantum structures see e.g. Feldmann *et al.* [63].

treated almost separately and their momenta become good quantum numbers. Optically excited electrons and holes quickly relax to the bottom of their subbands and create these loosely bound IXs. However, as electrons and holes are localised in opposite QWs, the minima of the corresponding subbands are mutually shifted in the reciprocal space by $eB_{\parallel}\Delta/\hbar$. Since only vertical transitions are allowed within the electric-dipole approximation, the radiative recombination of such excitons becomes very weak. The only signal we get from carriers thermally excited to states with higher energies, which explains the blueshift of the IX peak.

Parlangeli *et al.* applied the simple model of the Gaussian damping to explain their previously published data [67] and an impressive agreement was achieved. They observed with increasing $B_{\parallel}$ the quadratic increase of the IX recombination energy and also the damping of IX PL peak just according to the relation (5.2). However, the agreement with theory especially concerning the PL line damping is limited to a specific type of samples, in our opinion, and we will argue why in the following paragraphs.

The suggested model implicitly assumes a constant density of the IXs gas. This density is in an optically pumped system governed by the generation rate and by the exciton lifetime τ which combines both the radiative and non-radiative lifetimes: $\tau^{-1} = \tau_r^{-1} + \tau_n^{-1}$. Since the radiative lifetime τ_r is supposed to rise strongly with $B_{\parallel}$, a nearly constant exciton density can be maintained only when the non-radiative recombination channels dominate in the recombination process and simultaneously the condition $\tau_n \neq \tau_n(B_{\parallel})$ is fulfilled. Obviously, these very specific conditions can hardly be satisfied in DQW structures in general.

The results published by Parlangeli *et al.* [66] should be compared with those achieved by Butov *et al.* [68] who studied the kinetics of IX PL at a finite $B_{\parallel}$. A clear damping of the IX PL line is visible in their time-integrated PL spectra, but this damping was significantly slower with $B_{\parallel}$ than in [66], although the ratio Δ^2/T was higher in their sample. These data offer a nice demonstration of the limited validity of Parlangeli's model. Both experiments clearly showed the expected quadratic course of IX PL energy. However, very different exciton mass M was deduced in both papers. Whilst the mass $M = 0.42m_0$ was found in [66], the quadratic shift in [68] corresponds to $M = 0.21m_0$. The results of Butov's group were further confirmed in their following work [69], where the exciton mass as a function of $B_{\perp}$ was investigated using the in-plane component $B_{\parallel}$ for scanning of the IX dispersion. At $B_{\perp} = 0$ they obtained the IX mass $M = 0.22m_0$. The huge difference in results of both groups remains unexplained.

The behaviour of IX PL at a finite $B_{\parallel}$ has been investigated also by our group and we have carried out several experiments on different types of samples. In our opinion, the most important results are summarised in [34, 70, 71]. The former two papers are enclosed in Appendices C and D. The published experiment was performed on the sample TP313, which is described in Chapter 7 in detail. This sample contains three different symmetric DQWs placed in the intrinsic region of a *p-i-n* structure. The DQWs can be biased applying an appropriate bias U_{pn}.

We briefly summarise results of our experiments: The investigated DQWs in the sample TP313 were characterised by a very low non-radiative recombination rate in comparison with the radiative one and the PL signal of IXs clearly survived up to high magnetic fields $B_{\parallel}$ contrary to [66, 67]. The total PL intensity of IXs remained unchanged or slightly decreased, but no gaussian damping was found. The energy of the IX transition

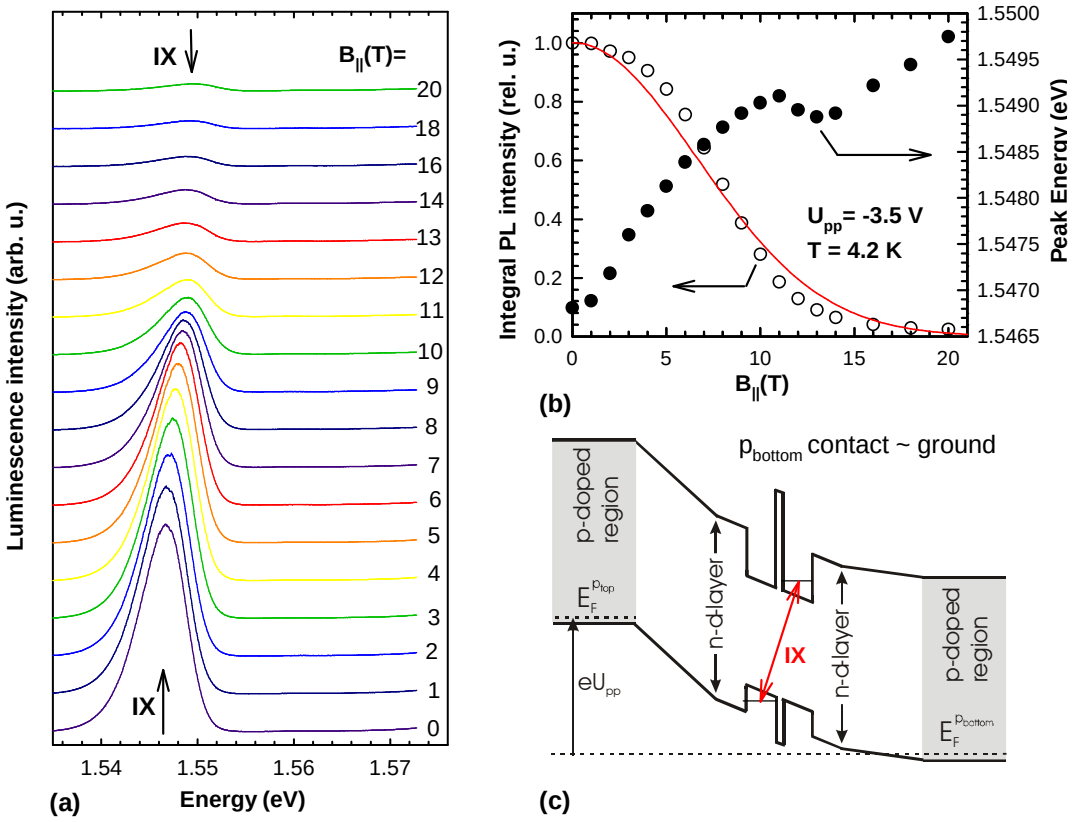

Figure 5.2: (a) PL spectra from sample TP811 at $U_{pp} = -3.5$ V and $T = 4.2$ K as a function of $B_{\|}$. The corresponding peak energies and integral intensities are depicted in the part (b). The red curve represents the fit of the intensity damping according to relation (5.2). The part (c) shows the schematic band structure of sample TP811 under experimental conditions. Lengths are not in scale.

underwent a blueshift with $B_{\|}$, but this could not be simply assigned to the quadratic shift observed by Parlangeli's and Butov's group. Our sample appears to be of the quality comparable to those studied by other groups, as follows e.g. from the comparison of FWHMs of corresponding peaks. The discussion of the achieved results led us to the conclusion that we actually observed PL of localised indirect excitons. This localisation is probably supported by a very high non-radiative recombination time τ_n. The localised IXs states were clearly identified in the dependence of PL spectra on the excitation power, see [34].

Other (until now unpublished) results are presented in Fig. 5.2. These spectra were measured on the sample TP811, when a high U_{pp} bias was applied and the electrical contact to the quantum well (n-doped) region remained disconnected, see Fig. 5.2c. The electron density in this strongly tilted DQW can be estimated to $n^{(2)} < 10^{11}$ cm^{-2}, see [37] in Appendix B, and therefore an excitonic-like PL is observed. The IX peak intensity clearly declines nearly following the gaussian function of $B_{\|}$, but the increase of the IX line energy is not quadratic which is again in contradiction to the simple model of Parlangeli's group. For the sake of completeness, the PL damping in Fig. 5.2b was fitted according to

the gaussian course (5.2), even though this simple model is hardly acceptable for analysis of these data. As a result, we obtained the product $(M/m_0).T \doteq 6.7$ K. Since high cooling rates of IXs were reported several times, see e.g. [23], we cannot assume the temperature of the IX gas significantly above 10 K. Therefore, we might expect that the exciton effective mass can achieve rather high value, similar to the mass determined by group of Parlangeli. Nevertheless, the model of the Gaussian damping is inadequate and thus no meaningful value of M can be attained. These results are mentioned just to emphasise the strong dependence of IX PL on specific parameters of samples including the exciton density, the presence of shallow and deep localisation and/or recombination centres etc.

In conclusion, we have demonstrated in [34, 70, 71] that the damping of the IX PL line as well as the quadratic increase of its energy with $B_{\parallel}$ are not general effects. Instead, the performed experiments revealed distinctively different behaviour of the IX line with increasing $B_{\parallel}$ in investigated samples. This effect can be explained by different ratio of radiative to non-radiative recombination rates in the individual samples. In the sample TP313, the very long non-radiative recombination lifetime indirectly leads to the optical recombination of IXs via weakly localised states, which was observed even in high in-plane magnetic fields [70]. The mechanism of this IX localisation requires further investigation. The samples with a reduced non-radiative recombination rate are potentially more suitable to prepare the saser, proposed by Lozovik *et al.* (see above), as such samples allow of an accumulation of IXs in DQWs, which would enhance the phonon emission. The increase of the IX lifetime could be also important for the potential BEC in the IX gas discussed in Chapter 2. The samples with the low non-radiative recombination rate might be used to achieve higher IX density and consequently a higher critical temperature of BEC.

Chapter 6

Superlattice in in-plane magnetic fields as a source of terahertz radiation

In this chapter we describe a simple concept of terahertz oscillations in superlattices (SLs) that are apparently different from standard Bloch oscillations (BOs) currently studied in such structures. The new type of THz oscillations are induced when crossed magnetic and electric fields are applied to SL in the in-plane directions and their frequency and amplitude are tunable by both these fields. The reader could be slightly astonished by a sudden jump from DQW to SL structures, but we only naturally extend our discussion of the properties of DQWs at non-zero $B_{\parallel}$ to an infinite periodic system. Therefore, this topic is very closely linked to the previous chapters, in our opinion.

The concept of SL structures was introduced by Esaki and Tsu in their famous paper [72]. In spite of its revolutionary impacts on the contemporary semiconductor physics, the basic idea was actually very simple. They suggested an artificially created structure with a spatial period Δ significantly larger than is the typical lattice constant in crystals. Such structures can be prepared e.g. by the periodic alternation of semiconductor materials of different band gap energies or by the periodic doping. The reason to enhance strongly the lattice constant was apparent. Esaki and Tsu tried to decrease the size of the Brillouin zone $2\pi/\Delta$ and reduce thus the time needed by an electron to fly through it, when a dc electric field is applied. They expected that this time can be shorter in the suggested structures than the characteristic scattering times of electrons, and opened thus a way to the experimental evidence of Bloch oscillations (BOs) proposed by Zener in 1930s, see [73]. Nowadays, the experimental evidence for BOs in SLs has been found several times, see e.g. [74, 75, 76]. Note that BOs have recently been achieved also in atomic [77] and photonic [78] systems.

Let us now recall some basic features of BOs in SLs. Having the z-axis oriented along the SL growth direction, we get the electron dispersion periodic in the momentum k_z, $E(k_z) = E(k_z + 2\pi/\Delta)$. The electron motion in this system can be described by the quasi-classical equation $\hbar\dot{k}_z = eF_z$. The frequency of BOs is then simply obtained, $\omega_{BO} = |e|F_z\Delta/\hbar$. To get experimentally detectable BOs, appropriate values of F_z and Δ have to be taken to achieve BO period $2\pi/\omega_{BO}$ significantly shorter than are typical electron scattering times in semiconductors. The frequency ω_{BO} then lies in the terahertz region and BOs in SLs are therefore considered as a promising source of coherent THz

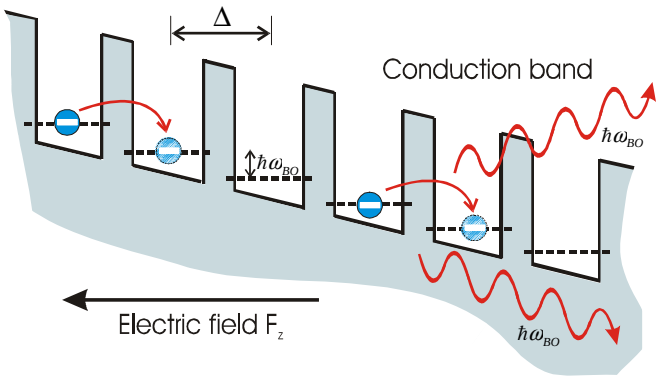

Figure 6.1: A schematic picture of the Wannier-Stark ladder in a strongly tilted SL discussed in the framework of standard BOs.

radiation. Note that in a fully quantum mechanical description, the Bloch oscillations correspond to electron transitions between stationary states[1] equidistantly arranged into the so-called Wannier-Stark ladder [80], see Fig. 6.1.

Let us compare these well-known BOs with another type of oscillations that can be induced in SLs when crossed dc electric and magnetic fields are applied, both in the in-plane direction, see Fig. 6.2. We confine ourselves just to the comparison, since a proper description of these novel oscillations is available on the preprint server [46], see Appendix E. Note that this in-plane orientation of the magnetic field in SLs appears rather rarely in the literature, but still several interesting papers can be found, see e.g. Goncharuk *et al.* [47], Wang and Cao [81] or Miller and Laikhtman [82].

The influence of $B_\parallel$ on SL can be understood on the basis of the Hamiltonian (3.1). When the periodic potential of SL is assumed, $V(z) = V(z + \Delta)$, the Hamiltonian (3.1) becomes invariant under simultaneous transformations $z \to z - \Delta$ and $k_x \to k_x + K_0$, where $K_0 = eB_\parallel \Delta/\hbar$. As the shift of the coordinate itself cannot change the energy spectrum of the system, the electron dispersion generally becomes K_0-periodic. Hence, solving the eigenvalue problem we obtain the energy spectrum in the form of minibands $E_i(k_x) = E_i(k_x + K_0)$, $i = 1, 2, 3 \ldots$ In [46], we took only the lowest lying subband $E_1(k_x) \equiv E(k_x)$ into account. The period K_0 of these minibands is tunable by $B_\parallel$ in contrast to the fixed period $2\pi/\Delta$ of the standard periodic dispersion $E(k_z)$ in SL at $B_\parallel = 0$. For the sake of completeness, when the Hamiltonian (3.1) is directly solved for a given value of k_x we get the electron wave functions each localised mostly in one QW and the momentum has to be taken from the interval $k_x \in (-\infty, +\infty)$. When we look for the electron eigenstates with respect to the periodicity of SL in the z-direction we can reduce our considerations to momenta in the interval $k_x \in (-K_0/2, K_0/2)$. Apparently, each state with given k_x then becomes infinitely degenerate. Both extended or reduced schemes are fully equivalent.

Since the miniband profiles cannot be simply guessed directly from the Hamiltonian (3.1), we have utilised the simple TB approximation in [46], which is sketched in Chapter 3, to get some numerically calculated curves. We obtained the results analogous to

[1] More accurately, quasi-stationary states or resonances, when the influence of other bands is taken into account, see e.g. [79] and references therein.

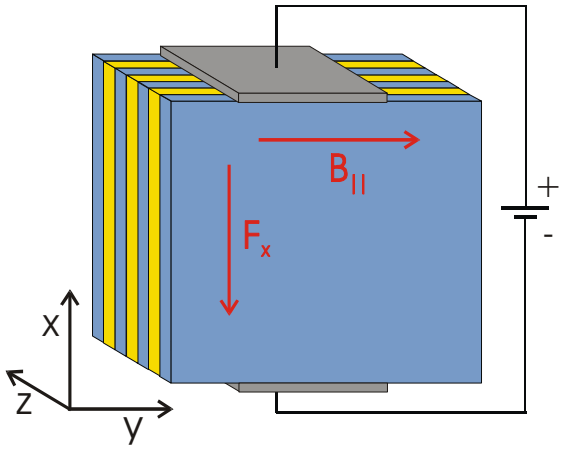

Figure 6.2: A schematic picture of a SL structure in crossed electric and magnetic fields, both applied in the in-plane directions. This configuration corresponds to the situation considered in the text and in [46] as well.

those in [47]. For an illustrative purpose, we show dispersion curves for the three lowest lying minibands at $B_{\parallel} = 10$ T, see Fig. 6.3. The parameters of SL chosen for this calculation correspond to the GaAs/GaAlAs system. Additionally, the velocity of the electron in the lowest subband depicted in the lower part of the figure was calculated using $v_x = \hbar^{-1} dE(k_x)/dk_x$. We clearly see that the calculated $E(k_x)$ strongly differs from the well-known cosine profile that is obtained for $E(k_z)$ within the standard TB model. A notice should can be also addressed to the miniband widths for $E(k_z)$ and $E(k_x)$. Whereas the width of the former one is fixed by the tunnelling rate between adjacent wells and within the TB model is equal to $4|t|$, the latter one can be continuously tuned by $B_{\parallel}$. For $E(k_x)$, the width E_0 can be within the TB approximation estimated to $E_0 \approx \hbar^2 (K_0/2)^2/(2m) = e^2 B_{\parallel}^2 \Delta^2/8m$ as explained in [46].

A striking difference between standard miniband profiles $E(k_z)$ and $E(k_x)$ arises when a finite number of wells in SL is assumed. The standard periodic miniband profile $E(k_z)$ is only formed when SL contains so many wells that discrete energy levels in this system of coupled QWs can be described as a quasi-continuum of states. The condition of many wells is not necessary, when $E(k_x)$ is taken at finite $B_{\parallel}$. The profile $E(k_x)$ becomes partly periodic when only few QWs are taken into account. The number of minima in the profile $E(k_x)$ simply corresponds to the number of wells in SL. In the very extreme case, when the number of wells in SL is reduced to two, i.e. a symmetric DQW is considered, we get the dispersion $E(k_x)$ with two minima as investigated in Chapters 3 and 4.

Having discussed the miniband profile $E(k_x)$, we can now apply a dc electric field F_x oriented in the x-direction. Similar to standard BOs, the quasi-classical equation of motion $\hbar \dot{k}_x = eF_x$ can be used to describe the time evolution of the electron state. Note that this method is applicable only when the electric-field-induced (Zenner-like) tunneling to the other minibands is negligibly small [79]. This condition leads to the requirement of a sufficiently strong coupling of wells in SL, which is expressed in the TB model by the parameter t. The high value of $|t|$ leads to better separation of individual minibands, see the upper part of Fig. 6.3. Taking account of the Brillouin zone size K_0, the oscillatory

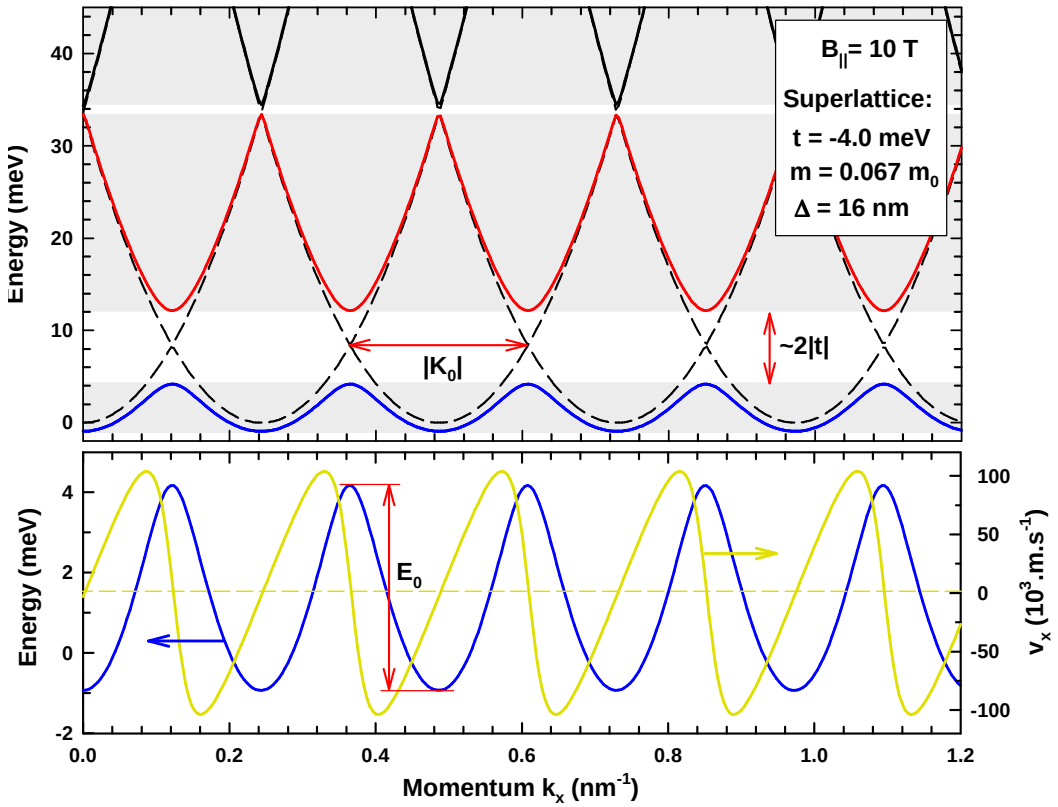

Figure 6.3: Upper part: The electron dispersion $E(k_x)$ curves for three lowest lying subbands calculated within the TB approximation at $B_\parallel = 10$ T for parameters of SL specified in the inset. Individual minibands are distinguished by colors. The dashed lines show the band structure in the limit of fully isolated QWs, i.e. $t = 0$. Note that the energy gap between lowest two minibands is roughly equal $2|t|$. Lower part: Dispersion curve of the lowest subband (blue curve) with the corresponding electron velocity $v_x = \hbar^{-1} dE(k_x)/dk_x$ (yellow curve).

frequency is easy to be obtained, $\omega_{B_\parallel} = 2\pi F_x/(B_\parallel \Delta)$. This frequency is tunable by $B_\parallel$ and not only by the electric field as in the case of ω_{BO}. Hence, we can independently set the frequency and the amplitude of these oscillations $x_0 = E_0/(2|e|F_x)$. Explicitly, the constant ratio $F_x/B_\parallel$ fixes the frequency $\omega_{B_\parallel}$ and a further change in $B_\parallel$ allows a variation in the amplitude of oscillations $x_0 \propto B_\parallel/\omega_{B_\parallel}$. The independent tuning of the frequency and amplitude can be useful for maximising of the total emitted power. Note that just the low emitted power due to a weak coupling of the oscillating electrons to the electromagnetic field is one of the problems encountered in the study of BOs, see Leo [83].

It is interesting to investigate also the direction characteristics of the expected radiation. Since the radiation is generated by the electron oscillatory motion in the x-direction, the radiation should be emitted mainly in the plane perpendicular to the x-axis, i.e. in the plane perpendicular to the oscillating dipoles. Hence, whereas terahertz emitters based on BOs are essentially edge-emitting, the suggested device working with $B_\parallel$-controlled oscillations could emit both from the surface and the edge.

The expected $B_\parallel$-controlled oscillations have one special feature – the oscillatory mo-

tion in the x-direction is accompanied by a steady shift in the z-direction as discussed in detail in [46]. Hence, each (e.g. optically generated) electron undergoes the oscillatory motion until it achieves the last well in SL and is subsequently removed into the electrical contact. The number of oscillation periods thus cannot exceed the number of wells in SL. The number of wells in SL thus limits the width of the generated terahertz pulse. In addition, electrons do not remain in SL much longer than is necessary for their coherent motion. This is not true for electrons exhibiting common BOs which survive in SL until they recombine either in radiative or non-radiative way. This recombination time usually significantly exceeds scattering (and also dephasing) times that are typical for electrons in semiconductor systems.

The application of the in-plane electric field needs to be discussed closely, since this was omitted in [46] for the sake of brevity. To apply such a field, the lateral size of the mesa structure cannot exceed several microns, because the field could be effectively screened inside SL due to free holes originating in inevitable residual acceptors. The required mesa size probably represents a limit for applicability of the standard optical lithography, but also other lithography techniques could be used.

A final note should be added to verify the use of the quasi-classical approach in our considerations. This intuitive way is satisfactory for a qualitative discussion of BOs, but a fully quantum-mechanical model has to be established if quantitatively correct results are needed. The quasi-classical study of the momentum time evolution is then replaced by considerations based on the Wannier-Stark ladder. The completely equivalent problem is encountered in the case of $B_{\parallel}$-controlled oscillations as well. We can work with a quasi-classical model as far as only the qualitative properties are important and a proper quantum theory has to be applied to get the accurate quantitative results.

Chapter 7

Experimental details

7.1 Sample preparation

All experimental results presented in this thesis have been achieved on two different samples denoted as TP313 and TP811. Their names correspond to the scheme used at the Institute of Technical Physics I, University Erlangen-Nuremberg, where these samples were grown by the MBE and photolithographically processed as well. The results of the PL experiment performed on sample TP811 were published in [36, 37] and those measured on sample TP313 in [70, 34] , see Appendices A,B and C,D, respectively.

The MBE growth was performed at the temperature of 600°C on the n-doped (TP313) or semi-insulating (TP811) GaAs substrate oriented in the [001] direction. To avoid possible misunderstandings, we should note that Soubusta *et al.* [20] incorrectly declared a semi-insulating substrate in the same sample TP313 instead of the actual n-doped one. Obviously, this formal mistake has absolutely no influence on conclusions in [20]. The growth interruptions were used during the growth of both samples where appropriate. The samples were capped by a pure GaAs to evade degradation of upper GaAlAs layers. In all cases, n- and p-regions were doped by silicon and carbon, respectively.

The grown wafers were photolithographically processed in a standard way, i.e. the mesa structures were prepared by the wet chemical etching and selective electrical contacts were deposited. Contacts to p-regions were created by the sequence of metal layers Au/Zn/Au and the n-contacts contain metal layers in the following order Ge/Au/Ni/Au (Au on the top). After deposition, these contacts were alloyed at the temperature of 350°C in the nitrogen atmosphere to achieve their near-Ohmic properties. The conducting channels on the mesa surface were suppressed by an insulating polyimid layer. The prepared mesa structures had square-shaped excitation windows of the size ranging from 50×50 μm^2 up to 300×300 μm^2 covered by the SiO antireflection coating. The coating thickness of ≈ 85 nm was designed for the perpendicular incidence of the light emitted by the red He-Ne laser (633 nm). Standard electrical measurements of I-V characteristics were performed on all prepared mesa structures to select the most appropriate ones for the optical experiment. PL spectra obtained on different mesa structures from one wafer were almost identical. A typical mesa device used in our experiments is depicted in Fig. 7.1.

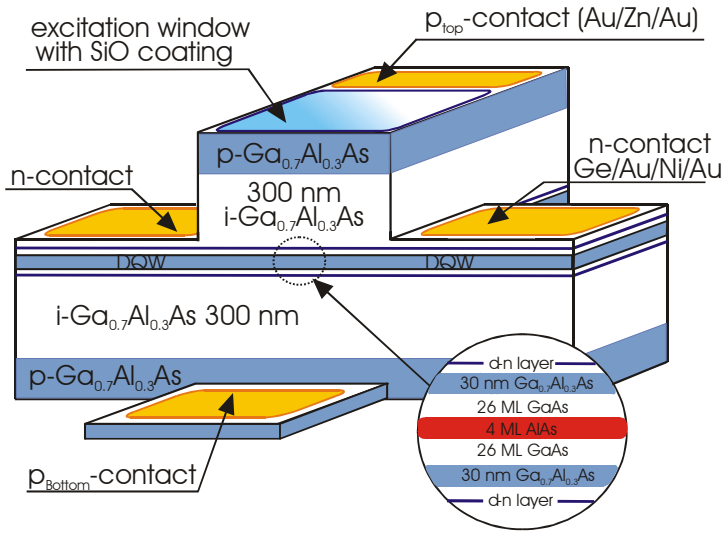

Figure 7.1: A typical mesa structure used in our PL experiment. In this case the device was photolithographically prepared from the wafer of sample TP811. The thicknesses of individual layers are not in scale.

7.2 Sample parameters

The schematic band structures of samples TP313 and TP811 on which our experiments were performed are plotted in Figs. 7.2a and 7.2b. The reader can consult Figs. 7.3a and 7.3b to get the concrete values of the thickness, the aluminium content and the doping level for the individual layers in both samples. All given parameters represent the intended values. Apparently, the actual parameters can be slightly different in real samples. In this respect, we suppose that the most critical parameter is the area density of the doping level in the δ-layers, see e.g. [36], where the experimental data suggest that the doping density is about 15% higher than originally intended.

The sample TP313 was designed for a study of direct and indirect excitons in DQWs. Therefore, three symmetric DQWs were inserted into an intrinsic region of a p-i-n junction.

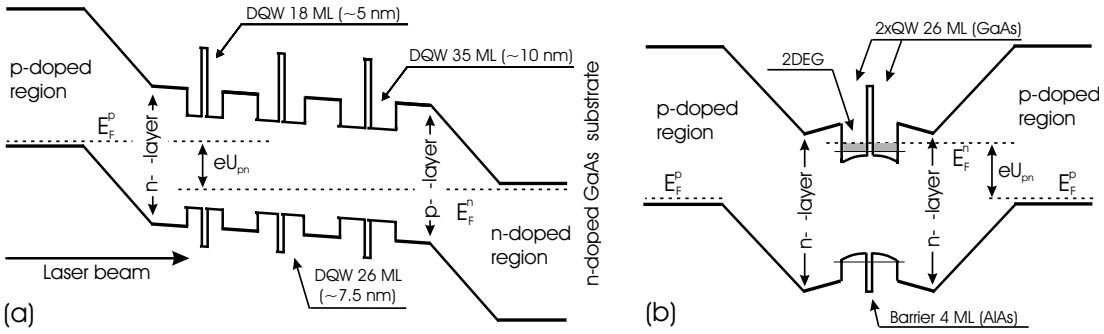

Figure 7.2: A schematic band structure of samples (a) TP313 and (b) TP811 under applied bias U_{pn}. Lengths are not in scale.

Figure 7.3: The MBE-grown sequence of layers for samples TP313 and TP811. The widths of layers are not in scale.

Each DQW consists of two identical GaAs QWs (18 ML, 26 ML and 35 ML) separated by a 4 ML wide AlAs barrier. The mutual independence of DQWs is ensured by a spacer 100 nm wide. Selective electric contacts to the upper p-doped and bottom n-doped regions allow the tilting of DQWs applying a bias U_{pn}. Additional δ-p and δ-n doped layers were introduced to compensate for the built-in electric field in the middle part of the intrinsic region and to achieve thus the flat band position around DQWs at a nearly zero bias U_{pn}. The carrier densities in all DQWs are in dark negligible in this sample.

The second sample TP811 is a p-i-δn-DQW-δn-i-p structure with relatively weakly doped δ-n layers placed symmetrically around DQW. The modulation of the band structure caused by this doping is insufficient to supply 2DEG into the DQW in dark, instead the Fermi level lies deep in the band gap of GaAs. The electron density in the DQW can be tuned by the applied bias from a nearly zero at $U_{pn} = U_{pp} = 0$ up to the density $\approx 3.5 \times 10^{11}$ cm^{-2} at $U_{pn} = +1.8$ V and $U_{pp} = 0$, which approximatively corresponds to the total doping of both δ-n layers. An additional variation in the bias U_{pp} introduces an asymmetry into the DQW, but this asymmetry cannot be set independently of the electron density in a wide interval of U_{pp}. For deeper discussion see [36] and [37] in Ap-

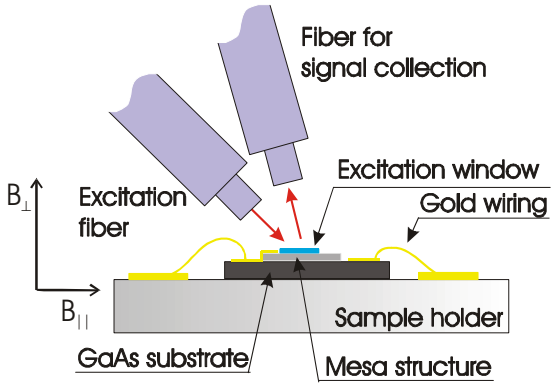

Figure 7.4: The schematic view of the experimental setup including a wired mesa structure.

pendices A and B, respectively. Note that both GaAs/$Ga_{0.7}Al_{0.3}As$ heterojuctions in this sample were smoothed by 1 ML of pure AlAs. However, this layer cannot be treated as an unbroken one, instead it only contributes to the sharpness of the heterojunctions.

7.3 Experimental setup

All results presented in this thesis were measured in Grenoble High Magnetic Field Laboratory, CNRS. The sample was excited by a Ti:sapphire laser at the photon energy 1.72 or 1.75 eV (720 or 710 nm), i.e. below the band gap of $Ga_{0.7}Al_{0.3}As$ at the liquid helium temperature. If not specified, the laser had a standard power density $I_0 \approx 100$ mW/cm^2. Two optical fibers were used, one for the sample excitation and the second for the signal collection, as schematically depicted in Fig. 7.4. These fibers did not conserve the polarisation of the excitation beam or signal. The PL signal was dispersed in a single- or double-grating monochromator and detected by a cooled charge coupled camera in both cases. The helium bath cryostat, where the sample was immersed into the helium liquid, ensured a good stability of the sample temperature at 4.2 K or optionally at ≈ 2 K. All measurements were performed in a resistive solenoid up to the magnetic field of 22 T. The sample holder allowed measurements in the configuration with magnetic field oriented in the DQW plane ($B_{\|}$) or perpendicular to this plane ($B_{\perp}$). The important point is certainly the accuracy of the sample orientation with respect to the magnetic field. We estimate that the misalignment is better than 5°. We have performed repeated measurements for each experimental configuration and achieved almost equivalent results, even though in each case a different mesa structure was mounted to the holder providing thus a different misalignment. Therefore, we suppose that the unintended component of the magnetic field does not negatively affect the obtained results.

References

[1] H. Kawai, I. Hase, K. Kaneko, and N. Watanebe, J. Crystal Growth **68**, 406 (1984).

[2] H. Kawai, J. Kaneko, and N. Watanebe, J. Appl. Phys. **58**, 1263 (1985).

[3] A. Yariv, C. Lindsey, and U. Sivan, J. Appl. Phys. **58**, 3669 (1985).

[4] E. J. Austin and M. Jaros, J. Phys. C **19**, 533 (1986).

[5] L. Kappei, J. Szczytko, F. Morier-Genoud, and B. Deveaud, Phys. Rev. Lett. **94**, 147403 (2005).

[6] S. B.-T. de Leon and B. Laikhtman, Phys. Rev. B **67**, 235315 (2003).

[7] J. P. Eisenstein and A. H. MacDonald, Nature **432**, 691 (2004).

[8] M. Kellogg, J. P. Eisenstein, L. N. Pfeiffer, and K. W. West, Phys. Rev. Lett. **93**, 036801 (2004).

[9] R. D. Wiersma, J. G. S. Lok, S. Kraus, W. Dietsche, K. von Klitzing, D. Schuh, M. Bichler, H.-P. Tranitz, and W. Wegscheider, Phys. Rev. Lett. **93**, 266805 (2004).

[10] M. Kellogg, J. P. Eisenstein, L. N. Pfeiffer, and K. W. West, Phys. Rev. Lett. **90**, 246801 (2003).

[11] K. Kheng, R. T. Cox, Y. M. d'Aubigné, F. Bassani, K. Saminadayar, and S. Tatarenko, Phys. Rev. Lett. **71**, 1752 (1993).

[12] R. J. Warburton, C. Schäflein, D. Haft, F. Bickel, A. Lorke, K. Karrai, J. M. Garcia, W. Schoenfeld, and P. M. Petroff, Nature **405**, 926 (2000).

[13] A. J. Shields, J. L. Osborne, D. M. Whittaker, M. Y. Simmons, M. Pepper, and D. A. Ritchie, Phys. Rev. B **55**, 1318 (1997).

[14] V. B. Timofeev, A. V. Larionov, M. G. Alessi, M. Capizzi, A. Frova, and J. M. Hvam, Phys. Rev. B **60**, 8897 (1999).

[15] M. Zvára, R. Grill, P. Hlídek, M. Orlita, and J. Soubusta, Physica E **12**, 335 (2002).

[16] X. G. Peralta, S. J. Allen, M. C. Wanke, N. E. Harff, J. A. Simmons, M. P. Lilly, J. L. Reno, P. J. Burke, and J. P. Eisenstein, Appl. Phys. Lett. **81**, 1627 (2002).

[17] Y. J. Chen, E. S. Koteles, B. S. Elman, and C. A. Armiento, Phys. Rev. B **36**, 4562 (1987).

[18] J. W. Little and R. P. Leavitt, Phys. Rev. B **39**, 1365 (1989).

[19] T. Westgaard, Q. X. Zhao, B. O. Fimland, K. Johannessen, and L. Johnsen, Phys. Rev. B **45**, 1784 (1992).

[20] J. Soubusta, R. Grill, P. Hlídek, M. Zvára, L. Smrčka, S. Malzer, W. Geißelbrecht, and G. H. Döhler, Phys. Rev. B **60**, 7740 (1999).

[21] L. V. Butov, A. Imamoglu, A. V. Mintsev, K. L. Campman, and A. C. Gossard, Phys. Rev. B **59**, 1625 (1999).

[22] L. V. Butov, C. W. Lai, A. L. Ivanov, A. C. Gossard, and D. S. Chemla, Nature **417**, 47 (2002).

[23] L. V. Butov, A. C. Gossard, and D. S. Chemla, Nature **418**, 751 (2002).

[24] D. Snoke, J. P. Wolfe, and A. Mysyrowicz, Phys. Rev. Lett. **59**, 827 (1987).

[25] A. V. Larionov, V. B. Timofeev, J. Hvam, and C. Soerensen, JETP Letters **71**, 117 (2000).

[26] L. V. Butov and A. I. Filin, Phys. Rev. B **58**, 1980 (1998).

[27] V. V. Krivolapchuk, E. S. Moskalenko, and A. L. Zhmodikov, Phys. Rev. B **64**, 045313 (2001).

[28] D. Snoke, S. Denev, Y. Liu, L. Pfeiffer, and K. West, Nature **418**, 754 (2002).

[29] L. V. Butov, L. S. Levitov, A. V. Mintsev, B. D. Simons, A. C. Gossard, and D. S. Chemla, Phys. Rev. Lett. **92**, 117404 (2004).

[30] R. Rapaport, G. Chen, D. Snoke, S. H. Simon, L. Pfeiffer, K. West, Y. Liu, and S. Denev, Phys. Rev. Lett. **92**, 117405 (2004).

[31] A. Gärtner, D. Schuh, and J. P. Kotthaus, Physica E , in press (2006).

[32] Z. Vörös, R. Balili, D. W. Snoke, L. Pfeiffer, and K. West, Phys. Rev. Lett. **94**, 226401 (2005).

[33] C. W. Lai, J. Zoch, A. C. Gossard, and D. S. Chemla, Science **303**, 503 (2004).

[34] M. Orlita, R. Grill, M. Zvára, G. H. Döhler, S. Malzer, M. Byszewski, and J. Soubusta, Physica E **30**, 1 (2005).

[35] V. Negoita, D. W. Snoke, and K. Eberl, Phys. Rev. B **61**, 2779 (1999).

[36] M. Orlita, R. Grill, P. Hlídek, M. Zvára, G. H. Döhler, S. Malzer, and M. Byszewski, Phys. Rev. B **72**, 165314 (2005).

[37] M. Orlita, M. Byszewski, G. H. Döhler, R. Grill, P. Hlídek, S. Malzer, and M. Zvára, Physica E , in press (2006).

[38] J. H. Davies, *The Physics of Low-Dimensional Semiconductors: An Introduction*, Cambridge University Press, 1997.

[39] L. Smrčka and T. Jungwirth, J. Phys.: Cond. Mat. **7**, 3721 (1995).

[40] D. Huang and S. K. Lyo, Phys. Rev. B **59**, 7600 (1999).

[41] J. Hu and A. H. MacDonald, Phys. Rev. B **46**, 12554 (1992).

[42] S. K. Lyo, Phys. Rev. B **50**, 4965 (1994).

[43] S. K. Lyo, Phys. Rev. B **51**, 11160 (1995).

[44] J. Soubusta, *Optical properties of double quantum well in electric and magnetic fields*, PhD thesis, Charles University in Prague, 1999.

[45] M. Orlita, R. Grill, and M. Zvára, in *Week of Doctoral Students - Proceedings*, edited by J. Šafránková, p. 618, Matfyzpress, 2003.

[46] M. Orlita, R. Grill, L. Smrčka, and M. Zvára, cond-mat/0601446 (2006).

[47] N. A. Goncharuk, L. Smrčka, J. Kučera, and K. Výborný, Phys. Rev. B **71**, 195318 (2005).

[48] G. M. G. Oliveira, V. M. S. Gomes, A. S. Chaves, J. R. Leite, and J. M. Worlock, Phys. Rev. B **35**, 2896 (1987).

[49] G. S. Boebinger, A. Passner, L. N. Pfeiffer, and K. W. West, Phys. Rev. B **43**, 12673 (1991).

[50] J. P. Eisenstein, T. J. Gramila, L. N. Pfeiffer, and K. W. West, Phys. Rev. B **44**, 6511 (1991).

[51] L. Zheng and A. H. MacDonald, Phys. Rev. B **47**, 10619 (1993).

[52] J. A. Simmons, S. K. Lyo, N. E. Harff, and J. F. Klem, Phys. Rev. Lett. **73**, 2256 (1994).

[53] L. Smrčka, P. Vašek, J. Koláček, T. Jungwirth, and M. Cukr, Phys. Rev. B **51**, 18011 (1995).

[54] T. Jungwirth, T. S. Lay, L. Smrčka, and M. Shayegan, Phys. Rev. B **56**, 1029 (1997).

[55] M. A. Blount, J. A. Simmons, and S. K. Lyo, Phys. Rev. B **57**, 14882 (1998).

[56] O. N. Makarovskii, L. Smrčka, P. Vašek, T. Jungwirth, M. Cukr, and L. Jansen, Phys. Rev. B **62**, 10908 (2000).

[57] D. M. Whittaker, T. A. Fisher, P. E. Simmonds, M. S. Skolnick, and R. S. Smith, Phys. Rev. Lett. **67**, 887 (1991).

[58] D. Huang and S. K. Lyo, J. Appl. Phys. **83**, 4531 (1998).

[59] H. Kissel, U. Zeimer, A. Maassdorf, M. Weyers, R. Heitz, D. Bimberg, Y. I. Mazur, G. G. Tarasov, V. P. Kunets, U. Muller, Z. Y. Zhuchenko, and W. T. Masselink, Phys. Rev. B **65**, 235320 (2002).

[60] Y. Kim, C. H. Perry, J. A. Simmons, and F. Klem, Appl. Phys. Lett. **77**, 388 (2000).

[61] A. A. Gorbatsevich and I. V. Tokatly, Semicond. Sci. Technol. **13**, 288 (1998).

[62] K. Chang and F. M. Peeters, Phys. Rev. B **63**, 153307 (2001).

[63] J. Feldmann, G. Peter, E. O. Göbel, P. Dawson, K. Moore, C. Foxon, and R. J. Elliott, Phys. Rev. Lett. **59**, 2337 (1987).

[64] Y. E. Lozovik, S. P. Merkulova, and I. V. Ovchinnikov, Physics Letters A **282**, 407 (2001).

[65] Y. E. Lozovik and I. V. Ovchinnikov, Solid State Communications **118**, 251 (2001).

[66] A. Parlangeli, P. C. M. Christianen, J. C. Maan, I. V. Tokatly, C. B. Soerensen, and P. E. Lindelof, Phys. Rev. B **62**, 15323 (2000).

[67] A. Parlangeli, P. C. M. Christianen, J. C. Maan, C. B. Soerensen, and P. E. Lindelof, phys. status solidi (a) **178**, 45 (2000).

[68] L. V. Butov, A. V. Mintsev, Y. E. Lozovik, K. L. Campman, and A. C. Gossard, Phys. Rev. B **62**, 1548 (2000).

[69] L. V. Butov, C. W. Lai, D. S. Chemla, Y. E. Lozovik, K. L. Campman, and A. C. Gossard, Phys. Rev. Lett. **87**, 216804 (2001).

[70] M. Orlita, R. Grill, M. Zvára, G. H. Döhler, S. Malzer, M. Byszewski, and J. Soubusta, Phys. Rev. B **70**, 075309 (2004).

[71] M. Orlita, M. Byszewski, R. Grill, and M. Zvára, in *Week of Doctoral Students - Proceedings*, edited by J. Šafránková, p. 553, Matfyzpress, 2004.

[72] L. Esaki and R. Tsu, IBM J. Res. Dev. **14**, 61 (1970).

[73] C. Zener, Proc. R. Soc. London A **145**, 523 (1934).

[74] J. Feldmann, K. Leo, J. Shah, D. A. B. Miller, J. E. Cunningham, T. Meier, G. von Plessen, A. Schulze, P. Thomas, and S. Schmitt-Rink, Phys. Rev. B **46**, 7252 (1992).

[75] C. Waschke, H. G. Roskos, R. Schwedler, K. Leo, H. Kurz, and K. Köhler, Phys. Rev. Lett. **70**, 3319 (1993).

[76] R. Martini, G. Klose, H. G. Roskos, H. Kurz, H. T. Grahn, and R. Hey, Phys. Rev. B **54**, 14325 (1996).

[77] M. B. Dahan, E. Peik, J. Reichel, Y. Castin, and C. Salomon, Phys. Rev. Lett. **76**, 4508 (1996).

[78] R. Morandotti, U. Peschel, J. S. Aitchison, H. S. Eisenberg, and Y. Silberberg, Phys. Rev. Lett. **83**, 4756 (1999).

[79] V. Grecchi and A. Sacchetti, Phys. Rev. B **63**, 212303 (2001).

[80] G. H. Wannier, Phys. Rev. **117**, 432 (1960).

[81] C. Wang and J. C. Cao, Phys. Rev. B **72**, 045339 (2005).

[82] D. Miller and B. Laikhtman, Phys. Rev. B **52**, 12191 (1995).

[83] K. Leo, Semicond. Sci. Technol. **13**, 249 (1998).

Appendix A

Authors:	M. Orlita, R. Grill, P. Hlídek, M. Zvára, G. H. Döhler, S. Malzer, and M. Byszewski,
Title:	Luminescence of double quantum wells subject to in-plane magnetic fields
Journal:	Physical Review B
Volume:	72
Year:	2005
Article Number:	165314

Luminescence of double quantum wells subject to in-plane magnetic fields

M. Orlita,* R. Grill, P. Hlídek, and M. Zvára
Faculty of Mathematics and Physics, Charles University, Institute of Physics, Ke Karlovu 5, CZ-121 16 Prague 2, Czech Republic

G. H. Döhler and S. Malzer
Max-Planck-Research Group, Institute of Optics, Information and Photonics, Universität Erlangen-Nürnberg, D-91058 Erlangen, Germany

M. Byszewski
Grenoble High Magnetic Field Laboratory, Boîte Postale 166, F-38042 Grenoble Cedex 09, France
(Received 13 April 2005; revised manuscript received 19 August 2005; published 11 October 2005)

We report on photoluminescence (PL) measurements of a symmetric GaAs/AlGaAs double quantum well (DQW) in high magnetic fields. For this study, a selectively contacted p-δn–DQW–δn-p structure was chosen, allowing an independent tuning of the electron density in the DQW and thus a creation of a two-dimensional electron gas. Our attention was focused on phenomena in in-plane magnetic fields, where the field-induced depopulation of the antibonding subband observable in the PL spectra as a so-called N-type kink was predicted by Huang and Lyo (HL) [Phys. Rev. B **59**, 7600 (1999)]. Whereas the equivalent behavior has been observed several times in the electric transport measurements and a proper theoretical description has been found, to the best of our knowledge, no PL experiment in a direct comparison with the theoretical model developed by HL has ever been published. We carried out a self-consistent calculation based on their model and achieved a good agreement with our experimental results. Additionally, the influence of the excitonic interaction on the PL spectra, not taken into account by HL, is also discussed. This enables us to explain small deviations from the HL theory. The interpretation of the in-plane magnetic field measurements is supported by the experiment with the magnetic field in the perpendicular orientation that allows a sufficiently accurate estimation of the electron density in the DQW. Distinctive renormalization effects of DQW subbands at various electron densities are also observed and discussed.

DOI: 10.1103/PhysRevB.72.165314 PACS number(s): 78.67.De, 78.55.Cr, 73.21.Fg, 78.20.Ls

I. INTRODUCTION

Double quantum wells (DQW) have been attracting a great deal of attention owing to their challenging properties, particularly formation of spatially direct and indirect excitons and their possible condensation to a cold exciton gas at low temperatures.[1,2] While in the configuration with the magnetic field perpendicular to the quantum well (QW) plane a free in-plane motion of charge carriers is quantized into Landau levels, an in-plane magnetic field (parallel to the layers) changes the carrier energy dispersion in the QW plane in the direction perpendicular to the field. Since Lyo's theoretical prediction of a saddle point type van Hove singularity in the density of states of a DQW, induced by an in-plane magnetic field,[3] much effort has been devoted to confirm this prediction experimentally. Another simple bi-layer quantum structure, similar to DQW, can be created in a rather broad modulation-doped single quantum well by a sufficiently high parallel magnetic field.[4,5] The predicted singularity in the magnetic-field-dependent density of states was at first successfully confirmed on both types of bi-layer systems in electric transport measurements—a modulation of the in-plane electric conductance[6–8] and of the cyclotron mass[9] in the in-plane magnetic field was reported. Among latest results concerning these effects, we mention thermopower measurements on the DQW system performed by Fletscher *et al.*[10] They have measured a clear dependence of the thermopower on the applied in-plane magnetic field and supported the experimental results by a convincing theoretical description.

It has become a challenge to find a manifestation of phenomena predicted for the in-plane magnetic field also in optical experiments. The photoluminescence (PL) calculation of DQW in the in-plane magnetic field, neglecting excitonic interaction between electron and hole, was published by Huang and Lyo.[11] The PL investigation of a similar bi-layer system in the in-plane magnetic field was reported by Whittaker *et al.*,[12] where the one-side modulation doping of a wide QW ensured a large separation of electrons and holes due to the strong built-in electric field. The observed strong quadratic shift of the luminescence maximum with in-plane magnetic field was interpreted as a result of the field-induced indirect gap. Similar measurements on wide QWs and heterojunctions have very recently been carried out by Ashkinadze *et al.*[13] Other in-plane magneto-optical measurements, in this case already on symmetric DQW structures, were published by Kim and co-workers.[14,15] In a parallel field, they observed two resolved peaks and their shift to the higher energy with increasing magnetic field. The peaks were related to the recombination of electrons from an upper (antibonding) subband-created by an antisymmetric linear combination of wave functions of a single QW, and from a lower (bonding) subband formed by a symmetric combination of electron states of a single well. In accordance with theoretical predictions,[11] they observed a $\mathcal{N}$-type kink, i.e., a gradual depopulation of the electron and hole antibonding subband resulting in a redshift of the PL maximum followed by its

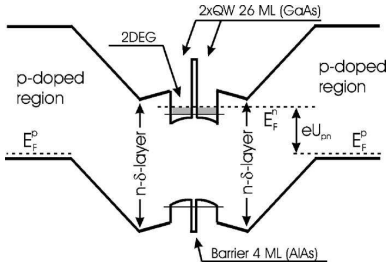

FIG. 1. The schematic picture of the studied sample under a typical operational condition $U_{pn}>0$. E_F^p and E_F^n denote Fermi level in p-doped regions and 2DEG, respectively. Lengths are not in scale.

blueshift, reflecting a diamagnetic increase of the bonding subband energy. However, no comparison with theoretically calculated spectra was performed.

In this paper, we present a study of PL from a symmetric DQW with various electron density in the magnetic field in perpendicular (Faraday), as well as in parallel (Voigt), orientation. The paper is organized as follows. In Sec. II a brief description of experiment and the studied sample is provided. The simple theory of phenomena in the in-plane magnetic field is summarized in Sec. III. Section IV concerns us with experimental results. These are compared with the suggested theory and the applicability of the used theoretical model is discussed with respect to the excitonic interaction, whose effects dominate the PL spectra at low carrier densities. Finally, the conclusions are given in Sec. V.

II. EXPERIMENT

Our magnetoluminescence measurements were carried out on a p-i-δn–DQW–δn-i-p structure grown by molecular beam epitaxy (MBE). A simple scheme of this structure under a typical operational condition is shown in Fig. 1. The symmetric DQW consists of two 26 ML, i.e., ≈7.5-nm-thick GaAs QWs with a 4 ML AlAs barrier in between. This DQW is separated from δ-n-doped layers by 30-nm-thick $Ga_{0.7}Al_{0.3}As$ spacers. Both $GaAs/Ga_{0.7}Al_{0.3}As$ interfaces in the DQW are smoothed by a 1 ML AlAs layer. The δ-n doping is realized by a 1-nm-thick n-doped $Ga_{0.7}Al_{0.3}As$ (Si, 1.5×10^{18} cm^{-3}) layer, which corresponds to the 2D donor density $n_D^{(2)}=1.5\times10^{11}$ cm^{-2}. The thickness of the $Ga_{0.7}Al_{0.3}As$ intrinsic part located between the δ-n layer and p-doped region is 350 nm on both sides. A doping density (C, 2.0×10^{18} cm^{-3}) is used in both p-doped regions. The sample was photolithographically processed, i.e., the structure was mesa etched, isolated and selectively contacted to the p-doped regions and to the region involving the DQW and the δ-n layers. The design of the sample was chosen to allow for a tuning of the electron density by applying a p-n bias with both p contacts kept at the same potential. When no bias is applied to the sample in the dark, the relatively weakly doped δ-n layers supply a negligible electron density in the DQW. As schematically depicted in Fig. 1, a two-dimensional electron gas (2DEG) with a tunable density is created at a positive bias U_{pn}. In the flat-band regime, when no electric field is present in intrinsic regions, the 2DEG density close to the δ-n doping ($\approx3\times10^{11}$ cm^{-2}) is achieved. The influence of the optical excitation on the electron density will be discussed later on. The PL spectra presented in this paper were gained from several mesa structures taken from the same wafer. All investigated structures exhibited almost identical behavior showing thus a very good homogeneity of MBE growth.

The sample was excited by a Ti:sapphire laser with a standard power density $I_0\approx100$ mW/cm^2 at the photon energy 1.72 eV, i.e., below the band gap of $Ga_{0.7}Al_{0.3}As$ at a helium temperature. An optical fiber was used for the excitation, as well as for the signal collection. The PL spectra were analyzed by a monochromator and detected by a cooled charge coupled camera. The helium bath cryostat ensured a good sample temperature stability at 4.2 K. All measurements were performed in a resistive solenoid up to the magnetic field of 22 T in the Voigt or Faraday configuration.

III. THEORY

The theoretical description discussed below follows a simplified model suggested by Huang and Lyo,[11] where no excitonic effects are included. In zero magnetic field, the electron subband energies E_e^i and corresponding wave functions $\chi_i(z)$ can be obtained straightforwardly using a common self-consistent procedure. This involves a simultaneous solution of the one-dimensional (1D) Schrödiner equation written in the envelope function approximation (EFA):

$$\left(-\frac{\hbar^2}{2m_e}\frac{d^2}{dz^2}+V_e(z)\right)\chi_e^i(z)=E_e^i\chi_e^i(z), \tag{1}$$

and the Poisson equation:

$$\frac{d^2}{dz^2}V_H(z)=-\frac{e^2n^{(2)}}{\epsilon_0\epsilon_r}\sum_i|\chi_e^i(z)|^2, \tag{2}$$

where $V_H(z)$ is the Hartree potential, which appears also in the potential energy $V_e(z)$:

$$V_e(z)=V_H(z)+E_c(z)+V_{xc}(z), \tag{3}$$

together with $E_c(z)$ and $V_{xc}(z)$ denoting the DQW conduction band profile and the exchange-correlation potential, respectively. In accordance with HL,[11] the approximation for $V_{xc}(z)$ was taken from Hedin and Lundqvist.[16] Overall in the paper, the lowest lying bonding $i=1$ and antibonding $i=2$ subbands are taken into account only. ϵ_0 and ϵ_r denote vacuum and relative permittivity, respectively. Because the 2D electron density $n^{(2)}$ serves as an input parameter of our calculation and the symmetric DQW only is considered, we can use the boundary condition:

$$\lim_{z\to-\infty}\frac{dV_H}{dz}=-\lim_{z\to+\infty}\frac{dV_H}{dz}=\frac{e^2n^{(2)}}{2\epsilon_0\epsilon_r}. \tag{4}$$

All z-dependent material parameters such as the relative permittivity ϵ_r or the relative mass of electron and hole m_e, m_h, are taken as an averaged value in our calculation.

Henceforth we take the in-plane magnetic field $\mathbf{B}=(0,B_\parallel,0)$ with the vector potential gauge $\mathbf{A}=(B_\parallel z,0,0)$ into account. The field modifies the Schrödinger equation (1), where an additional $B_\parallel$-dependent term parabolic in z appears:[11]

$$\left[-\frac{\hbar^2}{2m_e}\frac{d^2}{dz^2}+\frac{\hbar^2}{2m_e}\left(k_x-\frac{eB_\parallel z}{\hbar}\right)^2+V_e(z)\right]\chi^i_{e,k_x}(z) = E^i_e(k_x)\chi^i_{e,k_x}(z). \quad (5)$$

In the in-plane magnetic field, the electron in-plane motion becomes coupled with the motion in the z direction and thus the electron wave function χ^i_{e,k_x} and subband energy $E^i_e(k_x)$, are implicitly dependent on the electron momentum in the x direction k_x. The motion in the y direction, i.e., along the applied magnetic field $B_\parallel$, remains uncoupled and therefore the whole electron energy in the ith subband can be written in the form

$$\mathcal{E}^i_e(k_x,k_y)=E^i_e(k_x)+\frac{\hbar^2k_y^2}{2m_e}. \quad (6)$$

In general, Eq. (5) requires again a self-consistent solution to find $V_e(z)$. However, we suppose that the magnetic-field-induced changes in the potential $V_e(z)$ are small in comparison with a strong additional z-dependent parabolic term in Eq. (5). Therefore, we use the potential $V_e(z)$ achieved at zero magnetic field and avoid thus a complicated calculation. This assumption cannot be successfully used for asymmetric DQWs, where magnetic field $B_\parallel$ induces a significant redistribution of the total charge between wells, which strongly affects the Hartree term $V_H(z)$ contained in the total potential $V_e(z)$.

Up to now, we dealt with electron states only. To calculate hole states in the DQW, we solve again Eq. (1) or optionally in the nonzero magnetic field Eq. (5). In this case, we have to take an appropriate hole mass m_h and replace the total electron potential $V_e(z)$ by the total potential for holes $V_h(z)$, which includes the valence band profile $E_v(z)$ and the Hartree term $-V_H(z)$. In accord with our experiment, the density of the photogenerated holes is supposed to be much less than $n^{(2)}$. Hence, the Hartree term is given by the spatial distribution of electrons only and the exchange-correlation effects in the hole gas are neglected. Note that we consider the heavy hole states only in agreement with HL.[11] No nonparabolic or valence band mixing effects are included.

The luminescence intensity $I(\omega)$ roughly corresponds to the local joint density of states modified by the Fermi-Dirac statistical distribution of electrons and holes $f_e(E)$, $f_h(E)$:

$$I(\omega)\propto\sum_{k_x,k_y,i,j} f_e(E^i_e),f_h(E^j_h)|\langle\chi^j_h|\chi^i_e\rangle|^2\,\delta(E^i_e-E^j_h-\hbar\omega). \quad (7)$$

Optical transitions between bonding and antibonding subbands ($j\neq i$) must be included, because this recombination becomes allowed at a finite in-plane magnetic field.

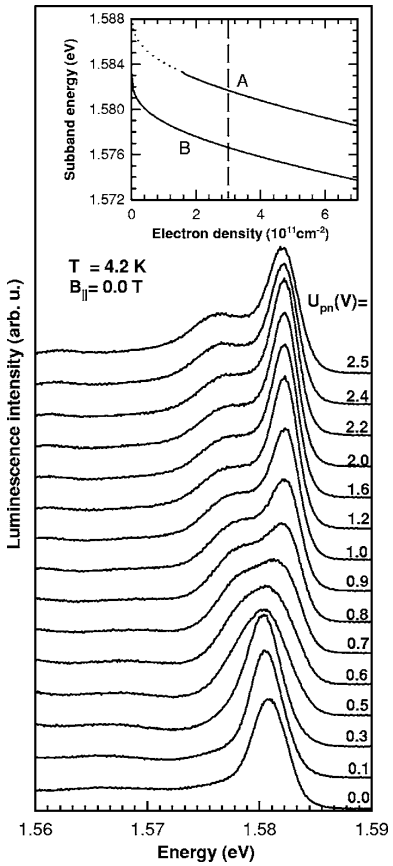

FIG. 2. PL spectra at zero magnetic field for various applied positive bias U_{pn}. The p contacts were kept at the same potential. The inset contains recombination energy calculated for electrons in the bottoms of the B and A subbands as a function of the electron density in DQW. The dotted line shows the unoccupied antibonding subband at lower electron densities. The dashed line denotes the total intended doping of δ-n layers.

IV. RESULTS AND DISCUSSION

A. PL as a function of applied bias

We start the discussion with the analysis of results in Fig. 2, which shows PL spectra of the studied sample at zero magnetic field as a function of the applied bias U_{pn}. Both p contacts were kept at the same potential, as well as in all other measurements presented in this paper. The observed spectrum consists of a well pronounced PL structure in the spectral range 1.575–1.585 eV and of a significant low-energy tail that will be commented on later. The sample was designed to obtain a depleted DQW at $U_{pn}=0.0$ V and a 2DEG density corresponding to the total charge of δ-n doping ($2n_D^{(2)}=3\times10^{11}$ cm^{-2}) in the flat-band regime. The flat-band regime is achieved for $U_{pn}\cong+1.8$ V at liquid helium temperature. Taking account of this, the relatively narrow PL line at $U_{pn}=+0.0-0.3$ V can be assigned to the excitoniclike

recombination and the line broadening observed above $U_{pn}=+0.5$ V reflects the formation of 2DEG and further increase of its density at higher bias. Simultaneously, the low-energy edge of the PL line shifts towards lower energies due to the subband renormalization, confirming the gradual increase of the electron density. At $U_{pn}\approx+1.2$ V, a steplike shape of the PL spectrum is achieved and this shape remains practically unchanged up to the bias of $U_{pn}\approx+2.0$ V, then a further redshift of the low-energy edge appears, showing thus a further increase of the electron density. The interpretation of the PL spectra at U_{pn} above the flat-band regime is not straightforward. In this case, the total applied bias U_{pn} can drop not only on the *p*-*n* junction, being in the forward regime, but also in the *p*- and *n*-contact layers themselves. However, an approximately exponential course of the current through the *p*-*n* junction with U_{pn} suggests that the voltage lost in the contacts is not dominant in the chosen interval of bias voltage ($U_{pn}<2.6$ V).

The shape of the spectrum can be interpreted on the basis of the self-consistent calculation depicted in the inset of Fig. 2, where the recombination energies for electrons in the bottom of the bonding (B) and antibonding (A) subbands are shown as a function of the 2D electron density. Hence, these values represent the energies of steps in the joint density of states, or in corresponding points of inflection in the PL spectra, when the realistic broadening of the PL spectra is taken into account. The difference in transition energies is given by the splitting of electron subbands B and A only, holes are supposed to be localized, having their energy at the bottom of the hole subband B, as is elucidated later on. The presented calculation predicts a relatively steep decline of the recombination energy at very low densities $n_e<10^{11}$ cm^{-2}. However, this expectation is unrealistic due to the excitonic effects completely neglected in the calculation. Instead, we can roughly say that the PL is dominated by excitonic interactions up to the electron density at which the renormalization energy is comparable with the exciton binding energy. Approximately at this density, excitons become unstable, or in other words the excitonic interaction is significantly screened by free electrons, and at higher densities, the recombination of practically unbound electrons and holes mainly appears. The same effect has been observed by Kappei *et al.*[17] They reported PL measurements on a QW with a wide range of electron-hole pair densities (from excitonic to the free carrier regime) and the maximum of the PL line remained almost unchanged. In our case, the excitonic origin of the PL at $U_{pn}=0.0-0.3$ V was proven also by the quadratic shift of the PL energy with $B_\perp$ as will be shown later. The mutual electron-hole Coulomb interaction plays an important role in the optical recombination also at higher electron densities, when particles are not bound to a stable exciton. This occurs for electrons close to the Fermi level, in particular. We will deal with this problem later.

Another important feature not closely discussed up to now is the behavior of holes in our DQW. In general, a relatively broad PL spectrum is usually observed in a high density electron-hole plasma[18] or at low hole densities, when holes are localized in a disordered potential. The spread of hole wave function in the reciprocal space then allows the recombination of electrons from the bottom of the subband, as well as from the Fermi level. Figures 3(a) and 3(b) summarize the spectra gained under excitation intensities I_0, $0.1I_0$, and $0.05I_0$ at the particular bias and magnetic field. These figures illustrate that the shape of PL spectra gained at the bias close to the flat-band regime ($U_{pn}\cong+1.8$ V) or lower is almost insensitive to the excitation intensity in the chosen interval. Hence, we can conclude that the hole localization should be responsible for a relatively broad PL spectrum (up to 8 meV). We suppose that holes have a small localization energy and are strongly scattered by large inhomogeneities and potential fluctuations. This type of hole localization, enabling electron recombination in a wide interval of momentum, was identified by Tarasov *et al.*[19] Therefore, the localization energy was neglected in our calculation and hole energy was taken at the bottom of the hole subband B. For the sake of completeness, the spectra insensitive to the excitation intensity could be obtained also when the low density hole gas is Boltzmann distributed, but this possibility would lead to peaks in the PL spectra much narrower than observed.

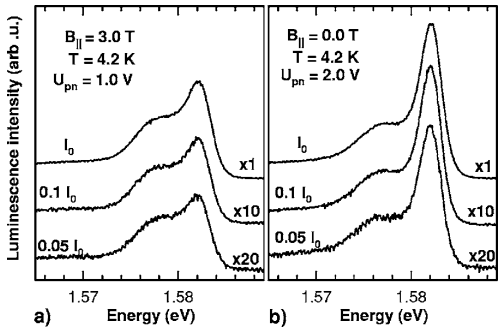

FIG. 3. The PL spectra at excitation intensities I_0, $0.1I_0$ and $0.05I_0$ for (a) $U_{pn}=+1.0$ V, $B_\parallel=3.0$ T and (b) $U_{pn}=+2.0$ V, $B=0.0$ T. The PL intensities are multiplied by the factor 10 and 20 for excitation intensity $0.1I_0$ and $0.05I_0$, respectively.

Independently, also another assertion can be done on the basis of Fig. 3. The optical excitation in the chosen interval of intensities does not practically affect the electron density. Hence, the photogenerated electrons with energies above the quasi-Fermi level in DQW, which is fixed by the applied bias U_{pn}, are drained from 2DEG into the electric contact. The photogenerated electrons arise not only in DQW but also in the undoped ternary regions near the DQW. Note that the absorption of photons with energy below the band gap of $Ga_{0.7}Al_{0.3}As$ is allowed by the Franz-Keldysh effect, as indicated by the observed photocurrent that was in the range of $\lesssim$100 nA at $U_{pn}=0.0$ V and intensity I_0.

B. PL in perpendicular magnetic field

The PL experiment in perpendicular field $B_\perp$ was performed in order to obtain a deeper insight into the electron subband structure due to the expected quantization of a 2DEG into Landau levels (LLs). The PL spectra at the constant bias $U_{pn}=+1.0$ V as a function of $B_\perp$ are shown in Fig. 4. The LLs are observable in the PL spectra as soon as the magnetic field achieves the value of $B_\perp=3.0$ T and in the

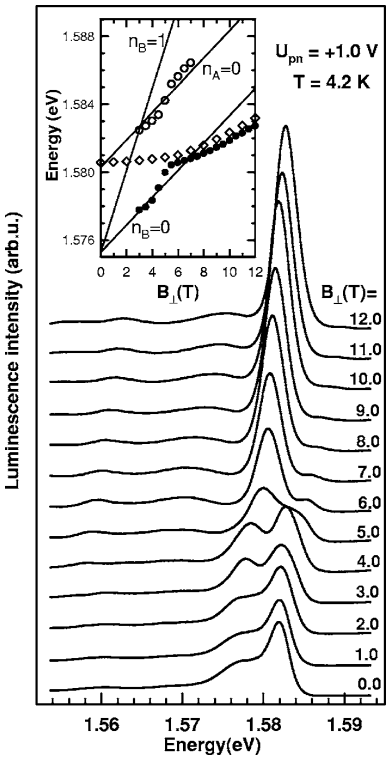

FIG. 4. Evolution of PL spectra with the magnetic field $B_\perp$ perpendicular to the layer at the bias $U_{pn}=+1.0$ V. The inset contains the fan diagram, where the full circles (●) correspond to the LL $n_B=0$ and open circles (○) to LL $n_A=0$. The full lines show calculated energies of LLs $n_{A,B}=0$ and $n_B=1$ for electron mass $m_e=0.072m_0$. Diamonds (◇) show the diamagnetic shift of the magnetoexciton line with $B_\perp$ observed at $U_{pn}=0.0$ V.

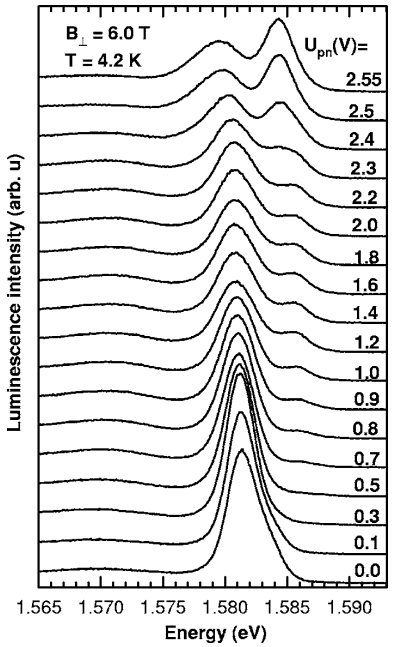

FIG. 5. Bias dependence of PL spectrum at $B_\perp=6.0$ T.

interval $B=3.0-4.5$ T, two local maxima are clearly observed. The maximum with a lower energy corresponds to the recombination from the zero LL of the bonding subband ($n_B=0$) and the maximum at the higher energy originates from the recombination of electrons from LL $n_A=0$. The peaks related to excited LLs $n_{A,B}\geqslant 1$ were not directly resolved in our PL spectra. We explain this by the fact that above $B_\perp=3.0$ T, when the splitting into LLs becomes distinguishable, all excited LLs including the lowest lying one $n_B=1$ are significantly exhausted. Furthermore, the peak corresponding to the weakly populated LL $n_B=1$ is likely hidden in the high energy side of the LL $n_A=0$ peak. We also speculate that the effect of LL $n_B=1$ could be identified from weak irregularities observed in the $B_\perp$ dependence of LLs $n_{A,B}=0$. The steep blueshift of the PL peaks at $B_\perp=4-5$ T could correspond to the reduced renormalization connected with the complete depletion of LL $n_B=1$, but the detailed study of this feature is out of the scope of this paper.

With the increasing field $B_\perp$, the enhanced degeneracy of LLs $\zeta=eB_\perp/\pi\hbar$ leads to a gradual depopulation of LL $n_A=0$ that becomes completely depopulated above $B_\perp\approx 7.0$ T. Whereas at $B_\perp<7.0$ T the LL energies apparently follow the expected linear dependence, above $B_\perp>7.0$ T the only partially occupied LL $n_B=0$ (we neglect the spin splitting here) allows the formation of excitons, whose binding energy gradually increases with the magnetic field. The LL blueshift then becomes slower and comparable to the shift of the magnetoexciton line at the low electron density maintained by $U_{pn}=0.0$ V, see the inset of Fig. 4.

The PL spectrum at $B_\perp=6.0$ T as a function of bias U_{pn} has been plotted in Fig. 5. At this magnetic field, LLs $n_B=0$ and $n_A=0$ are occupied only and the U_{pn} dependence enables a rough estimation of the total electron density in the DQW at the given bias. Results of the spectra decomposition, i.e., energies of LLs with $n_{B,A}=0$, as well as their peak area ratio, are shown in Fig. 6. As can be inferred, the distance between LL energies declines with the increasing electron concentration. However, this effect is relatively weak and thus we can say that the splitting of B and A subbands amounts to $\approx$5 meV. The ratio of peak areas in Fig. 6 roughly corresponds to the relative occupation of LLs. The LL $n_A=0$ appears in the spectra above $U_{pn}=+0.7$ V and its intensity increases rapidly up to $U_{pn}=+1.2$ V. Above this value, the peak area ratio and thus also the total electron density rises slowly and a further strong increase follows at $U_{pn}>+2.0$ V. Let us recall that the same behavior has already been shown at zero magnetic field in Fig. 2.

As Fig. 6 shows, the electron density is well stabilized in the interval $U_{pn}\approx+1.2-2.2$ V, i.e., in the interval around the flat-band regime, which is estimated to $U_{pn}\cong+1.8$ V. At lower bias, the electron concentration in DQW can be enhanced due to photon absorption in the ternary layers near the DQW. The generated electrons accumulate in the DQW resulting in a slightly increased density compared to that in

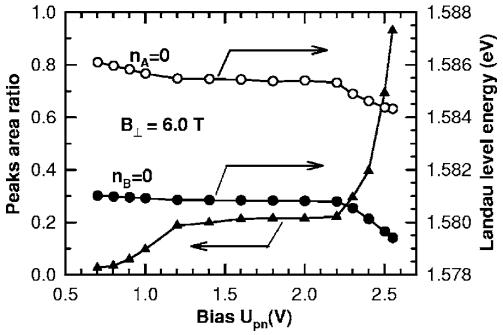

FIG. 6. The decomposition of PL spectra shown in Fig. 5. The figure summarizes the energies for $n_B=0$ (full circles, ●) and $n_A=0$ (open circles, ○) LLs at given bias U_{pn}. The ratio of the antibonding to bonding peak areas (triangles) roughly shows the relative occupation of levels. Lines serve as a guide for the eye only.

dark at the same bias. However, the total electron density in DQW is still mainly driven by the applied bias U_{pn}, as concluded above. In the flat-band position, $n^{(2)}$ should correspond to the total δ-n doping $2n_D^{(2)}$. Taking account of the relative occupation of $n_B=0$ and $n_A=0$ LLs (see Fig. 6) and the LL degeneracy at $B_\perp=6.0$ T, $\zeta=2.9\times10^{11}$ cm^{-2}, we obtain an electron density $n^{(2)}\cong3.5\times10^{11}$ cm^{-2} in the flat-band regime, i.e., only slightly above the intended value $2n_D^{(2)}$. The densities attained in this way can serve as a rough estimation only due to the neglected excitonic effects at the Fermi level. Electrons close to the Fermi level, i.e., in the partially filled LL $n_A=0$, are in the recombination process much strongly influenced by the excitonic interaction than those in the almost full LL $n_B=0$. Hence, the PL from antibonding subband could be intensified by the excitonic interaction causing thus a possible overestimation of $n^{(2)}$.

A note should be addressed to the intensity of peaks in Fig. 5. Even if the peak of LL $n_A=0$ transition at a bias $U_{pn}>+2.5$ V is higher than for the LL $n_B=0$ transition, the peak area ratio in Fig. 6 remains smaller than unity for all values of applied bias. This clearly indicates a larger peak broadening of the LL $n_B=0$ transition than that of LL $n_A=0$. We can bring out two main reasons to explain this: (i) The lower lying subband B is more affected by the potential fluctuations in the bottom of the well. (ii) Electrons in the subband A, having a node in their wave functions, are less scattered by imperfections of the very thin middle barrier in comparison with electrons in the subband B. We will include this different line broadening in our calculations later on.

The spectra in Fig. 4 were plotted in a broader spectral region to show the whole low-energy tail. With increasing $B_\perp$, a clear modulation of this tail appears. The field-induced maxima in the tail shift together with PL coming directly from DQW with increasing $B_\perp$ to higher energies. The low-energy tail, as well as its field-induced shape modulation were almost identical in the PL of all investigated structures taken from the grown wafer. Therefore, it should not be related to the defect of DQW in one particular mesa structure. However, we have to admit that the origin of the tail is not clear now. We suggest that it can be correlated with shake-up processes or with plasmon effects. The latter one is less probable because the shape of the tail is rather insensitive to the increasing electron concentration by applying higher bias voltages U_{pn}. Another explanation could be based on a PL experiment published by Tarasov *et al.*[19] Apart from the above discussed shallow localized hole states, significantly deeper lying states were also found there.

C. PL in in-plane magnetic field

In this section, the phenomena in the in-plane magnetic field $B_\parallel$ are discussed. Figure 7(a) summarizes the magnetic field dependence of the PL spectrum at a constant bias $U_{pn}=+1.8$ V, i.e., at a constant electron sheet density $n^{(2)}\cong3.5\times10^{11}$ cm^{-2}. As discussed above, the steplike shape of PL spectra at $B_\parallel=0$ T is given by the recombination of electrons from subbands B and A with heavy holes localized in the potential fluctuations, as concluded on the basis of Fig. 3. In this case, the wave functions of holes are widely spread in the reciprocal space, allowing the recombination of all electrons with a roughly equal probability. The experiment revealed a gradual damping of the PL line arising in subband A with increasing $B_\parallel$, even though the electron density $n^{(2)}$ was kept at the same level due to the constant applied bias U_{pn}. Around $B_\parallel=7.0$ T, the recombination from subband A diminishes completely and the PL from subband B takes over. A further rise of $B_\parallel$ leads to a further narrowing of the PL spectra accompanied by a moderate blueshift in its energy.

At this point, it is useful to look at Fig. 8, where PL spectra at $B_\parallel=6.0$ T are depicted as a function of U_{pn}. The spectrum develops with U_{pn} analogous to that in Figs. 2 and 5. We can observe a significant broadening of PL line above $U_{pn}=+0.5$ V, which corresponds to the creation of 2DEG and in the interval $U_{pn}=+1.2-2.0$ V, the shape of the PL spectrum remains nearly unchanged. A further increase of electron density is then observed above $U_{pn}=+2.0$ V resulting in an enhanced occupation of subband A, again in agreement with results in Figs. 2 and 5. However, the steplike shape of the PL spectrum attained at $B_\parallel=0$ T is thus not achieved even at the highest applied bias. The characteristic redshift of the PL band induced by the subband renormalization with increasing $n^{(2)}$ is also clearly seen. Hence, the dependence on U_{pn} brings analogous behavior both in the in-plane and in the perpendicular magnetic field. This observation indirectly indicates that the applied bias ensures in the in-plane magnetic field the same electron density in DQW as deduced from measurements at $B_\perp$.

D. Comparison with theory

Prior to the comparison of the experimental results with the suggested theory, a brief description of the performed calculations should be given. Our calculations are based on parameters summarized in Table I, which were taken from Davies.[20] The electron mass m_e was slightly enhanced above the bulk GaAs value due to the expected tunneling into barriers. The height of the AlAs barrier separating two QWs was adjusted to achieve a splitting of 5 meV between subbands A and B, determined experimentally at $B_\perp$. Namely, the offset[20]

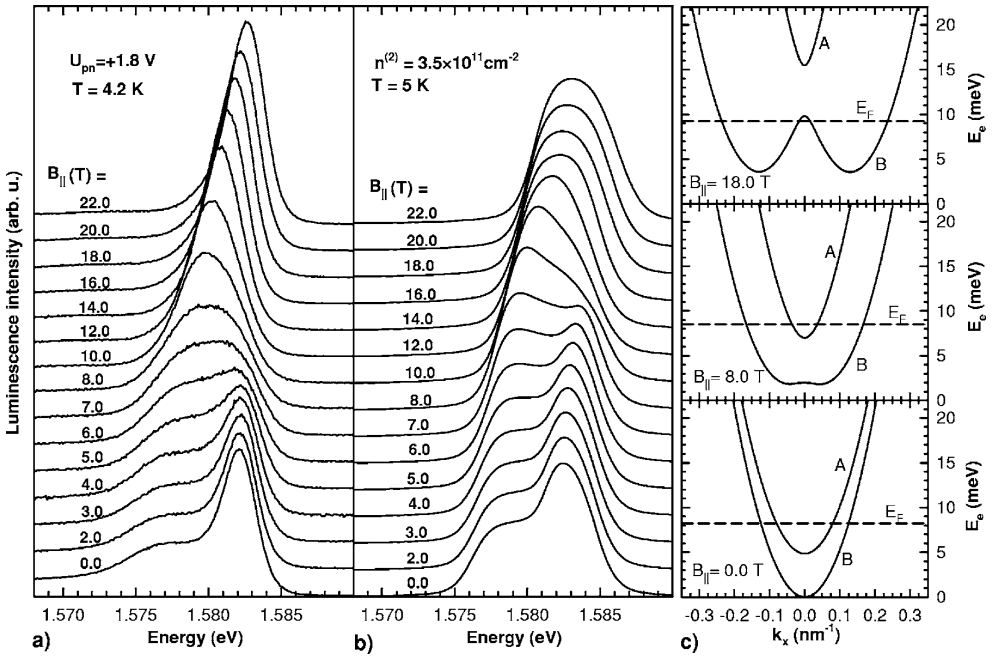

FIG. 7. (a) Normalized PL spectra in the in-plane magnetic field at the constant bias $U_{pn}=+1.8$ V. (b) Calculated PL spectra at $n^{(2)}=3.5\times10^{11}$ cm^{-2} and temperature $T=5$ K. (c) Electron dispersion in subbands B and A at $B_{\|}=0.0$, 8.0, and 18.0 T. The dashed line shows the Fermi-level energy in each case. Energies are plotted with respect to the bottom of subband B at $B_{\|}=0.0$ T.

$\Delta E_c=1120$ meV for the AlAs barrier (taken at the Γ point) was increased by an amount of 15%. We attribute that to a limited validity of the EFA method in case of a very thin, 4 ML wide, middle barrier.

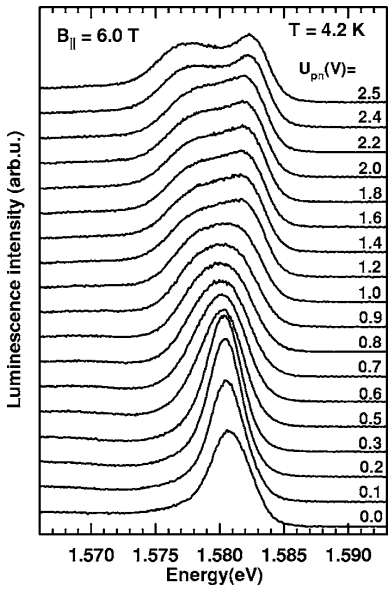

FIG. 8. PL spectra taken at $B_{\|}=6.0$ T for selected positive bias U_{pn}, i.e., at various electron densities in the DQW.

The PL spectra calculated for $n^{(2)}=3.5\times10^{11}$ cm^{-2} at a temperature of 5 K as a function of $B_{\|}$ are depicted in Fig. 7(b). These spectra were obtained using Eq. (7), where the δ function was replaced by a simple sum of the Gaussian and Lorentzian functions with the same weight in order to include both homogeneous and inhomogeneous mechanisms of PL line broadening. Another choice of the broadening function, which would prefer one of the mechanisms, would not lead to the significant changes in the results of the calculation. The lower line broadening of the PL from subband A than from subband B was used, $\sigma_B=1$ meV and $\sigma_A=0.7$ meV, as discussed above and as seen in Fig. 5. The sum in Eq. (7) runs over both occupied electron subbands ($i=1,2$) and a single energetic level E_h of localized holes. This energy of shallow localized holes was taken at the bottom of the hole subband B. Owing to the hole localization, the overlap integral in Eq. (7) is supposed to be independent of k_x and is thus not involved in the calculation.

Our calculations have also shown that 1 ML AlAs layers placed in the heterojunctions are improper to be included in our calculations using the common EFA method, because it

TABLE I. Parameters used in the calculations. The valence and conduction band offsets ΔE_v, ΔE_c, and GaAs band gap energy E_g^{GaAs} are given in meV. The value ΔE_c is valid for the molar fraction $x<0.45$ only. m_0 represents the free electron mass.

m_e	m_h	ϵ_r	ΔE_v	ΔE_c	E_g^{GaAs}
$0.072m_0$	$0.5m_0$	12.5	$474x$	$773x$	1519

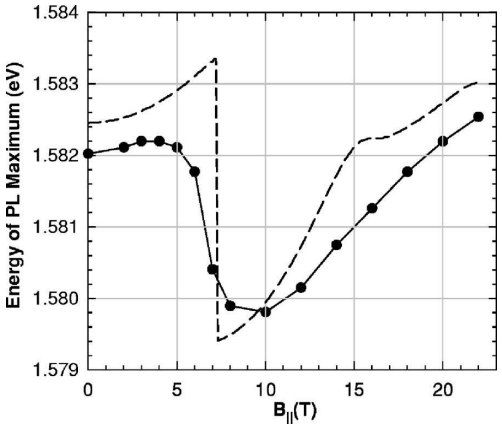

FIG. 9. The energy of the PL maximum as a function of $B_\parallel$ (closed circles) in comparison with the theoretical line (dashed line) attained for $n^{(2)}=3.5\times10^{11}$ cm^{-2}. The experiment corresponds to the measurements at $U_{pn}=+1.8$ V. The line connecting the experimental points serves as a guide for the eye only.

gives unacceptable high recombination energies in comparison with the experiment. Hence, we suppose that these layers only smooth the roughness of the heterojunctions and do not form a homogeneous AlAs monolayer. However, also in this case, these smoothing layers likely enhance the observed recombination energy. This fact together with the neglect of the hole localization energy limits the accuracy of our calculations. The calculated position of PL structure is thus given with the accuracy of several meV. We should take this into account, when the theory and experiment are compared (Figs. 2 and 7).

The calculation at $B_\parallel=0.0$ T provides an expected steplike spectrum reflecting recombination from both occupied subbands. The strength of the subband A in the PL spectra gradually declines with $B_\parallel$ in comparison with strength of subband B and slightly above $B_\parallel=7.0$ T the recombination from subband B takes over. This so-called $\mathcal{N}$-type kink effect was predicted by HL (Ref. 11) and can be more deeply understood on the basis of Fig. 7(c), where the calculated electron dispersions in the k_x direction, i.e., perpendicular to the applied in-plane magnetic field, are shown at $B_\parallel=0.0$, 8.0, and 18.0 T. The depicted position of the Fermi level E_F shows a gradual depopulation of subband A that is induced by a strong modulation of subband B dispersion. As Fig. 7(c) illustrates, two approximately parabolic-shaped minima are developed in the dispersion of the subband B at the high in-plane magnetic field. Roughly speaking, this effect doubles the total number of states close to the bottom of the subband B and induces thus the depopulation of the subband A, which is the main reason for the observation of the $\mathcal{N}$-type kink.

Another direct comparison between theory and experiment is shown in Fig. 9, where the measured and calculated $\mathcal{N}$-type kinks, i.e., position of the PL maximum as a function of $B_\parallel$, is plotted. Our simple calculation predicts a steep shift of the PL maximum from subband A to subband B at $B_\parallel=7.2$ T. This is in good agreement with the experiment, where the point of inflexion, which should correspond to the PL maxima change over from the upper to the lower subband, appears at $B_\parallel\approx6.5$ T.

The most significant feature, in which the calculation and our experiment differ, is the PL spectrum width above $B_\parallel\approx14$ T. This point must be addressed in detail. The calculated PL width above 5 meV is in contrast to the experimentally observed width $\approx3-4$ meV [cf. Figs. 7(a) and 7(b)]. To elucidate this problem, Fig. 7(c) can be consulted, where the dispersion of electrons in subband B at $B_\parallel=18.0$ T is depicted. Two minima in this dispersion curve show an effective separation of both wells in the DQW structure. Each electron in the subband B belongs to one QW only due to the Lorentzian force pushing electrons moving in the DQW plane either into the left or the right well. Hence, two parallel 2DEGs are developed and the observed PL is equivalent to the signal from two independent QWs, each with the electron density of $n^{(2)}/2$. One possible mechanism leading to the narrowing of the PL line is the electron localization in the middle of a QW, which limits the influence of imperfections in the DQW middle barrier. However, this effect itself cannot explain the whole peak narrowing because of the peak width, which is less than the calculated distance from the Fermi level to the bottom of the subband B. Therefore, we interpret the low line width as a result of the excitonic interaction, whose influence strongly increases at lower densities. Probably no stable excitons are formed, but also partially screened excitonic interaction leads to the peak narrowing.[17] In addition, the linewidth tends to increase rapidly at a higher bias (above $U_{pn}=+2.0$ V), when the electron density rises and causes probably again a transition from an excitonlike to free particlelike PL. We can also note that at high magnetic fields in the perpendicular orientation the magnetoexcitons close to the Fermi level are reported to be stable up to electron-hole plasma densities significantly higher than the electron density in our sample.[21] However, this finding cannot be easily applied to our case, when the magnetic field is oriented in the in-plane direction.

To make a short summary, our measurements were carried out on a DQW system with an electron density close to the value supposed by HL.[11] They have chosen a relatively low electron density $n^{(2)}=2.4\times10^{11}$ cm^{-2} to allow the observation of the $\mathcal{N}$-type kink effect in common DQW structures at in-plane magnetic fields of reasonable strength. PL spectra obtained from quantum well structures at densities close to $\cong10^{11}$ cm^{-2} are significantly influenced by the excitonic interaction[18] that precludes a straightforward single-particle description of the recombination process. However, our measurements have clearly demonstrated that the behavior predicted by HL can be observed. Furthermore, we are able to describe the observed effects in the quantitative way by a simple model based on the HL theory. Important deviations from their theory were registered at higher $B_\parallel$ only. Hence, the single particle model can be successfully used and even a rough quantitative description of the $\mathcal{N}$-type kink effects can be attained. At this point, we should also emphasize that with the exception of the slight adjustment of the DQW middle barrier height and of the obvious broadening factors $\sigma_{A,B}$ our calculation does not include any other free parameters.

A final note should be added for the sake of completeness. HL supposed a free hole gas instead of localized holes that

were found in our DQW structure. Therefore, our model is different in this particular way. The disordered potential as a necessary condition for a $\mathcal{N}$-type kink observation was also suggested by Kim *et al.*[15] They have identified this effect in the PL from only one particular sample that had the lowest mobility in the studied set of structures. Samples that allowed the observation of the $\mathcal{N}$-type kink are thus similar to those, where the Fermi edge singularity was studied.[19] The hole localization allows the recombination of electrons close to the Fermi level.

V. CONCLUSION

We have studied the influence of the in-plane magnetic field on the luminescence of the symmetric double quantum wells with the two-dimensional electron gas occupying two lowest subbands. A simple theoretical model similar to that suggested by Huang and Lyo[11] was applied and we have achieved a good agreement with our experimental data. Therefore, we conclude that the one-particle model can describe even in a quantitative way the luminescence of double quantum wells with the electron gas at a relatively low density under in-plane magnetic fields. Simultaneously, the effects connected with the excitonic interaction were discussed and are necessary for a more accurate description of the observed behavior.

ACKNOWLEDGMENTS

This work is a part of the research plan MSM0021620834 that is financed by the Ministry of Education of the Czech Republic. M.O. acknowledges support from the Grant Agency of Charles University under Contract No. 281/2004. The high magnetic field measurements were enabled by the program "Transnational Access to Infrastructures—Specific Support Action," Contract No. RITA-CT-2003-505474 of the European Commission.

*Electronic address: orlita@karlov.mff.cuni.cz

[1] L. V. Butov, C. W. Lai, A. L. Ivanov, A. C. Gossard, and D. S. Chemla, Nature (London) **417**, 47 (2002).
[2] L. V. Butov, A. C. Gossard, and D. S. Chemla, Nature (London) **418**, 751 (2002).
[3] S. K. Lyo, Phys. Rev. B **50**, 4965 (1994).
[4] L. Smrčka and T. Jungwirth, J. Phys.: Condens. Matter **7**, 3721 (1995).
[5] D. Simserides, J. Phys.: Condens. Matter **11**, 5131 (1999).
[6] J. A. Simmons, S. K. Lyo, N. E. Harff, and J. F. Klem, Phys. Rev. Lett. **73**, 2256 (1994).
[7] T. Jungwirth, T. S. Lay, L. Smrčka, and M. Shayegan, Phys. Rev. B **56**, 1029 (1997).
[8] O. N. Makarovskii, L. Smrčka, P. Vašek, T. Jungwirth, M. Cukr, and L. Jansen, Phys. Rev. B **62**, 10908 (2000).
[9] L. Smrčka, P. Vašek, J. Koláček, T. Jungwirth, and M. Cukr, Phys. Rev. B **51**, 18011 (1995).
[10] R. Fletcher, T. Smith, M. Tsaousidou, P. T. Coleridge, Z. R. Wasilewski, and Y. Feng, Phys. Rev. B **70**, 155333 (2004).
[11] D. Huang and S. K. Lyo, Phys. Rev. B **59**, 7600 (1999).
[12] D. M. Whittaker, T. A. Fisher, P. E. Simmonds, M. S. Skolnick, and R. S. Smith, Phys. Rev. Lett. **67**, 887 (1991).
[13] B. M. Ashkinadze, E. Linder, E. Cohen, and L. N. Pfeiffer, Phys. Rev. B **71**, 045303 (2005).
[14] Y. Kim, C. H. Perry, D. G. Rickel, J. A. Simmons, F. Klem, and E. D. Jones, in *Proceedings of the 23rd International Conference on The Physics of Semiconductors*, edited by M. Scheffler and R. Zimmermann (World Scientific, Singapore, 1996), p. 1859.
[15] Y. Kim, C. H. Perry, J. A. Simmons, and F. Klem, Appl. Phys. Lett. **77**, 388 (2000).
[16] L. Hedin and B. I. Lundqvist, J. Phys. C **4**, 2064 (1971).
[17] L. Kappei, J. Szczytko, F. Morier-Genoud, and B. Deveaud, Phys. Rev. Lett. **94**, 147403 (2005).
[18] R. Cingolani and K. Ploog, Adv. Phys. **40**, 535 (1991).
[19] G. G. Tarasov, U. Muller, Y. I. Mazur, H. Kissel, Z. Y. Zhuchenko, C. Walther, and W. T. Masselink, Phys. Rev. B **58**, 4733 (1998).
[20] J. H. Davies, *The Physics of Low-dimensional Semiconductors: An Introduction* (Cambridge University Press, Cambridge, 1997), p. 412.
[21] M. Bayer, A. Dremin, F. Faller, A. Forchel, V. D. Kulakovskii, B. N. Shepel, and T. Andersson, Phys. Rev. B **50**, 17085 (1994).

Appendix B

Authors:	M. Orlita, M. Byszewski, G. H. Döhler, R. Grill, P. Hlídek, S. Malzer, and M. Zvára
Title:	Photoluminescence of n-doped double quantum well – electron subbands under influence of in-plane magnetic fields
Journal:	Physica E
Year:	2006
Pages:	in press

Available online at www.sciencedirect.com
SCIENCE DIRECT
Physica E ▮ (▮▮▮▮) ▮▮▮–▮▮▮
PHYSICA E
www.elsevier.com/locate/physe

Photoluminescence of n-doped double quantum well—electron subbands under influence of in-plane magnetic fields

M. Orlita[a,*], M. Byszewski[b], G.H. Döhler[c], M. Grill[a], P. Hlídek[a], S. Malzer[c], M. Zvára[a]

[a]*Faculty of Mathematics and Physics, Institute of Physics, Charles University, Ke Karlovu 5, CZ-121 16 Prague 2, Czech Republic*
[b]*Grenoble High Magnetic Field Laboratory, Boîte Postale 166, F-38042 Grenoble Cedex 09, France*
[c]*Max-Planck-Research Group, Institute of Optics, Information and Photonics, Universität Erlangen-Nürnberg, D-91058 Erlangen, Germany*

Abstract

We report on photoluminescence (PL) measurements of a GaAs/AlGaAs double quantum well (DQW) in high magnetic fields. Measurements were carried out on a selectively contacted symmetric p-δn-DQW-δn-p structure, which allows a variation of the electron density in DQW by a p–n bias and simultaneously a tilting of DQW, when a p–p bias is applied. Attention was paid to phenomena in in-plane magnetic fields, theoretically studied by Huang and Lyo (HL), [Phys. Rev. B 59, (1999) 7600]. In this paper, we compare our results for both symmetric and asymmetric DQWs with the theoretical model made by HL. Whereas the spectra from a symmetric DQW fully confirmed the theoretical predictions, the results gained from DQW with an electric-field-induced asymmetry did not allow a proper study of anticipated effects. The reasons for that are discussed.

PACS: 78.67.De; 78.55.Cr; 78.20.ls

Keywords: Double quantum well; In-plane magnetic field; Luminescence

The properties of two-dimensional electron gas (2DEG) in bilayer systems under influence of in-plane magnetic fields ($B_{\|}$) has been widely studied over the last 15 years. Bilayer systems such as semiconductor double quantum wells (DQW) allow carrier tunnelling between layers, modulated by the Lorentzian force. This results in significant changes in the carrier in-plane dispersion and in related deviations from a step-like density of states typical of 2D systems. Whereas these effects have been studied several times in the electron transport, both theoretically and experimentally e.g. Refs. [1,2], only few works have dealt with optical properties of 2D systems with 2DEG at a finite $B_{\|}$. The first photoluminescence (PL) data on a single asymmetric quantum well (QW) were published by Whittaker et al. [3]. Later on, Huang and Lyo (HL) treated the problem of DQWs at finite $B_{\|}$ from a theoretical point of view and predicted a specific dependence of PL spectra on the applied in-plane magnetic field [4]. They considered symmetric as well as asymmetric DQWs and for the former one predicted so-called $\mathcal{N}$-type kink in PL spectra, given by the depopulation of the upper (anti-bonding) subband at $B_{\|}$ high enough. After these predictions, Kim et al. [5] published first experimental results on symmetric DQWs.

In this paper, we extend our previous results [6], where PL spectra from a symmetric DQW were compared with the calculated ones, based on a model similar to that HL used. This paper summarizes subsequent measurements on a symmetric DQW under modified experimental conditions and presents PL spectra obtained from the same DQW with an asymmetry induced by the electric field applied along the growth axis of the sample, as suggested by HL.

Our PL measurements were carried out on a p-i-δn-DQW-δn-i-p structure grown by molecular beam epitaxy. The symmetric DQW consists of two 26 monolayer (ML), i.e. ≈ 7.5 nm, thick GaAs QWs with a 4 ML AlAs barrier in between. This DQW is separated from δ-n doped layers (both Si, $1.5 \times 10^{11}\,\mathrm{cm}^{-2}$) by 30 nm thick $Ga_{0.7}Al_{0.3}As$ spacers. Both $GaAs/Ga_{0.7}Al_{0.3}As$ interfaces in the DQW

*Corresponding author. Tel.: +42 22 1911320; fax: +42 22 4922797.
E-mail address: orlita@karlov.mff.cuni.cz (M. Orlita).

1386-9477/$ - see front matter © 2006 Published by Elsevier B.V.
doi:10.1016/j.physe.2006.03.075

are smoothed by a 1 ML AlAs layer. The thickness of the $Ga_{0.7}Al_{0.3}As$ intrinsic part located between δ-n layer and p-doped region (C, $2.0 \times 10^{18}\,cm^{-3}$) is 350 nm on both sides. The sample was photolithographically processed and selective electrical contacts to the p-doped regions and to the central region involving the DQW and the δ-n layers were made. The design of the sample was chosen to allow for a tuning of the electron density by applying a p–n bias. When no bias is applied to the sample in the dark, the relatively weakly doped δ-n layers supply a negligible electron density to the DQW. A 2DEG with a tunable density is created at a positive (forward) bias U_{pn}. In the flat-band regime, when no electric field is present in the intrinsic regions, the 2DEG density approaches δ-n doping ($\approx 3 \times 10^{11}\,cm^{-2}$). In addition, the asymmetry of the DQW can be induced applying a p–p voltage. A schematic picture of the sample band structure under operational conditions is presented in Fig. 1.

The sample was excited by a Ti:sapphire laser with a power density $I_0 \approx 100\,mW/cm^2$ at the photon energy 1.75 eV, i.e. below the band gap of $Ga_{0.7}Al_{0.3}As$ at a helium temperature. Optical fibers were used for the excitation, as well as for the signal collection. The PL spectra were analyzed by a monochromator and detected by a cooled charge coupled camera. The helium bath cryostat ensured a good sample temperature stability at 4.2 K. All measurements were performed in a resistive solenoid up to the magnetic field of 20 T in the Voigt or Faraday configurations.

At first we turn our attention to Fig. 2 where PL spectra are depicted as a function of $B_\parallel$. Both p-contacts were kept at the same potential but the n-contact was not used, contrary to Ref. [6]. Under these conditions, the DQW is filled by electrons photo-generated in the intrinsic regions due to Franz–Keldysh absorption and the resulting band structure of the sample is almost flat. In this dynamical equilibrium, the density of the 2DEG nearly achieves the value of the total δ-n doping layers and this configuration thus appears to be practically equivalent to an applied forward bias of $U_{pn} \simeq +1.8\,V$, which also ensures flattening of the sample band structure. Therefore, the results shown here are analogous to that in Ref. [6]. The shape of the PL spectrum at $B_\parallel = 0\,T$ reflects the occupation of the bonding (B) and the anti-bonding (A) subband. We suppose that all electrons recombine with almost equal probability owing to a hole localization in potential fluctuations, as discussed in Ref. [6]. The final PL spectrum has thus a nearly step-like shape and the high-energy side of the PL band corresponds to the quasi-Fermi level of electrons in the DQW. With increasing $B_\parallel$ the intensity of the subband A in the PL spectrum declines, at $B_\parallel \approx 6.0\,T$ totally disappears and recombination from the subband B dominates in the PL spectrum. The resulting $\mathcal{N}$-type kink predicted by HL is shown in the inset of Fig. 2. So, the $\mathcal{N}$-type kink effect is observable also at simpler conditions (without applying a bias U_{pn}) than reported in Ref. [6], however, at one fixed electron density in the DQW only.

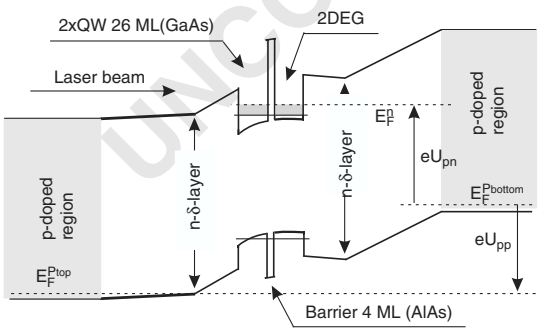

Fig. 1. A schematic band structure of the investigated sample under applied bias U_{pn} and U_{pp}. E_F^n, $E_F^{P_{top}}$ and $E_F^{P_{bottom}}$ denote quasi-Fermi levels in DQW and in both (top and bottom) p-regions.

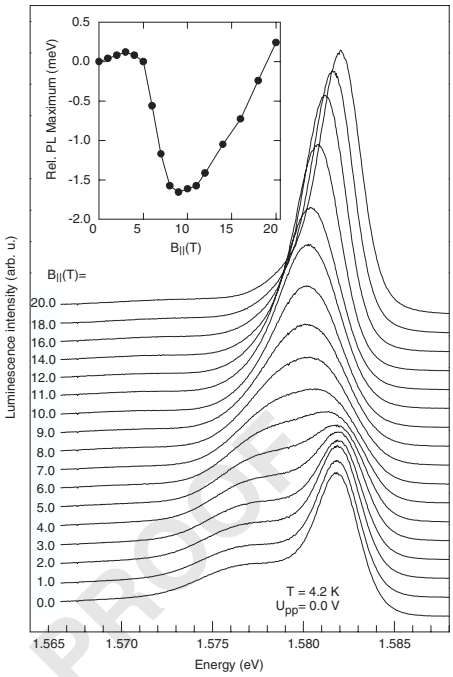

Fig. 2. PL spectra at $U_{pp} = 0.0\,V$ as a function of $B_\parallel$. The contact to DQW was not used. The inset shows $\mathcal{N}$-type kink, i.e. the relative shift of PL maximum energy with $B_\parallel$.

HL performed their calculations not only for symmetric but for asymmetric DQWs as well [4]. To induce an asymmetry in the DQW, they simply suggested applying an electric field along the sample growth direction. Fig. 3 demonstrates PL spectra as a function of bias U_{pp} at $B_\perp = 4.0\,T$. Again, no p–n bias was applied. The perpendicular orientation of the magnetic field can elucidate the changes in the occupied electron subbands, when the DQW is tilted. At a finite $B_\perp$ and $U_{pp} = 0.0\,V$ we can easily

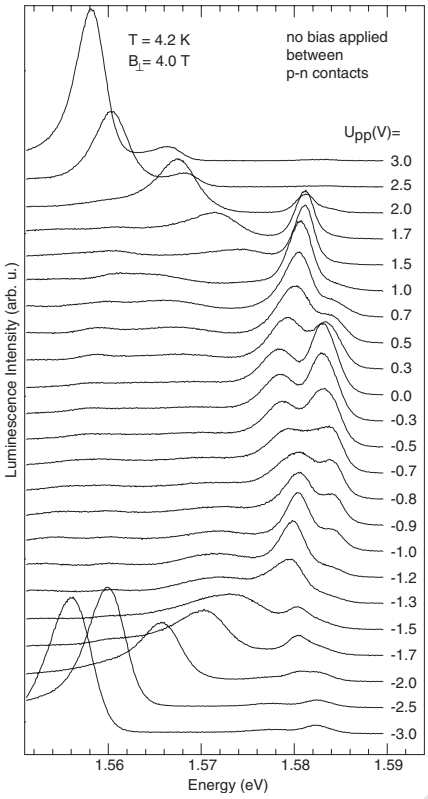

Fig. 3. PL spectra at $B_{\perp}$ as a function of U_{pp}. The contact to DQW remained disconnected.

distinguish two maxima in the PL spectrum, reflecting quantization of 2DEG into Landau levels (LL). The first maximum at the lower energy corresponds to the zeroth LL of the subband B, whereas the second one arises from the zeroth LL of the subband A and from higher LLs of the subband B. At a small bias U_{pp}, we clearly observe a gradual decrease of the upper peak intensity, even though the recombination probability for electrons in the subband A is for a tilted DQW higher than for those in the subband B. This is a consequence of the fact that even at a low bias U_{pp} holes become localized in the upper QW. The decline of the electron density, deduced from depopulation of the subband A, is also confirmed by an initial increase of the PL energy for a small bias U_{pp} due to the decrease of the electron subbands renormalization, as clearly seen in Fig. 3. At higher bias, positive or negative, the PL spectrum is dominated by a spatial indirect (interwell) recombination. Applying a bias U_{pp} also shows a good symmetry of our sample. The PL spectra obtained at positive U_{pp} correspond well to those measured at negative U_{pp} and the symmetrical configuration of the structure is achieved at a bias very close to zero, $U_{pp} \approx -0.1$ V. The main asymmetry in PL spectra was revealed for the intermediate bias $|U_{pp}| \approx 1.0$ V. The subband A is being depopulated faster and a narrower PL is observed at positive bias U_{pp}. We reckon that the main asymmetry in our structure is brought about by the one-side optical excitation and also by non-equivalent properties of GaAs/$Ga_{0.7}Al_{0.3}As$ interfaces in the DQW that results from the sample growth.

In the calculations of PL from asymmetric DQWs, HL considered a relatively large electric field applied to a symmetric DQW leading to the potential difference between the individual QW bottoms ≈ 10 meV. For the DQW with the electron density similar to the level of doping in our structures, they predicted a relatively broad PL spectrum, whose intensity on the high-energy side enhances with increasing $B_{||}$ thanks to the second minimum induced in the subband B dispersion. In order to keep the 2DEG density as high as possible in the tilted DQW we applied forward bias U_{pn}, see Fig. 1. Taking into account the sample design, the bias corresponding to the required potential drop on our DQW is slightly above $|U_{pp}| \simeq 1.0$ V. However, at this relatively high DQW tilting, the applied bias U_{pn} is not capable to supply a sufficient electron density and also leads to an inhomogeneous distribution of the 2DEG in the DQW. Therefore, we present measurements at a lower DQW tilting only. The representative PL spectra are shown in Fig. 4 as a function of $B_{\parallel}$. The DQW asymmetry was induced at bias voltages $U_{pp} = +0.4$ and $+0.6$ V in Figs. 4a and b, respectively. The electron density was enhanced by the forward bias $U_{pn} = +2.0$ V. In both cases, the in-plane magnetic field induces depopulation of the subband A and we can deduce that the PL from the subband A diminishes at lower $B_{\parallel}$ for higher U_{pp}, cf. spectra at $B_{\parallel} = 4.0$ T in Fig. 4.

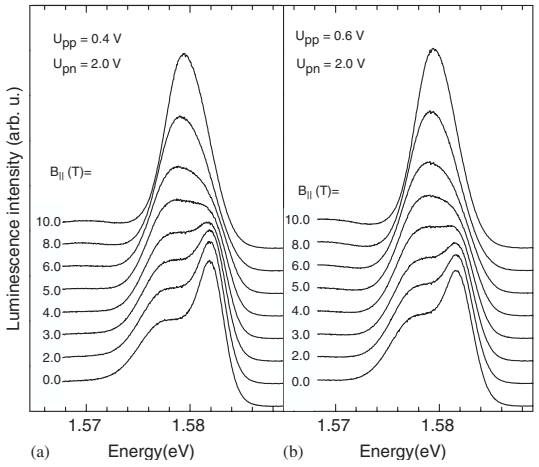

Fig. 4. PL spectra taken at $U_{pn} = 2.0$ V as a function of $B_{\parallel}$. The asymmetry of DQW was induced applying bias (a) $U_{pp} = +0.4$ V and (b) $U_{pp} = +0.6$ V.

The interpretation of the attained results must be done very cautiously. One possible explanation is that the DQW tilting increases the splitting between subband A and B, leading thus to the depopulation of subband A at lower $B_{\parallel}$. However, as discussed above, the 2DEG density gradually decreases with U_{pp}, even though a high bias U_{pn} is applied, having the same effect as the increase of the splitting. Furthermore, when both U_{pp} and U_{pn} are applied the actual tilting of DQW is hard to estimate. Hence, although the observed behavior agrees with expectations for the DQW with a slightly increased subband splitting, no definite conclusion can be drawn. Note that any optical experiment on an asymmetric DQW with 2DEG at a finite $B_{\parallel}$ has not been published up to our knowledge and there is no comparison with other results.

We reckon that the sufficient electron density in our DQW, where the asymmetry is induced by an external electric field only, is hard to achieve. Further, we suppose that similar problems can be encountered not only in our p-δn-DQW-δn-p structure but generally in other symmetric structures such as n-i-DQW-i-n structures as well. Instead, the design with a slightly asymmetric DQW doping, or better, with a DQW with different QW widths could be more appropriate. We intend to investigate this problem in future.

In conclusion, we have studied PL from a DQW with a 2DEG in in-plane magnetic fields. The spectra from a symmetric DQW exhibited the $\mathcal{N}$-type kink predicted by HL [4] and confirmed thus our previous results attained under different experimental conditions [6]. We have also performed measurements on DQWs with an electric field-induced asymmetry. These results do not allow confirmation of the effects expected by HL. A new design of structures with an asymmetric DQW with a sufficient electron density is discussed.

This work is a part of the research plan MSM 0021620834 that is financed by the Ministry of Education of the Czech Republic. M. O. acknowledges the support from Grant Agency of Charles University under Contract No. 281/2004. The high magnetic field measurements were enabled by the program "Transnational Access to Infrastructures-Specific Support Action" — Contract No. RITA-CT-2003-505474 of the European Commission.

References

[1] J.A. Simmons, S.K. Lyo, N.E. Harff, J.F. Klem, Phys. Rev. Lett. 73 (1994) 2256.
[2] O.N. Makarovskii, L. Smrčka, P. Vašek, T. Jungwirth, M. Cukr, L. Jansen, Phys. Rev. B 62 (2000) 10908.
[3] D.M. Whittaker, T.A. Fisher, P.E. Simmonds, M.S. Skolnick, R.S. Smith, Phys. Rev. Lett. 67 (1991) 887.
[4] D. Huang, S.K. Lyo, Phys. Rev. B 59 (1999) 7600.
[5] Y. Kim, C.H. Perry, J.A. Simmons, F. Klem, Appl. Phys. Lett. 77 (2000) 388.
[6] M. Orlita, M. Byszewski, G. H. Döhler, M. Grill, P. Hlídek, S. Malzer, M. Zvára, Phys. Rev. B (2005), in press.

Appendix C

Authors:	M. Orlita, R. Grill, M. Zvára, G. H. Döhler, S. Malzer, M. Byszewski, and J. Soubusta
Title:	Luminescence of coupled quantum wells: Effects of indirect excitons in high in-plane magnetic fields
Journal:	Physical Review B
Volume:	70
Year:	2004
Article Number:	075309

Luminescence of coupled quantum wells: Effects of indirect excitons in high in-plane magnetic fields

M. Orlita,* R. Grill, and M. Zvára
Institute of Physics, Charles University, Ke Karlovu 5, CZ-121 16 Prague 2, Czech Republic

G. H. Döhler and S. Malzer
Institute für Technische Physik I, Universität Erlangen-Nürnberg, D-91058 Erlangen, Germany

M. Byszewski
Grenoble High Magnetic Field Laboratory, Boîte Postale 166, F-38042 Grenoble Cedex 09, France

J. Soubusta
Joint Laboratory of Optics, Palacký University, 17. listopadu 50, CZ-772 07 Olomouc, Czech Republic
(Received 19 January 2004; revised manuscript received 5 April 2004; published 20 August 2004)

Luminescence measurements of a $Ga_{1-x}Al_xAs/GaAs$ double quantum well in in-plane magnetic fields up to 22 T are reported. The properties of spatially direct and indirect excitons are studied. We show that the strong indirect exciton luminescence survives in samples with low nonradiative recombination up to high in-plane magnetic fields. This contrasts with previously published results, where its strong suppression, observed for magnetic fields as low as of 10 T, was explained by the exciton center-of-mass momentum conservation. We attribute the discrepancy to a relatively low nonradiative recombination in the studied sample in comparison with the radiative recombination of localized indirect excitons.

DOI: 10.1103/PhysRevB.70.075309 PACS number(s): 78.67.De, 78.55.Cr, 73.21.Fg, 71.35.−y

I. INTRODUCTION

Double quantum well (DQW) represents a structure that allows for the study of basic quantum phenomena in the transition from two- (2D) to three-dimensional (3D) systems. In particular, a lot of attention has been paid to excitons, i.e., to the coupled electron-hole excitations. The DQW enables the formation of a spatially indirect exciton (IX) when an electron and a hole are located in opposite wells. The spatial separation leads to their very long lifetimes,[1,2] usually 3 orders of magnitude longer than for intrawell (direct) excitons (DX). Another special feature of excitons is their bosonic character. Thus, the gas of free excitons behaves according to Bose-Einstein statistics and in the case of long-living IXs a transition to a Bose-Einstein condensate is predicted at low temperatures. Recent experiments[1,2] in this field are very promising.

The spatial separation of electrons and holes in different wells leads in the in-plane magnetic field $B_\parallel$ to a shift of the IX ground state to a finite center-of-mass (CM) momentum in k space. Thus, the IX becomes indirect in the real, as well as in the reciprocal, space. The exciton dispersion in the DQW plane remains parabolic, but its minimum is displaced. For the magnetic field $\mathbf{B}=(0,B_\parallel,0)$ with the gauge $\mathbf{A}=(B_\parallel z,0,0)$ we get the indirect exciton dispersion,

$$E(K_x,K_y)=E_0+\frac{\hbar^2}{2M}\left[\left(K_x-\frac{eB_\parallel d}{\hbar}\right)^2+K_y^2\right], \qquad (1)$$

where d represents the center-to-center distance of wells when the intrawell Stark effect is neglected. E_0 and M denote the IX energy at rest and its in-plane mass, respectively, and e is the electron charge. For many experimental conditions, the Boltzmann statistics can be used for the description of the IX gas, instead of the Bose-Einstein distribution. Taking account of this assumption, the density of IX with CM momentum $K\approx 0$ decreases as a Gaussian function of the in-plane magnetic field: $\exp(-e^2d^2B_\parallel^2/2Mk_BT)$, where k_B is Boltzmann constant and T represents the IX gas temperature. Owing to the conservation of the particle's momentum, only the excitons with $K\approx 0$ can be optically active and thus the IX radiative recombination is strongly suppressed by the in-plane magnetic field. This effect was discussed theoretically by Gorbatsevich and Tokatly.[3] Simultaneously, the energy of IX optical transitions increases quadratically with the magnetic field by the amount of $e^2d^2B_\parallel^2/2M$. This simple model was used by Parlangeli *et al.*[4] to explain their photoluminescence (PL) measurements.[5] The authors observed the quadratic shift of the IX energy and the Gaussian suppression of the IX PL intensity with the magnetic field, and achieved a very good quantitative agreement between the simple theory and their experiment. However, the Gaussian quenching of the IX PL intensity is based on an assumption that the IX density remains unaffected by $B_\parallel$, and this is fulfilled only when the nonradiative recombination is dominant and independent of the magnetic field. Otherwise, the IX density has to increase with magnetic field, i.e., together with a decrease of the radiative recombination probability of the free IXs. The simple model is then no more valid and the IX PL intensity is governed by the variation of the radiative, as well as the nonradiative, decay rates. The IX luminescence in in-plane magnetic fields was also studied by Butov *et al.*[6] Even though the paper is primarily devoted to the time-resolved IX

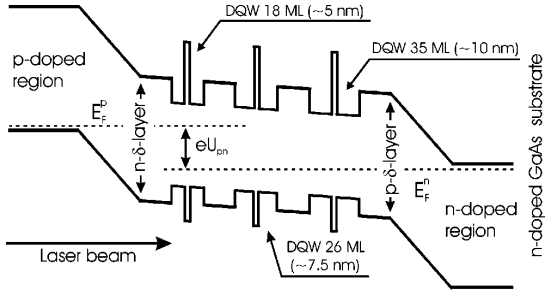

FIG. 1. The schematic picture of a sample studied under the typical operational condition $U_{pn}<0$. E_F^p and E_F^n denote Fermi level in *p*- and *n*-doped regions, respectively. Lengths are not in scale.

photoluminescence, the quadratic shift of IX energy was evaluated from time-integrated PL spectra according to $e^2d^2B_\parallel^2/2M$. Also the strong IX PL quenching was clearly observed and qualitatively described.

II. EXPERIMENT

The PL measurements were carried out on a $Ga_{1-x}Al_xAs/GaAs$ sample schematically depicted in Fig. 1, and prepared by molecular-beam epitaxy. The growth started on an *n*-doped substrate at a temperature of 600 °C with a 500-nm-wide *n*-doped GaAs region (Si, 1.4×10^{18} cm^{-3}) followed by *n*-doped and intrinsic $Ga_{0.7}Al_{0.3}As$ layers with thicknesses of 300 and 500 nm, respectively. The growth was continued with a 5-nm-thick *p*-δ layer (C, 3×10^{17} cm^{-3}) and 100 nm of an intrinsic region, both from $Ga_{0.7}Al_{0.3}As$. Afterwards, three symmetric GaAs DQWs separated always by 100 nm of $Ga_{0.7}Al_{0.3}As$ layers were added. Each DQW consists of 4 ML (ML=atomic monolayer) of AlAs central barrier separating two quantum wells with the same width of 35, 26, or 18 ML, respectively. Further $Ga_{0.7}Al_{0.3}As$ layers were grown as follows: 100-nm intrinsic, 5-nm *n*-δ layer (C, 4×10^{17} cm^{-3}), 500-nm intrinsic, and 300-nm *p* doped (C, 1.4×10^{18} cm^{-3}). The structure was closed by a 20-nm-wide *p*-doped (C, 2×10^{18} cm^{-3}) GaAs cap. The sample was photolithographically processed, i.e., the structure was mesa etched isolated and selectively contacted to the bottom *n* and top *p* regions. Hence, the DQWs can be tilted by the perpendicular electric field when a bias is applied to these contacts. Taking account of the distance of 1.45 μm between the *p* and *n* contacts, the bias change of $\Delta U_{pn}=1$ V represents the change of the electric field 6.9 kV/cm on the DQW. The compensating δ layers allow us to achieve a DQW flatband position for a relatively small bias voltage.

The sample was excited by a Ti:sapphire laser with the power density ~100 mW/cm^2 at the photon energy 1.75 eV, i.e., below the band gap of $Ga_{0.7}Al_{0.3}As$ at low temperature. Fiber optics were used for the excitation, as well as for the signal collection. The PL spectra were analyzed by a single-grating monochromator and detected by a cooled charge coupled camera. The helium bath cryostat that we used ensured a good temperature stability at 4.2 K. All measurements were performed in a resistive solenoid in the Voigt configuration up to the magnetic field of 22 T.

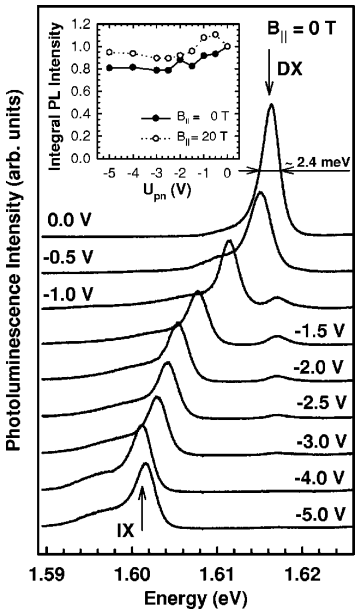

FIG. 2. PL spectra for selected negative bias at zero magnetic field. The corresponding voltages are indicated. The inset depicts integral PL intensity vs applied bias for $B_\parallel=0$ and $B_\parallel=20$ T. The values in the inset are normalized to zero bias for both magnetic fields.

III. RESULTS AND DISCUSSION

Figure 2 shows the PL spectra for selected values of bias U_{pn} taken at $B_\parallel=0$. The depicted spectra, as well as others presented in this paper, are related to the 18-ML-wide ($\approx$5 nm) DQW only. The remaining wells exhibited similar results. The applied U_{pn} tilts the DQW and a characteristic redshift of IX (interwell) transition for the increasing negative bias is observed, whereas the DX energy remains almost unaffected. These results are analogous to those published previously,[7] where PL of the same structure was studied at higher temperatures. The flatband regime was observed for a small forward bias $U_{pn}\simeq+0.5$ V, where more complex PL spectra were obtained, probably related to the formation of charged excitons-trions (not shown in this paper). These charged complexes were also identified in the PL spectra of the 35-ML ($\approx$10 nm) DQW in this sample under different experimental conditions.[8] For the bias in the range of $-3.0\text{ V}<U_{pn}<-1.0$ V, both IX and DX transitions are present in the PL spectra. The IX redshift is saturated for $U_{pn}<-4.0$ V. This effect can be explained by a screening of the external electric field caused by IXs with sufficiently high density n_{IX}. The fact that this saturation point appears in different DQWs for other bias U_{pn}, and that the energy of the

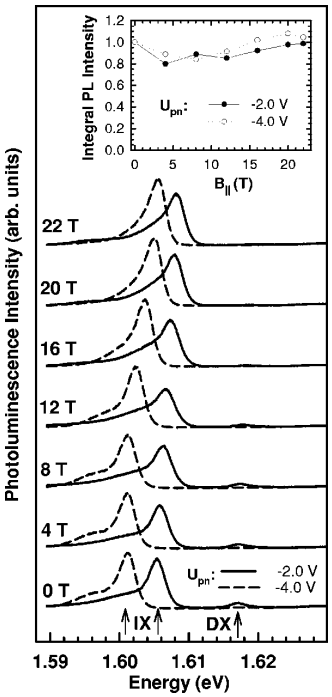

FIG. 3. The PL spectra in the dependence on the in-plane magnetic fields $B_\parallel$ for two selected biases, −2.0 and −4.0 V. The corresponding fields $B_\parallel$ are depicted near the curves. The inset shows the total PL intensity; values are normalized to zero magnetic field. The temperature was T_{bath}=4.2 K.

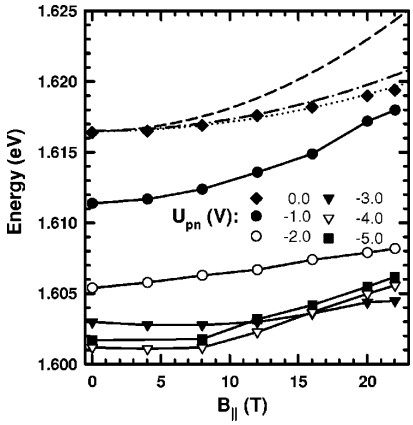

FIG. 4. The exciton peak energy for selected bias U_{pn}. The dotted line shows the parabolic DX shift 0.0065 meV/$T^2\times B_\parallel^2$. The dashed and dash-dotted lines represent the theoretical IX energy shift according to $e^2d^2B_\parallel^2/2M$ for the exciton mass $0.21m_0$ and $0.42m_0$, respectively. Other lines serve as a guide for the eye only.

IX transition strongly depends on excitation intensity (not shown in this paper), supports this interpretation. The simple formula for the electric field in a plate capacitor $en_{\mathrm{IX}}/\epsilon_0\epsilon_r$, where ϵ_0 and ϵ_r are the vacuum and relative permittivities, respectively, allows us to estimate the lower limit of IX concentration $n_{\mathrm{IX}}\gtrsim 5\times 10^{10}$ cm^{-2} for $U_{pn}\lesssim -4.0$ V. The inset of Fig. 2 contains the integral PL intensity for $B_\parallel=0$ and 20 T as a function of U_{pn}, normalized to $U_{pn}=0$. The integral intensity remains close to unity even for higher negative bias, when the radiative recombination lifetime of the IX is strongly enhanced. Hence, we can conclude that the nonradiative recombination rate is very small in comparison to the radiative one. The dominant radiative recombination and also the small full width at half maximum (FWHM) ~2 meV of the DX peak at 4.2 K (for IX FWHM=2.5–4 meV) are parameters that are characteristic for good quality samples, and thus the PL spectra can be compared to those published in Refs. 4 and 6.

Figure 3 summarizes the PL spectra measured in in-plane magnetic fields of up to $B_\parallel=22$ T for $U_{pn}=-2.0$ and −4.0 V. The integral intensities of these spectra have been plotted in the inset of this figure. The magnetic field $B_\parallel$ causes a blueshift of the IX peak, but no intensity degradation is present, contrary to previously published results.[4–6] Moreover, the PL of direct excitons declines relatively to the IX peak. For comparison, we can estimate the Gaussian suppression of IX peak intensity according to the simple model[4] sketched in the Introduction. However, we stress that its validity conditions are not fulfilled for our sample with a low nonradiative decay rate. The estimated intensity decrease at $B_\parallel=20$ T then varies within an interval of 10^2–10^8, due to the uncertainty in the exciton mass and the IX temperature. The values $M=0.42m_0$ and $0.21m_0$ (m_0 is the bare electron mass) were used for the exciton mass in Refs. 4 and 6, respectively, and in both cases in agreement with their experiments. The IX temperature is possibly higher than the lattice temperature T_{latt}=4.2 K, but we suppose that the temperature does not exceed 10 K, owing to high cooling rates of indirect excitons.[2]

We will now show that apart from the nonradiative and free IX recombination, another radiative recombination channel must be present to explain our measurements. As is shown in the insets of Figs. 2 and 3, the integral PL intensities are almost magnetic-field independent and are influenced only weakly by the applied electric field. Hence, the nonradiative recombination must be small. The probability of free IX radiative recombination with $K\approx 0$ is nearly magnetic-field independent[4] and thus the intensity of the IX peak is governed predominantly by the number of IXs at the corresponding energy level. If no other radiative channel were present, an increase of the IX density n_{IX} by the factor $\exp(e^2d^2B_\parallel^2/2Mk_BT)$ would be necessary to maintain the integral PL intensity constant. However, such a high IX density (more than 10^{12} cm^{-2} at $U_{pn}\lesssim -4.0$ V in higher magnetic fields) would cause a strong effective screening of the external electric field, resulting in a decrease of DQW tilting, and thus also in a strong blueshift of the IX peak. This is in contradiction with the experimentally determined IX maxima depicted in Fig. 4 for several values U_{pn}. Hence, the IX

luminescence observed in high in-plane magnetic fields cannot be related to the recombination of optically active free IXs (i.e., with the CM momentum $K \approx 0$) only. Therefore, another radiative recombination channel must be found. Although the repulsive interaction between IXs partially screens the potential fluctuations,[2] we suppose that the localization of the IXs plays a crucial role in the recombination process. In high magnetic fields, when the optical recombination of IX with a nonzero CM momentum is forbidden, the radiative recombination of localized IXs becomes dominant, whereas the nonradiative channel still seems to be negligible. The localized IX wave function is widely spread in the k space. Hence, the CM momentum conservation can be relaxed. The IX CM localization within the radius of 5 nm corresponds to the spread of wave function $\Delta K \approx 0.2$ nm^{-1} that is comparable with the shift $K_0 = edB_\parallel/\hbar$ of the IX dispersion parabola (1) induced by the in-plane magnetic field $B_\parallel \approx 20$ T. So we assume that a certain number of IXs becomes localized and therefore optically active also in high magnetic fields. This localization seems to be present, although our sample shows properties characteristic for a high quality structure. We interpret this fact as a result of a very low nonradiative recombination rate that leads to an enhancement of IX lifetime and thus supports the IX localization. So, the very low nonradiative recombination rate in our structure seems to be responsible for results different from those published previously.[4–6]

A clearly noticeable feature of our luminescence spectra is the low-energy tail of the IX peak developing with increasing magnetic field. We suppose that it is related to lower-lying localized IX states. We think that this interpretation is also supported by the PL measurements in Ref. 6, where a strong damping of the (unbound) IX peak in higher magnetic fields was observed while the low-energy tail survived. However, this effect was not discussed in detail there.

Some attention should be paid to Fig. 4. The peak maximum shift for $U_{pn} = 0.0$ V, i.e., for DX transition, is approximately quadratic in magnetic field, $\Delta E = 0.0065$ meV/T$^2 \times B_\parallel^2$, and corresponds to the commonly observed diamagnetic shift[4,5] of a DX. The shift for $U_{pn} = -1.0$ V is significantly higher, but this is caused by the mixing between the IX and DX states induced by $B_\parallel$. The PL maxima for $U_{pn} \leqq -2.0$ V correspond to the pure IX transition. The measured IX peak shifts can be compared to theoretical curves for free IXs, simultaneously plotted in Fig. 4. These curves were obtained using the formula $e^2d^2B_\parallel^2/2M$ for the electron-hole distance $d = 22$ ML (≈ 6.2 nm) and for two different values of the exciton mass[4,6] $M = 0.42m_0$ and $0.21m_0$. For comparison, the DX transition was chosen as the reference energy. Evidently, the IX maxima do not follow this simple quadratic dependence. Instead, the observed IX shift at $B_\parallel$ depends on the applied bias and is smaller for $U_{pn} = -2.0$ and -3.0 V than expected from theoretical curves. We relate this behavior to the IX localization and assume that the IX shift mainly represents the change in IX localization energy with the in-plane magnetic field. Also, slight but complex changes in the radiative recombination time of localized IX induced by the electric and magnetic fields can be expected. Because of the almost constant integrated PL intensity and the very low nonradiative recombination, the lifetime change affects predominantly the IX density. This effect becomes important close to the saturation point $U_{pn} \lesssim -4.0$ V, where the small changes in the IX density probably lead to different screenings of the external electric field and thus to different IX peak shifts. This can be clearly seen at $B_\parallel > 12$ T, when the PL maxima for $U_{pn} = -4.0$ and -5.0 V appear at a higher energy than for $U_{pn} = -3.0$ V. This blue shift of IX energy could be also supported by a possible charging of the DQW due to an exciton dissociation and electron tunneling out of the structure. Thus, although the shift for $U_{pn} = -4.0$ and -5.0 V is roughly comparable to the theoretical shift for the exciton with the mass $M = 0.42m_0$, we assume that it is of another origin than the plotted theoretical curve.

The shift of IX maxima with $B_\parallel$ should be compared to the results published by Butov *et al.*[9] They determined the IX mass as a function of the perpendicular magnetic field from the quadratic shift of the IX peak in the additionally applied magnetic field in the in-plane direction. They based the exciton mass evaluation on the simple relation $e^2d^2B_\parallel^2/2M$. In our case, owing to the localization of indirect excitons, the IX peak shift is influenced by the magnetic- and electric-field-induced changes of their localization energy and is smaller than the shift of free IX energy observed by Butov *et al.*[9] Using of the simple formula would thus lead to an overestimation of the IX mass.

IV. CONCLUSION

We have shown that the IX peak can survive in PL spectra of good quality sample even in high in-plane magnetic fields. The low rate of nonradiative recombination supports the localization of long-living IXs that enables their radiative recombination also in high magnetic fields. On the contrary, the higher nonradiative recombination rate reduces the time available for the IX localization and thus effectively decreases the probability of radiative recombination in high in-plane magnetic fields.[4]

We conclude that the dominating radiative recombination of localized indirect excitons does not allow us to observe the quenching of IX luminescence and the quadratic shift of their energy in the in-plane magnetic field that were reported in Refs. 4–6 and 9. The possibility of an exciton dispersion engineering[4,6,10] would then be limited in these kinds of samples.

ACKNOWLEDGMENTS

This work has been done within the research program, MSM113200002, financed by the Ministry of Education of the Czech Republic. M. O. acknowledges support from DAAD (German Academic Exchange Service, Bonn) and R. G., the support from the Alexander von Humboldt Foundation (AvH, Bonn, Germany). The high magnetic-field measurements were enabled by the program "Access to Research Infrastructure Action of the Improving Human Potential Programme" of EC.

*Electronic address: orlita@karlov.mff.cuni.cz

[1] L. V. Butov, C. W. Lai, A. L. Ivanov, A. C. Gossard, and D. S. Chemla, Nature (London) **417**, 47 (2002).
[2] L. V. Butov, A. C. Gossard, and D. S. Chemla, Nature (London) **418**, 751 (2002).
[3] A. A. Gorbatsevich and I. V. Tokatly, Semicond. Sci. Technol. **13**, 288 (1998).
[4] A. Parlangeli, P. C. M. Christianen, J. C. Maan, I. V. Tokatly, C. B. Soerensen, and P. E. Lindelof, Phys. Rev. B **62**, 15 323 (2000).
[5] A. Parlangeli, P. C. M. Christianen, J. C. Maan, C. B. Soerensen, and P. E. Lindelof, Phys. Status Solidi A **178**, 46 (2000).
[6] L. V. Butov, A. V. Mintsev, Y. E. Lozovik, K. L. Campman, and A. C. Gossard, Phys. Rev. B **62**, 1548 (2000).
[7] J. Soubusta, R. Grill, P. Hlídek, M. Zvára, L. Smrčka, S. Malzer, W. Geißelbrecht, and G. H. Döhler, Phys. Rev. B **60**, 7740 (1999).
[8] M. Zvára, R. Grill, P. Hlídek, M. Orlita, and J. Soubusta, Physica E (Amsterdam) **12**, 335 (2002).
[9] L. V. Butov, C. W. Lai, D. S. Chemla, Y. E. Lozovik, K. L. Campman, and A. C. Gossard, Phys. Rev. Lett. **87**, 216804 (2001).
[10] K. Chang and F. M. Peeters, Phys. Rev. B **63**, 153307 (2001).

Appendix D

Authors:	M. Orlita, M. Byszewski, G. H. Döhler, R. Grill, S. Malzer, J. Soubusta, and M. Zvára
Title:	Luminescence of indirect excitons in high in-plane magnetic fields
Journal:	Physica E
Volume:	30
Year:	2005
Pages:	1–6

Available online at www.sciencedirect.com
SCIENCE DIRECT®
Physica E 30 (2005) 1–6
PHYSICA E
www.elsevier.com/locate/physe

Luminescence of indirect excitons in high in-plane magnetic fields

M. Orlita[a,*], M. Byszewski[b], G.H. Döhler[c], R. Grill[a], S. Malzer[c], J. Soubusta[d], M. Zvára[a]

[a]*Faculty of Mathematics and Physics, Institute of Physics, Charles University, Ke Karlovu 5, CZ 121 16 Prague 2, Czech Republic*
[b]*Grenoble High Magnetic Field Laboratory, Boîte Postale 166, F 38042 Grenoble, Cedex 09, France*
[c]*Institut für Technische Physik I, Universität Erlangen-Nürnberg, D 91058 Erlangen, Germany*
[d]*Joint Laboratory of Optics, Palacký University, 17. listopadu 50, CZ 772 07 Olomouc, Czech Republic*

Received 3 February 2005; accepted 20 April 2005
Available online 6 September 2005

Abstract

We report on low-temperature magneto-luminescence measurements of biased $Ga_{1-x}Al_xAs/GaAs$ double quantum well structures. The luminescence of spatially indirect excitons (IX) is studied up to the magnetic field of 22 T. In contradiction to theoretical predictions and their several experimental confirmations, the IX line survives in PL spectra of our double quantum well structure up to high in-plane magnetic fields. We explain this difference by the IX localization which enables the relaxation of the IX in-plane momentum, whose conservation is responsible for the damping of the IX luminescence intensity observed by other groups. This localization is supported by a relatively weak non-radiative recombination in comparison to the radiative one observed in our double quantum well structure. The IX luminescence was studied under various excitation intensities to obtain deeper insight into the IX localization mechanism. This paper confirms and broadens our previously published results obtained from a double quantum well structure of other width.

PACS: 78.67.De; 78.55.Cr; 73.21.Fg; 78.20.ls

Keywords: Double quantum well; Indirect exciton; In-plane magnetic field

1. Introduction

A special feature of double quantum well (DQW) structures is the formation of a spatially indirect exciton (IX) under an applied electric field. This quasi-particle consists of an electron and a hole localized in neighboring quantum wells resulting in a small overlap of their wave functions. Therefore, IXs are characterized by a very long lifetimes, up to hundreds of nanoseconds, i.e. three orders of magnitude longer in comparison with spatially direct excitons (DX) in bulk or in a single quantum well [1]. Their extremely long lifetime, bosonic character and also low effective mass are key features for a potential Bose–Einstein condensation at liquid helium temperatures. This effect became a subject of an intensive research within recent years and has led to promising results published in Refs. [2,3].

A lot of attention has also been paid to IX properties in in-plane magnetic fields $B_{\parallel}$. Theoretical works, e.g. Ref. [4], predicted a gradual quenching of IX luminescence intensity with increasing magnetic field, accompanied by a quadratic increase of IX recombination energy. This was soon confirmed in photoluminescence (PL) experiments carried out independently by two groups [5–7]. The IX PL quenching is based on two features — on the shift of the IX in-plane dispersion minimum out from the zero point of the reciprocal space, proportional to the magnetic field $B_{\parallel}$ and on the IX in-plane momentum conservation in optical recombination [5,7]. A simple model was suggested and applied by Parlangeli et al. [7]. In this model, two main assumptions are made: the IX density is independent of the applied magnetic field and the IX gas obeys the Boltzmann statistics. The first assumption is fulfilled in samples with a strong non-radiative recombination that is independent of $B_{\parallel}$ and the second one is valid at low IX densities when Bose–Einstein statistics can be replaced by the Boltzmann distribution. Under these conditions, a Gaussian damping

*Corresponding author. Tel.: +420221911320; fax: +420224922797.
E-mail address: orlita@karlov.mff.cuni.cz (M. Orlita).

1386-9477/$ - see front matter © 2005 Elsevier B.V. All rights reserved.
doi:10.1016/j.physe.2005.04.014

of IX PL intensity can be experimentally indicated by

$$I \propto \exp\left(-\frac{e^2 d^2 B_{\parallel}^2}{2Mk_B T}\right) \quad (1)$$

together with an increase of IX recombination energy by amount of $e^2d^2B_{\parallel}^2/2M$. Here, M and d represent the exciton mass and center-to-center distance of the wells in the DQW, respectively. T is the IX gas temperature.

In this paper, we deepen the study of the IX luminescence published in Ref. [8], where no damping of IX line intensity was observed up to high in-plane magnetic fields and where IX localization leading to the exciton momentum relaxation was discussed. Here, we present spectra measured on a DQW structure of a different well width that exhibits similar behavior. The PL is studied under various excitation intensities in order to gain more information about IX localization. We show that the simple model applied by Parlangeli et al. [7] is not adequate for our DQW structures.

2. Experiment

The PL measurements were carried out on a $Ga_{1-x}Al_xAs/GaAs$ sample schematically depicted in Fig. 1, grown by molecular beam epitaxy. The growth started on an n-doped substrate at a temperature of 600 °C with a 500 nm-wide n-doped GaAs region (Si, $1.4\times10^{18}\,cm^{-3}$) followed by n-doped and intrinsic $Ga_{0.7}Al_{0.3}As$ layers with a thickness of 300 nm and 500 nm, respectively. The growth was continued with a 5 nm thin p-layer (C, $3\times10^{17}\,cm^{-3}$) and 100 nm of an undoped region, both of $Ga_{0.7}Al_{0.3}As$. Afterwards, three symmetric GaAs DQWs, each separated by 100 nm of $Ga_{0.7}Al_{0.3}As$ layers were added. The DQWs consist of 4 ML (ML = atomic monolayer) AlAs central barrier separating two quantum wells of equal width of 35 (≈ 10 nm), 26 (≈ 7.5 nm) or 18 ML (≈ 5 nm), respectively. Further $Ga_{0.7}Al_{0.3}As$ layers were grown as follows: 100 nm intrinsic, 5 nm n-layer (C, $4\times10^{17}\,cm^{-3}$), 500 nm intrinsic and 300 nm p-doped (C, $1.4\times10^{18}\,cm^{-3}$). The structure was capped by a 20 nm-wide p-doped (C, $2\times10^{18}\,cm^{-3}$) GaAs-layer. The sample was processed photolithographically by mesa etching, insulation, and selective contacting to the bottom n-region and to the top p-region. The DQWs can be tilted by the perpendicular electric field when a bias is applied to p–n contacts. Taking into account the distance of 1.45 μm between p- and n-contact, the bias change of $\Delta U_{pn} = 1$ V should correspond to a variation of the electric field of 6.9 kV/cm in the DQW. The thin n- and p-layers screen the built-in field and allow for a zero-field situation in the DQWs for a relatively small bias voltage.

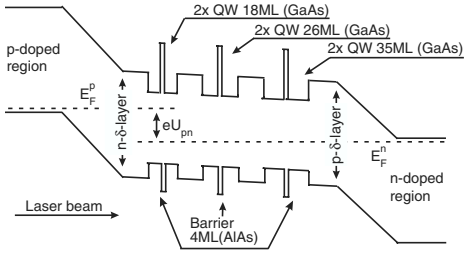

Fig. 1. Schematic bandstructure of the investigated sample. Symbols E_F^p and E_F^n denote the quasi-Fermi level in the p- and n-regions, respectively. Thicknesses of layers are not drawn to scale.

The sample was excited by a Ti:sapphire laser at a photon energy of 1.75 eV, i.e. below the band gap of $Ga_{0.7}Al_{0.3}As$ at low temperature. The standard intensity I_0 was about $\sim100\,mW/cm^2$. The PL signal was collected with an optical fiber, dispersed in a double-grating monochromator and detected by a cooled charge coupled camera. A helium bath cryostat was used to ensure a good temperature stability at 4.2 K. All measurements were performed in a resistive solenoid in the Voigt configuration up to a magnetic field of 22 T.

3. Results and discussion

In this paper, we focus our attention on IX PL gained from the 26-ML DQW in in-plane magnetic fields for various excitation intensities. All the results are discussed with respect to those published previously [8], where solely spectra from the 18-ML DQW were presented. Fig. 2 shows the PL spectra at $B_{\parallel} = 0$ T as a function of the applied voltage U_{pn}. We observe a typical shift of the IX peak to lower energies with increasing negative bias U_{pn}. As can be inferred from Fig. 2, the flat-band regime was achieved for small forward bias $U_{pn} = +0.5 - 1.0$ V. The complex shape of the PL peak close to the flat-band regime is probably governed by effects due to the formation of charged excitons (trions) that will require a further study. The upper inset of Fig. 2 contains the integral PL intensities for 26-ML DQW, normalized to the value at $U_{pn} = 0.0$ V. The IX peak related to 26-ML DQW overlaps with DX transitions in the 35-ML DQW for a bias voltage between $U_{pn} = -4.8$ and -5.0 V. Therefore, the corresponding integral PL intensities are rough estimations there. The IX PL integral intensity remains close to unity also for higher negative bias U_{pn} where the IX radiative lifetime should be strongly enhanced. Hence, the radiative recombination dominates in this DQW while non-radiative channels are relatively weak. This is in agreement with our observations on the 18-ML DQW [8].

The luminescence spectra taken at the standard excitation intensity I_0 in the in-plane magnetic field for the bias voltage in the range from $U_{pn} = -4.0$ to -4.9 V are depicted in Fig. 3a–c. The spectra in Fig. 3a measured at $B_{\parallel} = 6.0$ T show a relatively narrow IX line (FWHM ≈ 3–4 meV), narrower than in zero magnetic field (cf. to Fig. 2). The magnetic field also partially suppresses the low-energy tail, which is well pronounced at zero magnetic field. No intensity decline comparing to $B_{\parallel} = 0$ T was noted. The IX PL is clearly observed also at $B_{\parallel} = 12.0$ and

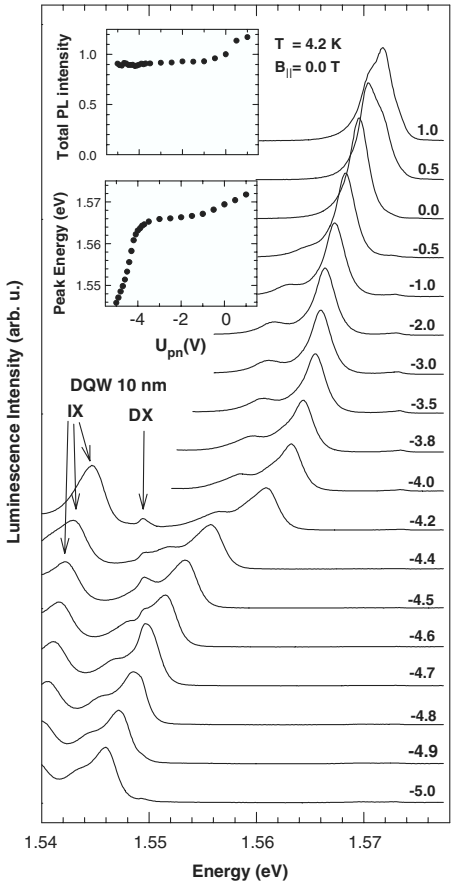

Fig. 2. PL spectra from 26-ML DQW at zero magnetic field. The applied bias U_{pn} is given at each curve. A standard excitation intensity I_0 was used. The lower inset shows the energy of the PL maximum in dependence on the bias U_{pn}. The corresponding integral PL intensities are depicted in the upper inset, values are normalized to $U_{pn} = 0.0$ V.

18.0 T, the PL peak intensity declines significantly but the integral IX PL intensity is not damped so strongly due to the evident peak broadening. Note that the simple model used by Parlangeli et al. [7] predicts according to relation (1) a strong IX PL damping for the field as low as $B_{\|} = 6.0$ T and the IX peak should practically diminish at $B_{\|} > 10.0$ T. However, this model is not adequate in our structure with a dominating radiative recombination. The absence of a strong IX peak intensity damping suggests that the observed IX line does not originate from the recombination of free IXs. We have already discussed this problem in connection with previously published results from 18-ML DQW in Ref. [8], where the IX localization was chosen as the most probable mechanism allowing the IX recombination.

This finding gave us a motivation for the study of PL at lower excitation intensities to obtain further information about IX localization. The results are presented in Fig. 4a–c for intensities $I = 0.5I_0$, $0.1I_0$ and $0.05I_0$, respectively. Whereas the difference in the spectra gained for intensities I_0 and $0.5I_0$ is not significant (cf. Fig. 3a and Fig. 4a), the further lowering of excitation intensity causes a clear IX peak broadening.

Similar effects have already been observed by Larionov et al. [9] at zero magnetic field, where the broad IX line at low excitation intensity was assigned to the PL of IXs strongly localized in potential fluctuations. The appearance of a relatively narrow IX peak at higher excitation intensity was associated with delocalized IXs there. Further, a significant collective behavior of delocalized IXs was stressed in order to explain an abrupt decrease of the IX line width with increasing excitation intensity and also strong temperature dependence of the observed effects.

Basically, our results exhibit behavior similar to the one observed by Larionov et al. [9], i.e. the broad IX line at low excitation intensity, which becomes narrower with increasing excitation power. However, the narrowing of IX line in our experiment appears gradually with increasing power and also an approximately linear increase of the IX PL intensity is observed instead of a superlinear course mentioned there. Likewise in Ref. [9], we relate the broad IX PL line at low excitation intensity to the PL from strongly localized IXs states. On the other hand, the narrow IX line at the standard excitation intensity I_0 cannot in our case correspond to the recombination of free (delocalized) IXs due to the above-mentioned absence of its damping with increasing in-plane magnetic field. Therefore, possible mechanisms of the in-plane momentum relaxation must be discussed. In principle, there are three ways of the IX momentum relaxation: (i) exciton–phonon interaction, (ii) exciton–exciton interaction, and (iii) exciton localization or collisions with structural defects. We reject the mechanism (i) because it characterizes PL constantly in all similar structures and thus cannot explain the discrepancy between our results and those published by other groups [5,7]. For the same reason we cannot accept the exciton–exciton interaction as a mechanism of the momentum relaxation because the IXs density and thus also exciton–exciton interaction strength in our sample seems to be similar to that in other experiments [5,7] that clearly showed the IX line damping with $B_{\|}$. The last mechanism (iii) seems to be the most probable to explain our results. At low intensities, IXs recombine localized at potential fluctuations of various depths resulting in a wide PL peak. At increased excitation power, the deep localization centers are largely occupied due to the finite lifetime of localized IXs and further occupation of these states is not allowed by the repulsive exciton–exciton (dipole–dipole) interaction. The enhanced IX density then results in dominant population of shallow localization centers with a weaker dispersion of the localization potential, which leads to the formation of a well-enhanced PL peak. The existence of shallow localization centers also intensifies the radiative recombination, which corresponds

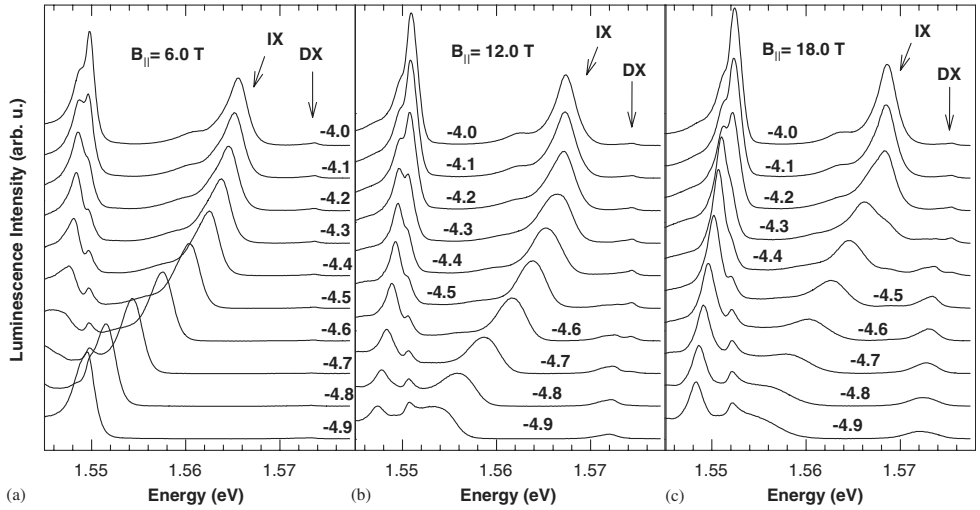

Fig. 3. The IX luminescence of 26-ML DQW at in-plane magnetic field (a) $B_{\parallel} = 6.0\,\mathrm{T}$, (b) 12.0 T and (c) 18.0 T for the bias between $U_{\mathrm{pn}} = -4.0$ and $-4.9\,\mathrm{V}$. The standard excitation intensity I_0 was used.

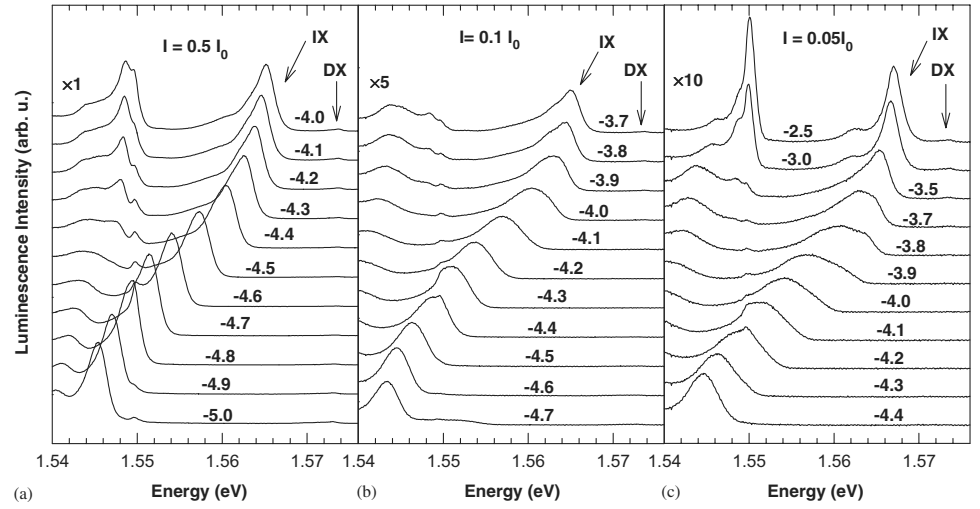

Fig. 4. PL spectra taken from 26-ML DQW at $B_{\parallel} = 6.0\,\mathrm{T}$ for excitation intensities $I =$ (a) $0.5I_0$, (b) $0.1I_0$ and (c) $0.05I_0$. PL intensities in parts (b) and (c) were multiplied by the factor of 5 and 10, respectively. The corresponding bias U_{pn} is indicated at each curve.

to the low non-radiative recombination rate discussed above.

We suppose that the presence of potential fluctuations leading to the IX localization does not contradict our observation of the low non-radiative recombination rate. All discussed IX states, whose localization was denoted above either as deep or shallow one, have a localization energy that owing to our experimental results does not significantly exceed 10 meV and hence, they are bound very weakly in comparison with the band gap energy. These weakly bound states do not themselves implicate strong non-radiative recombination channels, which are usually linked to states situated deep in the band gap (e.g. EL2 centers [10]).

A noticeable feature of IX PL is its non-linear redshift with applied bias (see lower inset in Fig. 2). A slow IX redshift for the lower negative bias becomes much steeper for higher negative voltages $U_{\mathrm{pn}} < -3.5\,\mathrm{V}$. The non-linear redshift is likely a result of the sample complexity. The current flowing through the p-i-n junction can affect the charge neutrality of each DQW and thus leads to a non-uniform distribution of the external electric field in

different parts of the structure. Even though the laser photon energy lies below the band gap of $Ga_{0.7}Al_{0.3}As$, the observed current was obviously induced by the optical excitation, enabled by the Franz–Keldysh absorption. We suppose that the charge accumulation in the 18-ML and 35-ML DQWs results in the screening of the external electric field on 26-ML DQW in the middle of the structure. The screening is less effective for the higher negative bias ($U_{pn} < -3.5$ V), probably due to the enhanced tunneling of carriers from the left and right DQWs. This leads to the abrupt increase of IX redshift, as can be seen in the lower inset in Fig. 2. The value of ≈ 15 meV of the IX redshift corresponding to the change of the applied bias from $U_{pn} = -4.0$ to -5.0 V, exceeds the value of 6 meV, which was roughly estimated from the sample design. Further support for this interpretation provide the measurements presented in Fig. 4a–c. The same value of the IX redshift and thus the same actual electric field in the 26-ML DQW was achieved at low excitation intensities for the lower negative bias voltages U_{pn} (cf. Fig. 4a with Fig. 4b,c). Hence, the polarization of the internal structure given by charging of 18-ML and 35-ML DQW at low excitation intensities is weakened by the strong decrease of the flowing photocurrent. We conclude that the actual electric field in the 26-ML DQW cannot be calculated directly from the applied bias and the distance of the p- and n-layers, but must be estimated from the value of the IX peak position with respect to the DX energy. The effects of DQWs charging were also mentioned in Ref. [8], but the PL from 18-ML DQW was less sensitive to the charge redistribution in the sample than the PL from the 26-ML DQW located in the middle of the sample structure.

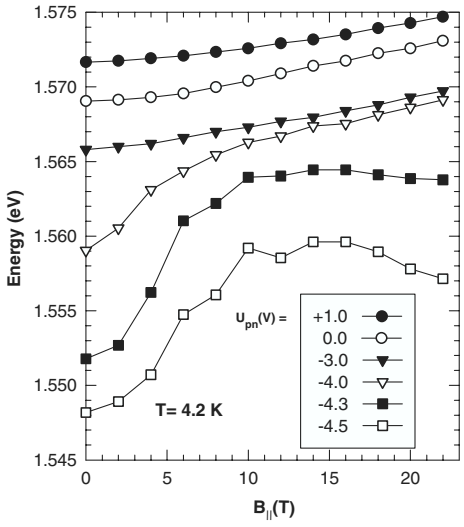

Fig. 5. PL maxima energy for 26-ML DQW as a function of the in-plane magnetic field $B_\parallel$ for several values of bias U_{pn}. The excitation intensity was $0.5I_0$. Lines serve only as a guide to the eye.

The effects of the charge redistribution in DQWs are also illustrated in Fig. 5, where the energy of PL maximum is plotted as a function of $B_\parallel$ for several values of bias U_{pn}. In case of localized IXs, a blueshift of IX peak with $B_\parallel$ is expected, which is lower than the quadratic blueshift $e^2d^2B_\parallel^2/2M$ reported for free IXs [5,7,11]. Instead, the blueshift of IX line for bias $U_{pn} < -3.0$ V in the interval $B_\parallel = 0$–5 T, even significantly, exceeds value $\sim$0.8 meV estimated at $B_\parallel = 5.0$ T for free IXs. The in-plane exciton mass $M = 0.21m_0$ was taken after Butov et al. [5] in this estimation (m_0 is the bare electron mass). Moreover, a redshift of IX peak is present for $U_{pn} = -4.5$ V at higher in-plane magnetic fields. Thus we conclude that the observed dependence of IX peak energy on $B_\parallel$ cannot be simply related to the blueshift of localized or free IXs. We suppose that the complex behavior is given by the charge accumulation in outlying 18-ML and 35-ML DQWs discussed in the previous paragraph, which is further influenced by $B_\parallel$. The photocurrent, leading to an excess of holes or electrons in DQWs, flows in the direction perpendicular to the in-plane magnetic field and thus its magnitude monotonically decreases with $B_\parallel$. This likely results in a consequent change of the total charge accumulated in 18-ML or 35-ML DQWs affecting strongly the actual electric field on the 26-ML DQW.

4. Conclusion

The photoluminescence study of our 26-ML DQW in an in-plane magnetic field has shown that a strong PL of IXs survives even in magnetic fields as high as 22 T. Hence, DQW structures of different widths show a behavior analogous to those previously published [8]. This is explained based on the assumption that IXs are localized in potential fluctuations allowing a relaxation of the momentum conservation in optical recombination. This localization is probably supported by a low non-radiative recombination rate in our structures in comparison with the radiative one. The effect of the IX localization was further studied under various excitation intensities. The low-excitation intensity measurements revealed a broadening of the IX emission line corresponding to the localization of IXs in potential fluctuations with a wide range of depths whereas the higher intensity led to a relatively narrow IX line reflecting IX localization in shallow potential fluctuations only.

Acknowledgements

This work is a part of the research plan MSM0021620834 that is financed by the Ministry of Education of the Czech Republic. The high magnetic field measurements were enabled by the program Access to Research Infrastructure Action of the Improving Human Potential Programme of EC.

References

[1] L.V. Butov, C.W. Lai, A.L. Ivanov, A.C. Gossard, D.S. Chemla, Nature 417 (2002) 47.
[2] L.V. Butov, A.C. Gossard, D.S. Chemla, Nature 418 (2002) 751.
[3] L.V. Butov, L.S. Levitov, A.V. Mintsev, B.D. Simons, A.C. Gossard, D.S. Chemla, Phys. Rev. Lett. 92 (2004) 117404.
[4] A.A. Gorbatsevich, I.V. Tokatly, Semicond. Sci. Technol. 13 (1998) 288.
[5] L.V. Butov, A.V. Mintsev, Y.E. Lozovik, K.L. Campman, A.C. Gossard, Phys. Rev. B 62 (2000) 1548.
[6] A. Parlangeli, P.C.M. Christianen, J.C. Maan, C.B. Soerensen, P.E. Lindelof, Phys. Status Solidi A 178 (2000) 46.
[7] A. Parlangeli, P.C.M. Christianen, J.C. Maan, I.V. Tokatly, C.B. Soerensen, P.E. Lindelof, Phys. Rev. B 62 (2000) 15323.
[8] M. Orlita, R. Grill, M. Zvára, G.H. Döhler, S. Malzer, M. Byszewski, J. Soubusta, Phys. Rev. B 70 (2004) 075309.
[9] A.V. Larionov, V.B. Timofeev, J. Hvam, C. Soerensen, JETP Lett. 71 (2000) 117.
[10] M. Kaminska, E.R. Weber, Imperfections in III/V Materials, in: R.K. Willardson, A.C. Beer, E.R. Weber (Eds.), Semiconductors and Semimetals, vol. 38, Academic Press, New York, 1993, p. 59 (Chapter 2).
[11] L.V. Butov, C.W. Lai, D.S. Chemla, Y.E. Lozovik, K.L. Campman, A.C. Gossard, Phys. Rev. Lett. 87 (2001) 216804.

Appendix E

Authors:	M. Orlita, R. Grill, L. Smrčka, and M. Zvára
Title:	Tunable terahertz oscillations in superlattices subject to an in-plane magnetic field
Preprint server:	http://de.arxiv.org/abs/cond-mat/0601446
Year:	2006

Tunable terahertz oscillations in superlattices subject to an in-plane magnetic field

M. Orlita,[1,2,*] R. Grill,[1] L. Smrčka,[2] and M. Zvára[1]

[1] *Charles University, Faculty of Mathematics and Physics, Institute of Physics, Ke Karlovu 5, CZ-121 16 Prague 2, Czech Republic*

[2] *Institute of Physics, Academy of Sciences of the Czech Republic, Cukrovarnická 10, CZ-162 53 Prague 6, Czech Republic*

(Dated: January 19, 2006)

We present a concept of terahertz oscillations in superlattices that are generated under conditions apparently different from standard Bloch oscillations. These oscillations are induced when crossed magnetic and electric fields are applied to the superlattice, both in the in-plane direction. The frequency of these oscillations is tunable by the applied fields.

PACS numbers: 73.21.Cd, 73.40.-c

INTRODUCTION

The possibility of Bloch oscillations (BOs), i.e. the periodic motion of an electron in a periodic system induced by a uniform electric field, was mentioned by Zener [1] relatively soon after the basic quantum mechanical theory of the solid state was established [2]. Taking a simple picture of electrons, which are not subject to scattering, Zener predicted an oscillatory motion in the real as well as in the reciprocal space with the frequency $\omega_{BO} = eF\Delta/\hbar$, where Δ and F are the system spatial period and the electric field, respectively. However, it took a long time before any experimental evidence of BOs has been found, see e.g. [3, 4]. The key feature for their observation was a pioneering concept of a superlattice (SL) suggested by Esaki and Tsu [5] that allowed to overcome problems of a strong electron scattering, which made the observation of BOs in bulk semiconductors hardly feasible.

In this paper, we present a simple idea of electron-in-plane-oscillations appearing when crossed in-plane magnetic and electric fields are applied to SL. We start with a general discussion of properties of SL subject to the in-plane magnetic field the effect of which cannot be described within the quasi-classical approximation. The findings are illustrated by simple numerical calculations based on the standard tight-binding (TB) model, see e.g. [6, 7].

Subsequently, we study influence of an additionally applied electric field and conclude that an oscillatory motion of electrons is induced. We present two models of these oscillations, the first quasi-classical and the second pure quantum-mechanical. The predicted oscillations are compared to common BOs.

SUPERLATTICE SUBJECT TO IN-PLANE MAGNETIC FIELD

Let us consider an infinite SL described by the periodic potential $V(z) = V(z+\Delta)$, where Δ is the period of SL.

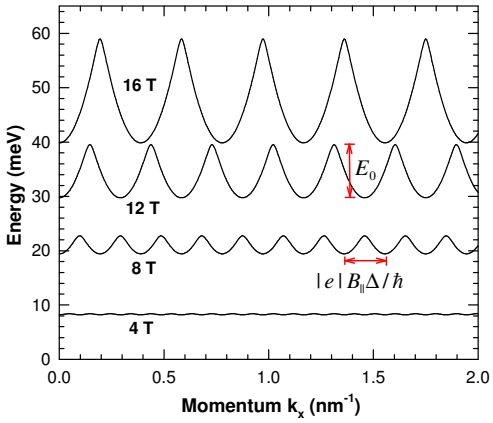

FIG. 1: Electron dispersion curves $E(k_x)$ calculated in TB approximation for several values of the magnetic field $B_\parallel$. Each curve is shifted upwards by a value of 2.5 meV/T$\times B_\parallel$ to prevent the confusing overlap. The parameters $m = 0.067m_0$, $\Delta = 16$ nm and $t = -2.5$ meV were used in the calculation.

We assume that the growth direction of SL is oriented along the z axis. When the in-plane magnetic field $\mathbf{B} = (0, B_\parallel, 0)$ with the vector potential gauge $\mathbf{A} = (B_\parallel z, 0, 0)$ is applied, the corresponding Hamiltonian of an electron in SL reads:

$$H = \frac{\hbar^2}{2m}\left(k_x - \frac{eB_\parallel z}{\hbar}\right)^2 + \frac{\hbar^2 k_y^2}{2m} - \frac{\hbar^2}{2m}\frac{d^2}{dz^2} + V(z). \quad (1)$$

We implicitly suppose the wave function in the form of plane waves in x- and y-directions. Evidently, the in-plane motion of an electron cannot be separated from the motion in the z-direction as commonly done in the solution of such problems at $B_\parallel = 0$. Instead, the coupling of motions in x- and z-directions appears and therefore the electron energy is no longer parabolic in momentum k_x and has a general form $E(k_x, k_y) = E(k_x) + \hbar^2 k_y^2/2m$.

Moreover, the dispersion is periodic in momentum k_x with period $K_0 = eB_\parallel\Delta/\hbar$, $E(k_x) = E(k_x + K_0)$. Hence, the Hamiltonian describes a system with a periodic dispersion $E(k_x)$, whose period K_0 is tunable by the applied magnetic field $B_\parallel$. This is in contrast to a fixed period $2\pi/\Delta$ of the electron dispersion in the growth direction of SL. The obtained result can be interpreted also as a formation of a 2D lattice in the $x-z$ plane induced in SL by a finite magnetic field in the y-direction. This lattice has spatial periods in x- and z-directions $2\pi/K_0$ and Δ, respectively. The magnetic flux trough the unit cell of the lattice is simply $2\pi B_\parallel\Delta/K_0 = h/e$, i.e. one magnetic flux quantum. Before we further utilize these findings, we use a simple TB approximation to get some numerical results, which can illustrate the studied problem.

Within the framework of the TB model, the Hamiltonian (1) is transformed into the matrix form and reads (see e.g. [8, 9]):

$$H_{i,j} = \frac{\hbar^2}{2m}(k_x + K_0 i)^2\delta_{i,j} + t\delta_{i,j\pm1}, \qquad (2)$$

where the coefficient t ($t < 0$) characterizes the tunneling between adjacent quantum wells (QWs) and where the motion in the y-direction is not included, since it is not affected by $B_\parallel$. Note that this TB Hamiltonian conserves the periodicity of the original Hamiltonian (1) in momentum k_x. The stationary Schrödinger equation with the tridiagonal Hamiltonian (2) can be easily solved numerically. The calculated dispersion curve in the x-direction for several values of the magnetic field $B_\parallel$ is plotted in Fig. 2 in the selected interval of k_x. We take only the lowest lying subband into account.

The results in Fig. 1 demonstrate both the expected periodicity of $E(k_x)$ and the shape of the dispersion curve, which cannot be predicted only from the periodicity of the Hamiltonian (1). We see that just one minimum per interval $(k_x, k_x + K_0)$ appears. The interpretation of this is rather straightforward: the increasing $B_\parallel$ leads to an effective decoupling of QWs and therefore, electrons with the momentum k_x become localized mainly in one QW only, in contrast to the case of zero magnetic field, when each electron is spread uniformly within the whole SL. Each minimum in $E(k_x)$ thus corresponds to a nearly parabolic dispersion of an electron localized just in one QW and the adjacent minimum corresponds to an electron localized in the next QW. The approximation assuming a nearly parabolic shape of each minimum allows also a rough estimation of the band width E_0 defined in Fig. 1. We simply take $E_0 \approx \hbar^2(K_0/2)^2/(2m) = e^2B_\parallel^2\Delta^2/8m$, which is again tunable by $B_\parallel$. Obviously, this approximation fails if $E_0 \approx |t|$.

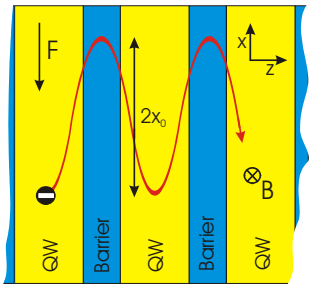

FIG. 2: A schematic picture of SL showing an expected trajectory of the electron under depicted conditions.

SEMI-CLASSICAL MODEL OF OSCILLATIONS

Having the periodic band structure $E(k_x)$ at a given fixed magnetic field $B_\parallel$, we use a semi-classical consideration to describe the electron motion if an additional constant electric field F_x in x-direction is applied. As the influence of $B_\parallel$ has already been included in the discussed energy spectrum, the semiclassical equation of motion takes a simple form $d(\hbar k_x)/dt = -eF_x$ and thus k_x increases linearly in time. Hence, the electron velocity $v_x = \hbar^{-1}dE(k_x)/dk_x$ becomes periodic in time and a specific oscillatory motion is generated. This motion is schematically shown in Fig. 2 and can be decomposed into a steady motion in the SL growth direction and the oscillation in the x-direction. The used equation of motion gives us also possibility to calculate the corresponding oscillatory frequency $\omega_{B_\parallel} = 2\pi F_x/(B_\parallel\Delta)$. Hence, $\omega_{B_\parallel}$ is tunable not only by the electric field, as in the the case of BOs but by $B_\parallel$ as well. Both frequencies ω_{BO} and $\omega_{B_\parallel}$ are functions of Δ – but whereas the first frequency is linear in Δ, the latter one has the reciprocal dependence. The oscillatory frequency $\omega_{B_\parallel}$ can be rewritten into $\omega_{B_\parallel} = 2\pi v_d/\Delta$, where $v_d = F_x/B_\parallel$ is the drift velocity introduced in 3D for the electron motion perpendicular to the crossed electric and magnetic fields, see e.g. [10]. The ratio Δ/v_d is then obviously the time needed to tunnel between adjacent QWs.

The semiclassical model allows us to determine the spatial amplitude of expected oscillations x_0 defined in Fig. 2. When we make use of the facts that the electron position is the time integral of the electron velocity and the velocity v_x is derivative of the dispersion curve, we obtain a simple relation $x_0 = E_0/(2eF_x)$. When the above discussed estimation for E_0 is used we get the final result $x_0 \approx e\Delta^2B_\parallel^2/(16mF_x)$.

QUANTUM-MECHANICAL MODEL OF OSCILLATIONS

The electron motion in a system with a periodic dispersion $E(k_x) = E(k_x + K_0)$ can be treated in a pure quantum-mechanical way as reviewed e.g. by Hartmann *et al.* [11]. The corresponding Hamiltonian is there conveniently written in the momentum representation:

$$H(k_x) = E(k_x) - \hat{\imath}eF_x\frac{d}{dk_x} \tag{3}$$

and thus, taking account of the periodicity in k_x, the eigenenergies can be easily calculated:

$$E_n = \frac{1}{K_0}\int_0^{K_0} E(k_x)dk_x + n\hbar\omega_{B_\parallel}. \tag{4}$$

Because the first term of this eigenenergy is constant at given $B_\parallel$, we receive an analog of the common Wannier-Stark ladder ($n \in \mathbb{Z}$) discussed in the framework of Bloch oscillations, see e.g. [11].

REMARKS ON A POSSIBLE REALIZATION

From the practical point of view, the emission of the terahertz radiation supposes a coherent motion of all electrons. To achieve detectable BOs, the electrons are usually generated in an un-doped SL by a femtosecond optical pulse ensuring the same phase of all electrons, see e.g. [3, 4, 12]. The photon laser energy is tuned to an appropriate electron-hole transition in SL. The same technique can be used in our case as well.

For a possible realization, we should also check the sample design and experimental conditions to observe the predicted oscillations in the terahertz region. Assuming $\omega_{B_\parallel} \approx \omega_{BO}$ and the same electric field in both cases, we obtain the corresponding magnetic field $B_\parallel \approx h/\Delta^2 e \cong 16$ T for $\Delta = 16$ nm. Hence, at $B_\parallel < 16$ T the oscillatory frequency is even higher than for BOs, since $\omega_{B_\parallel} \propto B_\parallel^{-1}$. Moreover, having two free parameters F_x and $B_\parallel$ we can independently optimize $\omega_{B_\parallel}$ and x_0 to achieve the maximal emitted power. This is more complicated for standard BOs, since ω_{BO} and the corresponding spatial amplitude are governed by the applied electric field only.

The important point in the observation of BOs is the achievement of an oscillation period significantly lower than is the scattering time due to phonons or plasmons. We predict our oscillation for SL systems, where common BOs are observed. Therefore, the same or very similar damping rates as observed in BO experiments could be expected in our case as well. Hence, the published experimental evidence of BOs, see e.g. [3, 4, 12], suggests that the predicted oscillations should be experimentally observable.

It is interesting to investigate also the direction characteristics of the expected radiation. Since the radiation is generated by the electron oscillatory motion in the x-direction, the radiation should be emitted mainly in the plane perpendicular to the x-axis, i.e. in the plane perpendicular to the oscillating dipoles.

CONCLUSIONS

We have investigated behavior of electrons in a superlattice when crossed magnetic and electric fields are applied, both in the in-plane direction. We predict a novel terahertz oscillations in superlattices that are different from Bloch oscillations that appears when the electric field is applied in the growth direction of the superlattice. We have also found a simple expression for the frequency of these oscillations. The suggested realistic design of the structures allows preparation of terahertz emitters controlled by the in-plane magnetic field.

This work is a part of the research plan MSM 0021620834 that is financed by the Ministry of Education of the Czech Republic. M. O. acknowledges the support from Grant Agency of Charles University under contract No. 281/2004 and L. S. from Grant Agency of ASCR under contract No. IAA1010408.

* Electronic address: orlita@karlov.mff.cuni.cz

[1] C. Zener, Proc. R. Soc. London A 145, (1934) 523.
[2] F. Bloch, Z. Phys. 52, (1928) 555.
[3] J. Feldmann, K. Leo, J. Shah, D. A. B. Miller, J. E. Cunningham, T. Meier, G. von Plessen, A. Schulze, P. Thomas, and S. Schmitt-Rink, Phys. Rev. B 46, (1992) 7252.
[4] C. Waschke, H. G. Roskos, R. Schwedler, K. Leo, H. Kurz, and K. Köhler, Phys. Rev. Lett. 70, (1993) 3319.
[5] L. Esaki and R. Tsu, IBM J. Res. Dev. 14, (1970) 61.
[6] N.A. Goncharuk, L. Smrčka, J.Kučera, and K. Výborný, Phys. Rev. B 71, (2005) 195318.
[7] A. G. Lebed, Phys. Rev. Lett. 95, (2005) 247003.
[8] U. Wulf, J. Kučera, and A. H. MacDonald, Phys. Rev. B 47, (1993) 1675.
[9] K. Výborný, L. Smrčka, and R. A. Deutschmann, Phys. Rev. B 66, (2002) 205318.
[10] J. H. Davies, The Physics of Low-Dimensional Semiconductors: An Introduction, Cambridge University Press, (1997) p. 229.
[11] T. Hartmann, F. Keck, H. J. Korsch, and S. Mossmann, New J. Phys. 6, (2004) 2.
[12] R. Martini, G. Klose, G. H. Roskos, H. Kurz, H. T. Grahn, and R. Hey, Phys. Rev. B 54, (1996) 14325.